UNIVERSITY OF AMSTERDAM

UvA-DARE (Digital Academic Repository)

Modelling and computational improvements to the simulation of single vector-boson plus jet processes for the ATLAS experiment

The ATLAS Collaboration

DOI
10.1007/JHEP08(2022)089

Publication date
2022

Document Version
Final published version

Published in
Journal of High Energy Physics

License
CC BY

Link to publication

Citation for published version (APA):
The ATLAS Collaboration (2022). Modelling and computational improvements to the simulation of single vector-boson plus jet processes for the ATLAS experiment. *Journal of High Energy Physics*, *2022*(8), Article 89. https://doi.org/10.1007/JHEP08(2022)089

General rights
It is not permitted to download or to forward/distribute the text or part of it without the consent of the author(s) and/or copyright holder(s), other than for strictly personal, individual use, unless the work is under an open content license (like Creative Commons).

Disclaimer/Complaints regulations
If you believe that digital publication of certain material infringes any of your rights or (privacy) interests, please let the Library know, stating your reasons. In case of a legitimate complaint, the Library will make the material inaccessible and/or remove it from the website. Please Ask the Library: https://uba.uva.nl/en/contact, or a letter to: Library of the University of Amsterdam, Secretariat, P.O. Box 19185, 1000 GD Amsterdam, The Netherlands. You will be contacted as soon as possible.

UvA-DARE is a service provided by the library of the University of Amsterdam (https://dare.uva.nl)

Download date:13 Sept 2026

Published for SISSA by Springer

Received: December 20, 2021
Revised: May 2, 2022
Accepted: June 30, 2022
Published: August 5, 2022

Modelling and computational improvements to the simulation of single vector-boson plus jet processes for the ATLAS experiment

The ATLAS collaboration

E-mail: atlas.publications@cern.ch

Abstract: This paper presents updated Monte Carlo configurations used to model the production of single electroweak vector bosons (W, Z/γ^*) in association with jets in proton-proton collisions for the ATLAS experiment at the Large Hadron Collider. Improvements pertaining to the electroweak input scheme, parton-shower splitting kernels and scale-setting scheme are shown for multi-jet merged configurations accurate to next-to-leading order in the strong and electroweak couplings. The computational resources required for these set-ups are assessed, and approximations are introduced resulting in a factor three reduction of the per-event CPU time without affecting the physics modelling performance. Continuous statistical enhancement techniques are introduced by ATLAS in order to populate low cross-section regions of phase space and are shown to match or exceed the generated effective luminosity. This, together with the lower per-event CPU time, results in a 50% reduction in the required computing resources compared to a legacy set-up previously used by the ATLAS collaboration. The set-ups described in this paper will be used for future ATLAS analyses and lay the foundation for the next generation of Monte Carlo predictions for single vector-boson plus jets production.

Keywords: Hadron-Hadron Scattering

ArXiv ePrint: 2112.09588

Open Access, Copyright CERN,
for the benefit of the ATLAS Collaboration.
Article funded by SCOAP^3.

https://doi.org/10.1007/JHEP08(2022)089

JHEP08(2022)089

Contents

1 Introduction **1**

2 Generator configurations **3**
2.1 Sherpa 3
2.2 MadGraph5_aMC@NLO+Pythia 5
2.3 Cross-sections 6

3 Theoretically motivated improvements **7**
3.1 Electroweak virtual corrections 7
3.2 Electroweak input scheme 10
3.2.1 Forward-backward asymmetry 10
3.2.2 Polarization of τ-leptons 10
3.3 Modified Catani-Seymour splitting kernels 12
3.4 Scale-setting scheme for unordered histories 13

4 Computational improvements **15**
4.1 Speed characterization 17
4.1.1 Perturbative accuracy 18
4.1.2 Additional features 20
4.1.3 Generator comparisons 21
4.2 Statistical enhancement methods 23
4.2.1 Sample biasing and statistical precision 23
4.2.2 Quantitative assessment 26
4.3 Impact on computing resources 30
4.3.1 Per-event CPU cost for production configurations 31
4.3.2 Generated effective luminosity 32

5 Conclusions **35**

A Equations for modified Catani-Seymour splitting kernels **36**
A.1 Final-initial dipoles 36
A.2 Initial-final dipoles 36
A.3 Initial-initial dipoles 37

The ATLAS collaboration **43**

JHEP08(2022)089

1 Introduction

The production of a single electroweak vector boson (W or Z/γ^*) in association with jets, collectively referred to as $V+$jets, is a fundamentally important process at the Large Hadron Collider (LHC) [1]. Measurements of electroweak bosons in the leptonic decay modes provide a clean experimental signature within the ATLAS detector [2] to test the electroweak sector of the Standard Model (SM) and perturbative quantum chromodynamics (QCD) in high-multiplicity final states. In addition, $V+$jets production is a significant irreducible SM background for a diverse range of analyses within the LHC physics programme: Higgs boson [3, 4] and top quark measurements [5, 6], and searches for new physics phenomena beyond the Standard Model (BSM) [7–9]. These analyses often rely on Monte Carlo (MC) simulation-based predictions for background estimation, and therefore an accurate description of the $V+$jets process with sufficient statistical precision across a wide phase space with many final-state jets is required. Consequently, multi-leg MC generators that combine multiple exclusive jet emissions with the highest possible perturbative accuracy in the strong and electroweak couplings are preferred.

In recent years, the statistical precision of $V+$jets MC samples has become an increasingly limiting factor for a broad array of ATLAS data analyses. This is primarily due to the long event-generation time of multi-leg MC predictions with high perturbative accuracy that is demanded by the ATLAS physics programme. The relatively large $V+$jets production cross-section and the rapidly growing integrated luminosity of the proton-proton collision dataset require MC event generators to provide enormous simulated samples, which results in a significant computational challenge for experiments. Current analyses exploring high cross-section regions of phase space already rely on simulated samples that contain many billions of events. Furthermore, the wide range of ATLAS physics searches continue to explore $V+$jets processes in increasingly extreme regions of phase space, with cross-sections that are many orders of magnitude lower than the inclusive cross-section. In order to meet the statistical demands of these analyses, specialized techniques are required to populate their selection regions. Meeting all of these requirements has historically resulted in a challenging workflow with computing demands that continue to stretch existing resources. With finite computational resources and a fixed computing budget for the High Luminosity LHC (HL-LHC) [10], fast and efficient MC event generation has already been identified as a potential bottleneck for the large integrated luminosity expected during the HL-LHC runs [11, 12].

The ATLAS collaboration has relied on a multi-leg Sherpa 2.2.1 [13, 14] $V+$jets prediction for the past several years, which has been used for a range of measurements and new-physics searches. This configuration, hereafter referred to as the 2.2.1 set-up, has been substantially extended to meet the statistical needs of these analyses. It required significant resources to produce, due to the long event-generation time, inefficient heavy-flavour filtering techniques, and a relatively large fraction of negative MC event weights. Moreover, many analyses that probe regions of phase space with poorly understood predictions required complex data-driven corrections to their background estimates. The recent efforts highlighted in this paper have focused on improving both the

JHEP08(2022)089

theoretical and computational aspects of the widely used Sherpa $V+$jets predictions in ATLAS. In addition, an alternative multi-jet merged next-to-leading-order (NLO) MadGraph5_aMC@NLO+Pythia [15, 16] configuration with similar perturbative accuracy to the Sherpa prediction has been produced for use by ATLAS for the first time. This configuration is used for an independent comparison with the Sherpa predictions.

The modelling improvements have focused on the level of agreement of the Sherpa 2.2.1 predictions with data using a series of well motivated theoretical changes. It is known that cross-sections predicted by the Sherpa 2.2.1 configuration disagree with the data in several important regions of phase space. In particular, those dominated by extremely energetic jets significantly overestimate the measured cross-section, requiring sophisticated data-driven corrections [17, 18]. Moreover, measurements of the transverse momentum of Drell-Yan lepton pairs show artificial discontinuities around the matrix-element and parton-shower merging scale [19]. Such discontinuities can arise from different cross-sections predicted by the matrix element and parton shower at the merging scale. This paper begins to address these issues through well-motivated theoretical changes including the inclusion of higher-order QCD and electroweak (EW) corrections, a dedicated scale-setting procedure for topologies with unordered parton-shower histories, modified Catani-Seymour parton-shower splitting kernels, and a careful treatment of input electroweak parameters. Comparisons of these changes, along with the newly available MadGraph5_aMC@NLO+Pythia predictions, are performed with publicly available ATLAS and CMS data to highlight the changes.

The computational resources required for large-scale production of any multi-jet merged MC prediction that meets the mentioned theoretical demands is significant. Furthermore, the techniques used to populate the low cross-section regions of phase space can significantly exacerbate the problem. In the Sherpa 2.2.1 configuration, a discrete phase-space slicing technique was used, which resulted in artificial features in the distribution of event weights that adversely impacted the statistical precision of the sample. In addition, the relatively large fraction of MC events with negative weights in the high cross-section regions of phase space, coupled with the long event-generation time, made it difficult to provide a simulated dataset with enough generated luminosity to match the collected data. Therefore, the focus of the computational improvements in this paper has been to reduce the per-event generation time, and the fraction of MC events with negative weights, whilst simultaneously including higher-order EW and QCD corrections. Moreover, a continuous statistical enhancement method is introduced in order to more efficiently populate the low cross-section regions of phase space. A detailed assessment of the CPU resources of the Sherpa configuration is shown, along with approximations that reduce the per-event generation time. In addition, the performance of various statistical enhancement methods is reported and is shown to improve on the approach adopted for the 2.2.1 configuration.

This paper is organized as follows. The Sherpa and MadGraph5_aMC@NLO+Pythia configurations are described in section 2. The theoretically motivated improvements are shown in section 3, in which comparisons with unfolded ATLAS and CMS data are performed where relevant. Section 4 is devoted to computational improvements, which include a characterization of the per-event CPU time consumption, an evaluation of the

JHEP08(2022)089

phase-space slicing and statistical enhancement techniques, and a real-world example of the impact that the aforementioned computational improvements have had on computing resources. Finally, conclusions are given in section 5.

2 Generator configurations

This section describes the Sherpa and MadGraph5_aMC@NLO+Pythia configurations and software versions used throughout the paper. An extensive software suite [20] is used for the generation of simulated MC samples shown in this paper. All predictions are normalized to the cross-sections obtained from the generator. Particular attention is given to settings that are highlighted in the modelling and numerical improvements in sections 3 and 4, respectively. For settings not mentioned below, the default values from the event generator are used.

2.1 Sherpa

A legacy Sherpa 2.2.1 configuration is included in this paper as a reference point, against which various improvements are quantified. Further performance studies of this set-up can be found in ref. [14]. An improved configuration is described below and is referred to as the Sherpa 2.2.11 configuration.

Both configurations are simulated with the Sherpa [13] MC generator. In this set-up, NLO-accurate matrix elements for up to two jets, and LO-accurate matrix elements for up to five (four) jets in the five-flavour scheme are calculated with Comix [21] for the 2.2.11 (2.2.1) configuration. The b- and c-quarks are treated as massless at matrix-element level and massive in the parton shower. Virtual QCD corrections for matrix elements at NLO accuracy are provided by OpenLoops [22–25]. The Hessian NNPDF3.0nnlo [26, 27] PDF set is used for the 2.2.11 configuration, whilst the 2.2.1 configuration used the MC replica version of NNPDF3.0nnlo. In the Sherpa $Z+$jets configurations the invariant mass of the charged leptons is required to be larger than 40 GeV, while the charged lepton plus neutrino invariant mass is required to be larger than 2 GeV for $W+$jets final states.

The 2.2.11 $Z+$jets configuration uses an electroweak input scheme specified by m_Z, the QED coupling constant evaluated at the Z resonance, $\alpha(m_Z)$, and the effective weak mixing angle $\sin^2\theta_{\text{eff}}$ [28], while the $W+$jets configuration uses the so-called G_μ scheme specified by the Fermi constant G_μ, m_Z and m_W. Remaining EW parameters are derived from these input parameters using tree-level relations. Further discussion and comparisons of these EW input schemes are presented in section 3.2. For the 2.2.1 configuration, all $V+$jets processes use an *effective EW input scheme* in which the masses of the W, Z and Higgs boson are taken as inputs, alongside $\sin^2\theta_{\text{eff}}$, $\alpha(m_Z)$, the vacuum expectation value (v), and Higgs self-coupling constant (λ). Such an input scheme allows certain tree-level relations between some parameters to be violated. Electroweak virtual corrections are included in the 2.2.11 configuration, and are available as an alternative generator weight based on the NLO EW_{virt} approach [29, 30]. The effect of these corrections using an additive, multiplicative, or exponentiated combination scheme for higher-order QCD and EW terms is explored in section 3.1. QED radiation to electron, muon, hadron and τ-lepton

JHEP08(2022)089

decays is implemented by the Yennie-Frautschi-Suura (YFS) algorithm. The default YFS Sherpa settings [31, 32] are used.

The NLO matrix elements of a given jet multiplicity are matched to the parton shower using a colour-exact variant of the MC@NLO algorithm [33]. Different jet multiplicities are then merged into an inclusive sample using an improved CKKW matching procedure [34, 35] which is extended to NLO accuracy using the MEPS@NLO prescription [36]. The merging cut is set to $Q_{\text{cut}} = 20\,\text{GeV}$. The default Sherpa Catani-Seymour dipole parton shower [37] scheme and the cluster hadronization model [38] are used. Modified splitting kernels, which give the probability for a given parton to split, are used in the Sherpa 2.2.11 set-up and they are shown to improve the modelling close to the merging scale, as discussed in section 3.3. In the Sherpa 2.2.11 set-up, unordered parton-shower histories are not allowed. If an unordered emission is found, the previous maximal scale will be used as described in section 3.4.

Heavy-flavour hadron production fractions in the Sherpa 2.2.1 set-up are known to disagree with the world average values [39]. A dedicated tuning was therefore performed by the ATLAS collaboration, which was subsequently implemented in the Sherpa event generator. The heavy-flavour baryon production rates previously modelled by a single hadronization parameter in the 2.2.1 configuration were extended to five unique parameters, in order to provide higher fidelity in the control of heavy-flavour baryon production. Two parameters for the charm and beauty baryons, and three for the charm-beauty, charm-strange, and bottom-strange baryons, were introduced. Heavy-flavour hadrons with unknown hadronic decay modes are forced to decay into diquark pairs which are then subsequently hadronised. The invariant mass and binding energy of the diquark pair characterize the hadronization process. The former was adjusted to reduce the low-energy photon ($\mathcal{O}$(0.1–1) GeV) production rate from such hadronic decays. Furthermore, the b-fragmentation function was altered to address an overabundance of jets with small b-momentum fraction ($x_b = p_{\text{T}}^b/p_{\text{T}}^{\text{jet}}$), in addition to updating the heavy-flavour decay tables to the world average values [40]. These changes are implemented in Sherpa versions 2.2.5 or later, and thus are present in the Sherpa 2.2.11 configuration.

The MEPS@NLO scale-setting algorithm for the infrared-regular part of the real emission component, commonly referred to as 'hard events' or '$\mathbb{H}$-events' [36], was studied from a CPU and modelling point of view. In the 2.2.1 configuration, the renormalization scale for these multi-jet configurations is calculated by probabilistically identifying parton-shower topologies through a k_{T}-type clustering algorithm [35]. The full scale-setting algorithm is referred to as the STRICT_METS scale-setting algorithm. The $\mathbb{H}$-events represent a large fraction of the total event generation time, which could be significantly reduced using a simplified event-level H'_{T} scale for this calculation. The H'_{T} scale is defined by [41]:

$$H'_{\text{T}} = \sum p_{\text{T}}^j + m_V, \tag{2.1}$$

where the sum extends over all final-state partons excluding those from the boson decay, p_{T}^j is the jet transverse momentum, and m_V denotes the invariant mass of the boson decay products. The STRICT_METS scale-setting algorithm is used for the remainder

JHEP08(2022)089

of the calculation. This scale scheme reduces the per-event generation time as shown in section 4.1. It is used in the Sherpa 2.2.11 configuration only.

All MC@NLO processes are affected by negative weights. The presence of negative weights degrades the statistical precision of a sample compared to the one without negative weights, and therefore it is desirable to reduce the fraction of negative weights as much as possible. In the Sherpa 2.2.11 configurations, the MC@NLO matching does not account for subleading gluon spin and colour correlations known to have small effects on final-state observables [42]. This results in an overall reduction in the fraction of negative weights, while preserving the essential features of the matched prediction [43]. In addition, the LO contributions are reweighed with a differential NLO/LO K-factor using a $2 \to 2$ core process obtained through an inverse parton-shower clustering. The clustering is first performed in an inclusive mode where both QCD and EW vertices are allowed to be clustered; if the inclusive clustering fails to find a suitable process to evaluate the NLO/LO K-factor, it is re-performed in an exclusive mode where the clustering of EW vertices is disabled [44]. This scheme is referred to as the inclusive+exclusive clustering mode. For the 2.2.1 set-up, the highest $2 \to n$ NLO QCD process in the inclusive mode is used as the core process. Using the $2 \to 2$ core process improves the statistical power of the MC sample in high cross-section regions of phase space as shown in section 4.1.

Control of the phase-space sampling is achieved via either a discrete slicing or continuous phase-space biasing technique. In the case of the Sherpa 2.2.1 configuration, the sample is divided into discrete $\max(H_{\mathrm{T}}, p_{\mathrm{T}}^{V})$ regions (slices), with boundaries at [0, 70, 140, 280, 500, 1000, 6500] GeV. The H_{T} variable is defined as the scalar sum of all partonic jet transverse momenta and p_{T}^{V} is the transverse momentum of the lepton pair. The Sherpa 2.2.11 configuration was statistically enhanced in the $\max(H_{\mathrm{T}}, p_{\mathrm{T}}^{V})$ variable using an analytic enhancement technique. Section 4.2.1 discusses the strengths and weaknesses of different enhancement techniques in terms of statistical performance.

QCD scale uncertainties have been evaluated on-the-fly using 7-point variations of the factorization and renormalization scales coherently in the matrix elements and the parton shower [45]. The scales are varied independently by factors of 0.5 and 2 while avoiding cases where the factorization and renormalization scales move in opposite directions. PDF uncertainties for the nominal NNPDF3.0nnlo PDF set are evaluated using the 100 variation replicas in case of the 2.2.1 set-up and using the Hessian eigenvector set for the 2.2.11 set-up, as well as ± 0.001 shifts of α_{S} around the nominal value of 0.118. Additionally, the central values of the CT18nnlo [46] and MSHT2020nnlo [47] PDF sets are included as additional generator weights.

A summary of the Sherpa configurations is shown in table 1.

2.2 MadGraph5_aMC@NLO+Pythia

An additional prediction using the MadGraph5_aMC@NLO 2.6.5 [15] program is used to generate weak bosons with up to three additional partons in the final state at NLO accuracy in the strong coupling. The renormalization and factorization scales are set to one half the transverse mass of all final state partons. The accuracy on the absolute value of the cross section obtained during the phase-space integration is required to be less than 0.0001.

JHEP08(2022)089

Configuration	Sherpa 2.2.1	Sherpa 2.2.11
Generator version	Sherpa 2.2.1	Sherpa 2.2.11
PDF set	NNPDF3.0nnlo	NNPDF3.0nnlo
EW input scheme	Effective	$\sin^2\theta_{\text{eff}}$
QCD accuracy	0–2j@NLO+3,4j@LO	0–2j@NLO+3,4,5j@LO
NLO EW_{virt} corrections	No	Yes
Subtraction scheme	Default	Modified Catani-Seymour
Special treatment for unordered histories	No	Yes
Scale for $\mathbb{H}$-events	STRICT_METS	H_{T}'
Gluon colour/spin exact matching	Yes	No
Core process for K-factor	$2 \to 4$	$2 \to 2$
Phase-space strategy	Sliced in $\max(H_{\text{T}}, p_{\text{T}}^{V})$	Analytic enhancement

Table 1. Summary of the Sherpa 2.2.1 and 2.2.11 configurations.

The showering and subsequent hadronization is performed using Pythia 8.240 [16] with the A14 tune [48], and the NNPDF2.3lo PDF set [49] with $\alpha_{\text{S}} = 0.130$. The different jet multiplicities are merged using the FxFx NLO matrix-element and parton-shower merging prescription [50]. The sampled phase-space is biased using a function equal to the square of sum of final state momenta (i.e leptons plus partons). Heavy-flavor hadron decays are handled by EvtGen 1.7.0 and QED radiation is added by Pythia 8. The inclusive fraction of generated events with negative weights is approximately 17%, and reaches 35% for p_{T}^{V} and H_{T} phase spaces above 100 GeV.

The MadGraph5_aMC@NLO+Pythia calculation uses a five-flavour number scheme with massless b- and c-quarks at the matrix-element level, and massive quarks in the Pythia 8 shower. At the event-generation level, the jet transverse momentum is required to be at least 10 GeV, with no restriction on the absolute value of the jet pseudorapidity. The PDF set used for event generation is NNPDF3.1nnlo supplemented with the LUXqed photon PDFs using $\alpha_{\text{S}} = 0.118$ [51]. The merging scale is set to $Q_{\text{cut}} = 20$ GeV. Scale variations where the renormalization and factorization scales have been varied independently by a factor of 2 or 0.5 in the matrix element are included as alternative generator event weights [52].

2.3 Cross-sections

The predicted cross sections from the Sherpa and MadGraph5_aMC@NLO+Pythia event generators for the configurations described above are shown in table 2. Additionally, an inclusive reference cross-section calculated with FEWZ [53] using the MSTW2008nnlo PDF set to NNLO QCD accuracy is shown for comparison. The effects of scale uncertainties are estimated by varying the factorization and renormalization scales independently around their central values by factors of 2 and 0.5. The PDF uncertainties are estimated from the NNPDF3.0nnlo and NNPDF3.1nnlo variations for the Sherpa and Mad-

JHEP08(2022)089

	$\sigma(pp \to \ell\ell)$ [pb]	$\sigma(pp \to \mu\nu)$ [pb]
Sherpa 2.2.1	2160 ± 86 (scale) ± 53 (PDF+α_S)	20697 ± 828 (scale) ± 507 (PDF+α_S)
Sherpa 2.2.11	2221 ± 155 (scale) ± 47 (PDF+α_S)	21781 ± 1525 (scale) ± 462 (PDF+α_S)
MG5_aMC@NLO+Pythia	2268 ± 92 (scale) ± 23 (PDF)	22163 ± 898 (scale) ± 225 (PDF)
NNLO QCD	$2067\ ^{+10}_{-14}$ (scale) $^{+52}_{-39}$ (PDF)	$20080\ ^{+100}_{-161}$ (scale) $^{+522}_{-401}$ (PDF)

Table 2. Event generator predicted cross-sections for each of the MC configurations. The reference NNLO QCD cross-section is calculated with FEWZ [53] using the MSTW2008nnlo PDF set.

Graph5_aMC@NLO+Pythia set-ups, while the inclusive NNLO PDF uncertainty is computed using the 68% C.L. MSTW2008nnlo PDF eigenvector error sets.

The cross-sections predicted by the different configurations can differ for numerous reasons, including the perturbative accuracy of the set-up, the choice of EW input scheme, and the choice of PDF set. The cross-section from the 2.2.11 configuration is larger than that from the Sherpa 2.2.1 configuration due to the inclusion of the 5j@LO matrix-elements. All cross-sections are larger than the inclusive NNLO QCD value since both the Sherpa and MadGraph5_aMC@NLO+Pythia configurations include contributions beyond an inclusive NNLO QCD calculation. The scale uncertainties in the Sherpa 2.2.11 set-up include variations in the 5j@LO matrix element as well as coherent variations in the parton shower, which together lead to a ∼40% increase in the total inclusive scale uncertainty relative to the Sherpa 2.2.1 configuration. All results presented in this paper are normalized to the respective event generator's cross-section prediction.

3 Theoretically motivated improvements

This section reports on the theoretical changes that are included in the Sherpa 2.2.11 configuration. They include four major topics: the inclusion of higher-order QCD and electroweak corrections, an electroweak input scheme for Z + jets events that specifies the weak mixing angle, specialized treatment of the dipole operators for the Catani-Seymour splitting kernels, and a special treatment of unordered parton-shower histories. These changes are described below and the performance of the Sherpa 2.2.11 and MadGraph5_aMC@NLO+Pythia configurations is compared with that of the 2.2.1 configuration. Rivet [54] is used to compare the predictions with previously published ATLAS or CMS data to highlight the theoretical changes.

3.1 Electroweak virtual corrections

Electroweak corrections to single boson production can play a significant role in regions of phase space where the boson is produced with large transverse momentum, owing to the appearance of EW Sudakov logarithms of the form $\log(s/m_V^2)$ [30]. These corrections are crucial for an accurate description of single vector bosons and will play an important role for BSM searches probing high-p_T^V phase-space regions. The full electroweak calculation contains contributions from virtual loops and from real emission of gauge bosons. The

JHEP08(2022)089

Sherpa 2.2.11 configuration presented in this paper only contains the virtual-loop terms, since applying the full NLO EW corrections is not currently possible in a multi-jet merged set-up. Moreover, the real emission of a gauge boson leads to a fundamentally different experimental signature that is typically produced in separate samples.

Amplitudes for the electroweak virtual corrections are calculated by OpenLoops and implemented in the Sherpa event generator for multi-jet merged set-ups. Results from MEPS@NLO merged set-ups with up to two additional jets at next-to-leading order in QCD for selected processes are shown in ref. [30]. In this paper, electroweak virtual corrections are included in the multi-jet merged set-ups with 0–2j@NLO+3–5j@LO QCD accuracy, and their effects are demonstrated relative to the NLO QCD-only prediction for all leptonic decay modes of the W and Z bosons. Moreover, multiple NLO QCD and NLO EW combination schemes are compared, and these are stored as alternative generator weights.

The cross-section calculated at NLO QCD and NLO EW accuracy for a $2 \to n$ final state, where the higher-order terms in QCD and EW couplings are summed (*additive scheme*), can be expressed as:

$$\sigma^{\text{NLO}}_{n,\text{QCD+EW}} = \sigma_{n,\text{LO}} + \Delta\sigma^{\text{NLO}}_{n,\text{QCD}} + \Delta\sigma^{\text{NLO}}_{n,\text{EW}_\text{virt}}$$

where $\sigma_{n,\text{LO}}$ denotes the Born-level cross-section and $\Delta\sigma^{\text{NLO}}_{n,\text{QCD}}$ the NLO QCD corrections to the Born process. The $\Delta\sigma^{\text{NLO}}_{n,\text{EW}_\text{virt}}$ term only contains the virtual-loop components, and in the NLO EW_virt approximation these are specified by [30]:

$$\Delta\sigma^{\text{NLO}}_{n,\text{EW}_\text{virt}} = \left[B_{n,\text{mix}}(\Phi_n) + V_{n,\text{EW}}(\Phi_n) + I_{n,\text{EW}}(\Phi_n)\right] \mathrm{d}\Phi_n, \tag{3.1}$$

where Φ_n represents the phase space of the n-particle final state, $B_{n,\text{mix}}$ are the mixed QCD-EW Born contributions with order α_S^{n-1} and α^3 in the strong and electroweak coupling, respectively, $V_{n,\text{EW}}$ is the exact one-loop virtual correction to the Born process with order α^3 in the electroweak coupling, and $I_{n,\text{EW}}$ is the approximated subtraction term used to render the above cross-section finite. The approximated electroweak virtual corrections in eq. (3.1) are denoted by NLO EW_virt in this paper. They were developed and shown to be in good agreement with the full NLO EW calculation in ref. [30] up to a few percent, with the exception of phase spaces dominated by real emission contributions such as the off-shell region of the $m_{\ell\ell}$ invariant mass distribution. Such phase-spaces are dominated by real QED emissions from charged leptons that are not included in the NLO EW_virt calculations, and instead supplemented by dedicated samples. In the results shown below, the one-loop contributions are included for final states with up to two extra jets.

Two additional NLO QCD and NLO EW combination schemes are provided by the Sherpa framework. The first is the *multiplicative scheme*, which is defined as:

$$\sigma^{\text{NLO}}_{n,\text{QCD}\times\text{EW}} = (\sigma_{n,\text{LO}} + \Delta\sigma^{\text{NLO}}_{n,\text{QCD}}) \times (1 + \Delta\sigma^{\text{NLO}}_{n,\text{EW}_\text{virt}}).$$

The second scheme is referred to as the *exponentiated scheme*, and is defined as:

$$\sigma^{\text{NLO}}_{n,\text{QCD}\times e^{\text{EW}_\text{virt}}} = (\sigma_{n,\text{LO}} + \Delta\sigma^{\text{NLO}}_{n,\text{QCD}}) \times e^{\Delta\sigma^{\text{NLO}}_{n,\text{EW}_\text{virt}}}.$$

JHEP08(2022)089

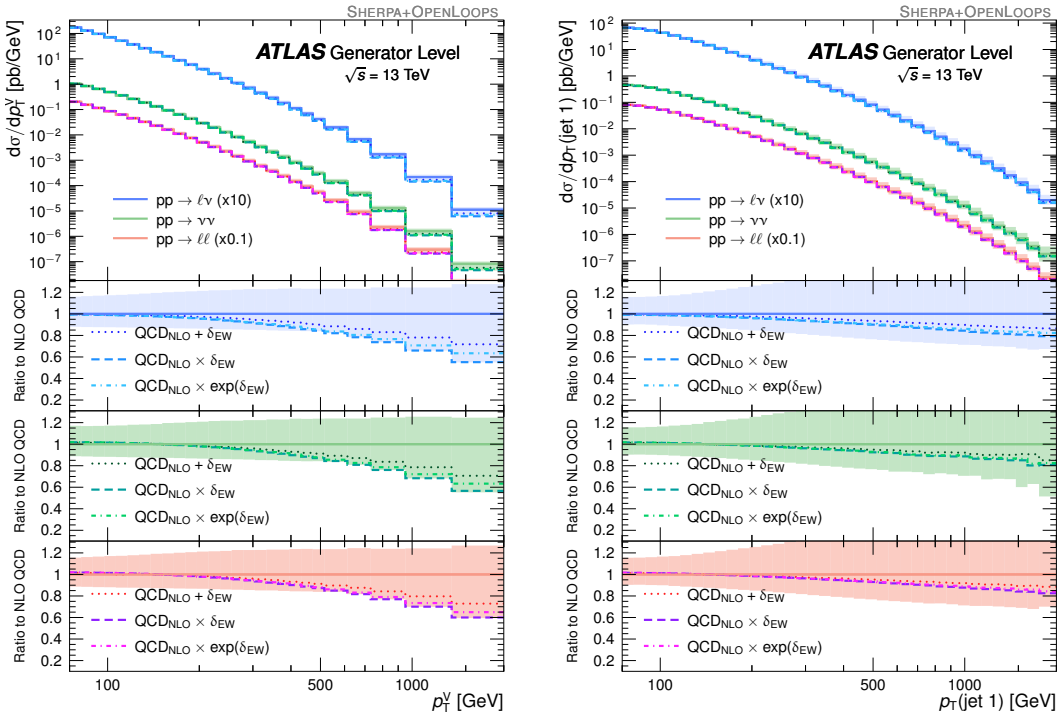

(a) (b)

Figure 1. Differential distributions of the transverse momentum of (a) the boson and (b) the highest transverse momentum jet for $pp \to \ell\ell, \nu\nu, \ell\nu$ processes. The QCD accuracy of all predictions is 0–2j@NLO+3–5j@LO. The electroweak virtual corrections are denoted by Δ_{EW}. The $\ell\ell$ and $\ell\nu$ final states have been averaged from electron, muon and τ-lepton final states. The shaded bands include scale uncertainties calculated from the envelope of renormalization and factorization variations.

The multiplicative and exponentiated schemes are motivated by the factorization of the QCD and EW Sudakov corrections at high energies [55].

Comparisons of the NLO QCD-only prediction with and without the virtual electroweak corrections are shown in figure 1 using the SHERPA 2.2.11 configuration. The corrections reach 30% around $p_{\text{T}}^{V} \sim 1\,\text{TeV}$ and qualitatively follow the expected logarithmic behaviour. The relative size of the corrections is in good agreement with those obtained from the fixed-order NLO EW calculations when including corrections for up to two additional jets at next-to-leading order [30]. The multiplicative and exponentiated contributions show the largest deviations from the NLO-only prediction and are in good agreement with each other. The difference between the additive and multiplicative or exponentiated predictions is interpreted as a source of systematic uncertainty for missing higher orders resulting from mixed QCD-EW contributions, and around p_{T}^{V} of 1 TeV the uncertainty is approximately 10% for all final states. Future measurements of vectors bosons produced with large transverse momentum will be crucial in testing these predictions, in addition to understanding NLO EW effects overall.

JHEP08(2022)089

3.2 Electroweak input scheme

An EW input scheme defines the set of input parameters which are use to derive any remaining EW parameters. Some choices of EW scheme can result in values that differ from experimentally determined values. In particular, using tree-level relations in the G_μ scheme the weak mixing angle is found to be:

$$\sin^2\theta_W = \left(1 - \left(\frac{m_W}{m_Z}\right)^2\right) \approx 0.223,$$

which disagrees with the experimentally determined value of $\sin^2\theta_{\text{eff}}$=0.23113±0.00014 [56]. Although the G_μ scheme is an attractive choice for Z + jets (Drell-Yan) processes at hadron colliders because it absorbs a large part of the radiative corrections in the LO prediction [28], this level of discrepancy causes measurable differences in the forward-backward asymmetry of leptons from Z boson decays and the τ-lepton polarization as highlighted below.

The $\sin^2\theta_{\text{eff}}$ scheme by construction ensures the correct value of $\sin^2\theta_{\text{eff}}$ since it is specified as one of the input parameters. The $\sin^2\theta_{\text{eff}}$ scheme based on ref. [28] was implemented by the OpenLoops and Sherpa authors [30] throughout the course of the work presented in this paper. It is used for the Sherpa 2.2.11 Z + jets configuration for both the NLO QCD and NLO EW_{virt} calculations. In this scheme, the derived W boson mass differs from its experimentally measured value, but for single Z boson production this has negligible impact on the physics performance.

3.2.1 Forward-backward asymmetry

The vector and axial-vector couplings in the $pp \to Z \to \ell\ell$ process lead to a forward-backward asymmetry (A_{FB}) in the polar angle of the lepton with respect to the incoming quark direction in the rest frame of the dilepton system. This forward-backward asymmetry has been measured as a function of the dilepton invariant mass by ATLAS in $\sqrt{s} = 7\,\text{TeV}$ proton-proton collisions and used to extract the weak mixing angle [57]. The measured asymmetry values are used to test the performance of the G_μ and $\sin^2\theta_{\text{eff}}$ schemes using the Sherpa 2.2.11 configuration.

The forward-backward asymmetry is most sensitive to the weak mixing angle close to the Z boson's pole mass since the size of A_{FB} is proportional to $\sin^2\theta_W$ at $m_{\ell\ell} \sim m_Z$. As shown in figure 2, with NLO QCD accuracy the G_μ scheme leads to an overestimate of A_{FB} near the Z-pole at the 1σ–2σ level. The inclusion of EW corrections provides a better overall description of the data in the G_μ scheme. The $\sin^2\theta_{\text{eff}}$ scheme provides a good description of the data with and without EW corrections, with a level of agreement with the data similar to that achieved with the NLO QCD+EW_{virt} G_μ scheme. The reduced dependency on EW corrections makes the $\sin^2\theta_{\text{eff}}$ scheme preferable to the G_μ scheme for Drell-Yan production.

3.2.2 Polarization of τ-leptons

Similarly to the forward-backward asymmetry, the polarization of τ-leptons in $Z/\gamma^* \to \tau\tau$ decays is sensitive to the value of $\sin^2\theta_{\text{eff}}$ since the Z boson couples differently to left-handed and right-handed τ-leptons due to the chiral coupling asymmetry. The expected

JHEP08(2022)089

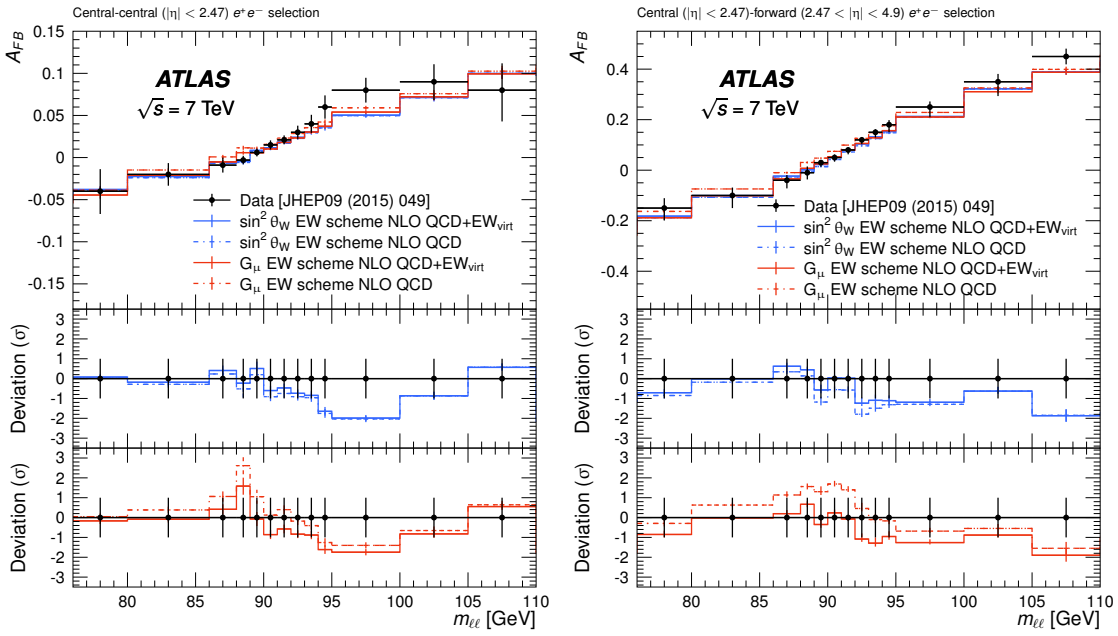

(a) (b)

Figure 2. The forward-backward asymmetry A_{FB} for the G_μ and $\sin^2\theta_{\mathrm{eff}}$ electroweak input schemes in the (a) central-central and (b) central-forward electron selections. MC simulation $pp \to e^{\pm}e^{\mp}$ predictions were obtained using the SHERPA 2.2.11 configuration at a centre-of-mass energy of $\sqrt{s} = 7\,\mathrm{TeV}$. Uncertainties in the predictions are statistical only. Data points are taken from ref. [57].

τ polarization for on-shell Z bosons is approximately -0.145 as obtained from precision measurements of the effective weak mixing angle at LEP [58], and more recently it was measured by ATLAS in proton-proton collisions at $\sqrt{s} = 8\,\mathrm{TeV}$ in $Z \to \tau\tau$ events and found to be $-0.14 \pm 0.02\,(\mathrm{stat}) \pm 0.04\,(\mathrm{syst})$ [59].

The polarization (P) of τ-leptons is extracted from a fit to the visible momentum fraction, $x_\pi = |\vec{p}(\pi)|/|\vec{p}(\tau)|$ in $\tau \to \pi\nu$ decay, using the following semi-analytic formula [60]:

$$\frac{1}{N}\frac{\mathrm{d}N}{\mathrm{d}x_\pi} = 1 + P(2x_\pi - 1). \tag{3.2}$$

Simulated events with two opposite-sign final-state τ-leptons with an invariant mass of $66 < m_{\tau\tau} < 116\,\mathrm{GeV}$ are selected. The distribution of x_π normalized to unity and corresponding fit results of eq. (3.2) for the G_μ and $\sin^2\theta_{\mathrm{eff}}$ schemes are shown in figure 3. The outlier point at low x_π arises from the finite pion mass and is excluded from the fit. The polarization of τ-leptons in the G_μ scheme is found to be $(-20.2 \pm 0.9)\%$ at NLO in QCD and $(-17.6 \pm 0.9)\%$ when including additive NLO $\mathrm{EW_{virt}}$ corrections. In the $\sin^2\theta_{\mathrm{eff}}$ scheme, a τ polarization value of $(-14.4 \pm 0.9)\%$ is extracted and is insensitive to EW virtual corrections. Given this value's better agreement with the SM prediction and the measured values from both LEP and ATLAS, and the reduced dependency on EW corrections, the $\sin^2\theta_{\mathrm{eff}}$ scheme is preferred.

JHEP08(2022)089

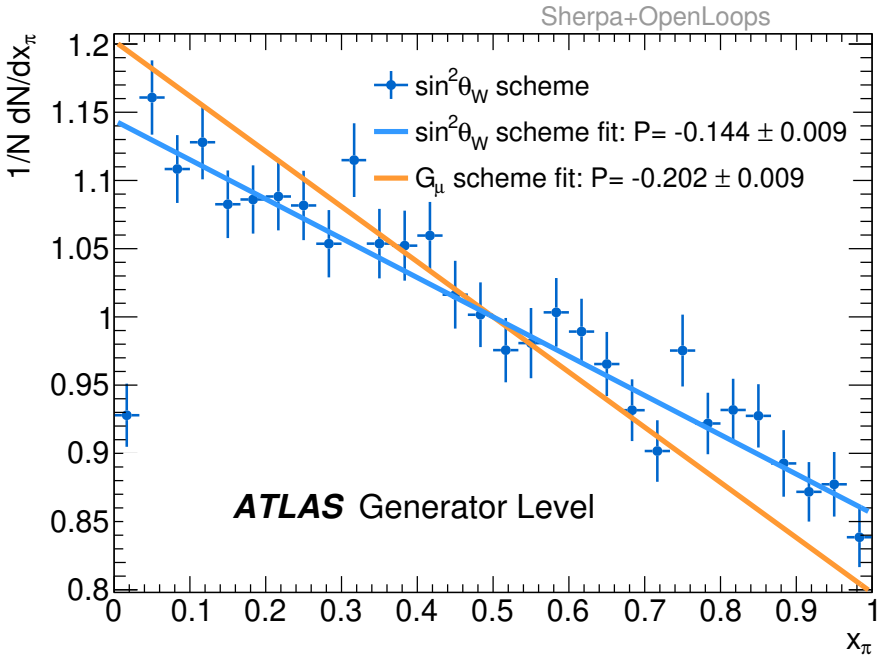

Figure 3. Comparison of the τ-lepton visible momentum fraction x_π for the G_μ and $\sin^2\theta_{\text{eff}}$ EW input schemes. Only data points in the $\sin^2\theta_{\text{eff}}$ scheme are shown. The fitted values are shown along with the extracted polarization of the τ-leptons. The distribution is normalized to unity. Uncertainties are statistical only.

3.3 Modified Catani-Seymour splitting kernels

The splitting kernels in the Catani-Seymour [61] based parton shower of SHERPA are known to exhibit non-singular corrections which can alter the radiation pattern significantly in the regions of phase space where the matrix element is not logarithmically enhanced. While a large part of these regions is covered by the hard matrix elements in an NLO-matched and multi-jet merged set-up, some part of it will always be populated by the parton shower. In addition, the radiation pattern of the shower also affects the Sudakov suppression in the hard region dominated by matrix elements.

In the SHERPA 2.2.11 configuration, the parton-shower splitting kernels are modified to better reflect the known soft limits of the hard matrix elements. The kinematic parameterization of an emission in the collinear kinematic region is modified to match the partial-fractioned soft eikonal part to the collinear limit. The modified splitting kernels can be found in appendix A. These changes are made consistently in both the parton shower and the NLO fixed-order and NLO matched calculations, and mainly affect the physics in the parton shower, thus being relevant for p_{T}^{V} around and below the merging scale (20 GeV). No significant effect was observed in the fraction of negative event weights due to these modifications.

The SHERPA 2.2.11 set-up contains the modified splitting kernels described above, while the 2.2.1 configuration does not and can be used to assess the modelling changes.

JHEP08(2022)089

Predictions from these set-ups are compared with a measurement of the transverse momentum $p_{\mathrm{T}}^{\ell\ell}$ of Drell-Yan lepton pairs in the mass range 66–116 GeV [19]. The measurement used 36.1 fb^{-1} of 13 TeV proton-proton collision data collected by the ATLAS experiment. The predictions from the Sherpa 2.2.11 and 2.2.1 configurations, along with the MadGraph5_aMC@NLO+Pythia FxFx configuration, are shown in figure 4 as a function of the unit normalized measured $p_{\mathrm{T}}^{\ell\ell}$ and ϕ_{η}^{*} [19] variables. The latter variable is constructed from only the angular separation of the leptons, which reduces the impact of the lepton momentum resolution at low-$p_{\mathrm{T}}^{\ell\ell}$ and depends only on the well-measured directions of the leptons. The red uncertainty band is shown on the NLO QCD prediction for the Sherpa 2.2.11 setup and includes scale and merging scale variations, where the merging scale was varied to 15 GeV and 30 GeV. The scale and merging scale uncertainties are added in quadrature. Additionally, the figure shows in blue the effect of adding the additive NLO EW$_{\mathrm{virt}}$ prediction. The blue uncertainty band is calculated from the envelope of multiplicative and exponentiated NLO EW$_{\mathrm{virt}}$ schemes.

The new splitting kernels used in the Sherpa 2.2.11 configuration significantly improve the description of the data below and around the merging scale ($p_{\mathrm{T}}^{\ell\ell} \sim 20$ GeV). The artificial discontinuity close to the merging scale is reduced, representing a closer match of cross-sections predicted by the matrix element and parton shower at the merging scale. As a result of these changes, the uncertainty due to variations of the merging scale is reduced by a factor of two compared to the Sherpa 2.2.1 set-up and contributes less than 5% around the merging scale. For intermediate-$p_{\mathrm{T}}^{\ell\ell}$ and large ϕ_{η}^{*} values, the predicted cross sections of the Sherpa 2.2.11 configuration is reduced by approximately 10% compared to the Sherpa 2.2.1 prediction. This is primarily a consequence of the scale changes for unordered histories discussed in the next section that reduce the cross sections for events with many jets. While the central value disagrees with the measured data points in the intermediate-$p_{\mathrm{T}}^{\ell\ell}$ and large ϕ_{η}^{*} regions, the predictions are in agreement within the scale uncertainties shown in red and the significant over-prediction observed in the Sherpa 2.2.1 for the highest $p_{\mathrm{T}}^{\ell\ell}$ values measured is reduced. The NLO EW$_{\mathrm{virt}}$ prediction reduces the cross-section further in the high $p_{\mathrm{T}}^{\ell\ell}$ and ϕ_{η}^{*} regions, as expected from figure 1. The uncertainties from different NLO EW$_{\mathrm{virt}}$ schemes is small for the majority of the phase-space, indicating good agreement between the three NLO EW$_{\mathrm{virt}}$ predictions.

The MadGraph5_aMC@NLO+Pythia FxFx prediction uses a different subtraction technique based upon the FKS method [62–64] and exhibits fundamentally different modelling behaviour than the Sherpa predictions in the low $p_{\mathrm{T}}^{\ell\ell}$ phase-space. Below the merging scale of 20 GeV, the MadGraph5_aMC@NLO+Pythia prediction models the data well, but around the merging scale it disagrees with the data in the opposite direction relative to the Sherpa configurations. For the intermediate and high-$p_{\mathrm{T}}^{\ell\ell}$ regions, the MadGraph5_aMC@NLO+Pythia prediction agrees very well with the Sherpa 2.2.11 NLO QCD prediction.

3.4 Scale-setting scheme for unordered histories

The MEPS@NLO algorithm used by the Sherpa event generator matches fixed-order perturbative calculations to parton showers by probabilistically identifying parton-shower to-

JHEP08(2022)089

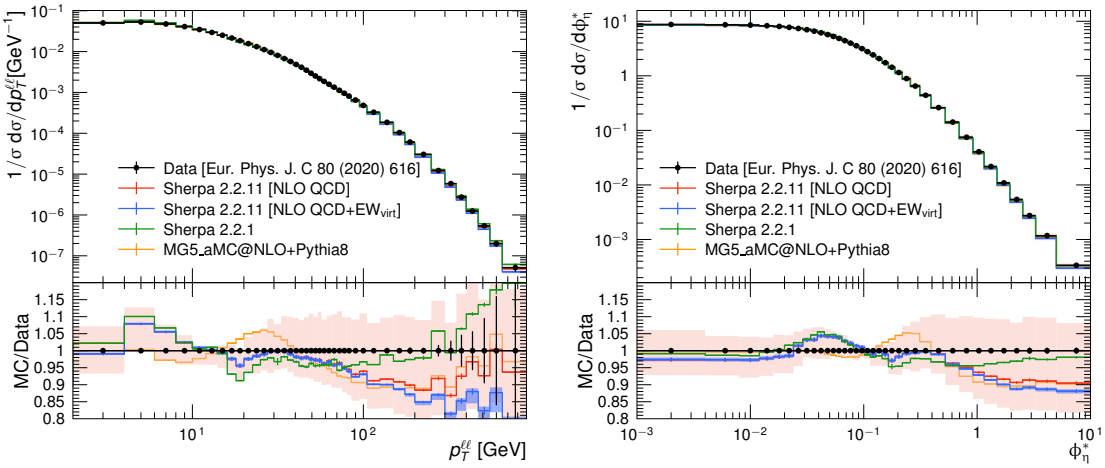

(a) (b)

Figure 4. Unit normalized cross-sections as a function of (a) the transverse momentum of the dilepton system and (b) ϕ^*_η. Predictions from the Sherpa and MadGraph5_aMC@NLO+Pythia are compared with data points taken from the ATLAS measurement [65]. The red uncertainty band corresponds to scale and merging scale variations in the 2.2.11 NLO+QCD Sherpa set-up. The blue uncertainty band is the envelope of multiplicative and exponentiated NLO $\mathrm{EW}_{\mathrm{virt}}$ schemes around the additive NLO $\mathrm{EW}_{\mathrm{virt}}$ prediction.

pologies through a k_{T}-type clustering algorithm [35]. In this approach, the first or hardest scale at which the parton shower starts needs to be identified. This is done by running the shower and clustering backwards to a core process that cannot be further decomposed. The strong coupling associated with each QCD branching in the parton-shower tree is then evaluated at the nodal k_{T} of the branching, and each propagator in the tree is dressed by a corresponding Sudakov factor. Such a process typically leads to a sequence of m nodal values whose k_{T} scales increase with each additional clustering step:

$$Q^{(m)} \leq Q^{(m-1)} \leq \cdots \leq Q^{(2)} \leq Q^{(1)} \leq Q^{(\mathrm{core})} = Q^2, \tag{3.3}$$

which leads to small Sudakov factors counteracting large values of the running strong coupling. However, in extreme regions of phase space, this scale hierarchy in eq. (3.3) may be violated. A prime example would be jets of similar transverse momentum that are widely separated in rapidity but not separated in the k_{T} scale used in the clustering. Such configurations would also be accompanied by Sudakov-type suppression factors, but these specific contributions are not taken into account in standard parton showers because they correspond to an evolution in rapidity. Due to the absence of the suppression factor, potentially large enhancements from evaluating the strong coupling at small transverse momenta can then not be compensated for, and the differential cross-section, together with its perturbative uncertainty, becomes uncontrollably large. The strong coupling associated with the production of jets in this 'unordered' region of phase space must therefore not be evaluated at the nodal k_{T} scales of the jet clustering. Instead it should be computed at a global hardness scale associated with the event.

JHEP08(2022)089

The Sherpa 2.2.11 configuration uses a new algorithm to handle these cases, where unordered histories are no longer used in the scale-setting algorithm. If the k_{T} scale decreases during the clustering, the largest previously identified scale will be used. In comparison to previous predictions from the Sherpa generator, this typically leads to reduced cross-sections and smaller uncertainties in regions of the phase space that contain multiple jets of similar hardness. In the reverse clustering procedure, nodes containing EW particles are only included if they involve a strongly interacting particle (e.g. u-quark clustered with W, but not e clustered with ν). The virtuality of the EW propagators is accounted for during the clustering.

The Sherpa 2.2.11 configuration includes the changes described above, while the Sherpa 2.2.1 configuration allowed for unordered histories. Comparisons of the Sherpa 2.2.11 and 2.2.1 predictions, along with the MadGraph5_aMC@NLO+Pythia FxFx prediction are shown in figures 5 and 6 for $Z+$jets and $W+$jets measurements, respectively. The NLO $\mathrm{EW}_{\mathrm{virt}}$ predictions are shown by the blue curves with an uncertainty band that includes the envelope of multiplicative and exponentiated NLO $\mathrm{EW}_{\mathrm{virt}}$ schemes around the additive prediction.

The $W+$jets data is based upon a CMS measurement of the differential cross-sections for the associated production of a W boson and jets in $2.2\,\mathrm{fb}^{-1}$ of proton-proton collisions at $\sqrt{s} = 13\,\mathrm{TeV}$ [66]. The predicted cross-section for events with at least three jets is significantly reduced and are in agreement with the data. In the old scheme, the predicted cross-section overestimated the data by up to 50% for jets produced with momentum greater than 300 GeV. In the new scheme, the rates are considerably reduced and in better agreement with the data. This improved agreement with the data for highly energetic jets is at the expense of a higher predicted cross section for events with low jet transverse momentum, and is observed to overshoot the data by as much as 15% as shown in figure 5(b). The NLO $\mathrm{EW}_{\mathrm{virt}}$ corrections reduce the QCD-only prediction by ∼10% for large jet momentum and improve agreement with data.

For the $Z+$jets comparisons, the data is based upon an ATLAS measurement of the production cross-section of a Z boson in association with jets in $3.16\,\mathrm{fb}^{-1}$ of pp collisions at $\sqrt{s} = 13\,\mathrm{TeV}$ [67]. The predicted cross-sections for each jet emission are in better agreement with the data when using the Sherpa 2.2.11 configuration. The cross-sections for large jet momenta are reduced by approximately 10% in the Sherpa 2.2.11 configuration when compared to the Sherpa 2.2.1 prediction. This introduces a small disagreement of the central values with the measured data points. However, the agreement is within the perturbative scale uncertainties. Similarly to the $W+$jets results, the NLO $\mathrm{EW}_{\mathrm{virt}}$ corrections reduce the QCD-only prediction by ∼5%–10% for large jet momenta.

4 Computational improvements

An accurate description of SM processes in proton-proton collisions, as discussed in the previous section, is paramount to the success of the ATLAS physics programme. At the same time, the generated effective luminosity of a MC sample should ideally exceed that of the data across the wide range of phase spaces explored by measurements and searches.

JHEP08(2022)089

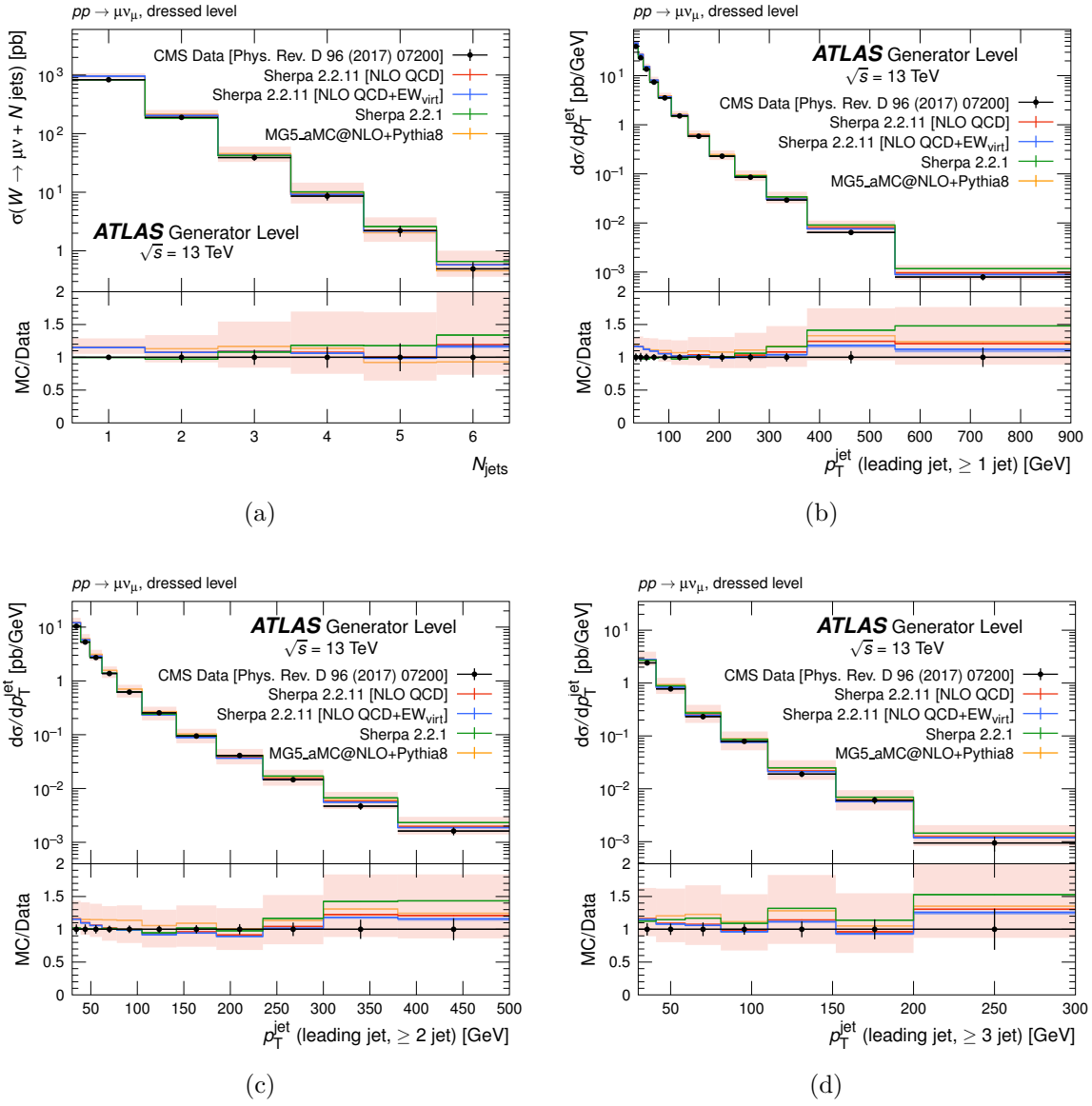

Figure 5. Comparisons between generator-level $W \to \mu\nu$ predictions and measured data points. The red uncertainty band includes the envelope of the 7-point scale variations around the SHERPA 2.2.11 NLO QCD prediction. The blue uncertainty band is the envelope of multiplicative and exponentiated NLO $\mathrm{EW}_{\mathrm{virt}}$ schemes around the additive NLO $\mathrm{EW}_{\mathrm{virt}}$ prediction. Data points are taken from CMS measurements at $\sqrt{s} = 13\,\mathrm{TeV}$ [66].

Looking towards the HL-LHC era [10], this is only possible if a reduction of the per-event generation time is achieved and smart sampling techniques are used that do not adversely impact the statistical performance of the generated events. The following section addresses these issues using $V+$jets processes as a case study. The per-event CPU time for various generator configurations is presented in section 4.1, while section 4.2 explores the statistical consequences of various sampling techniques to populate the low cross-section regions of phase space.

JHEP08(2022)089

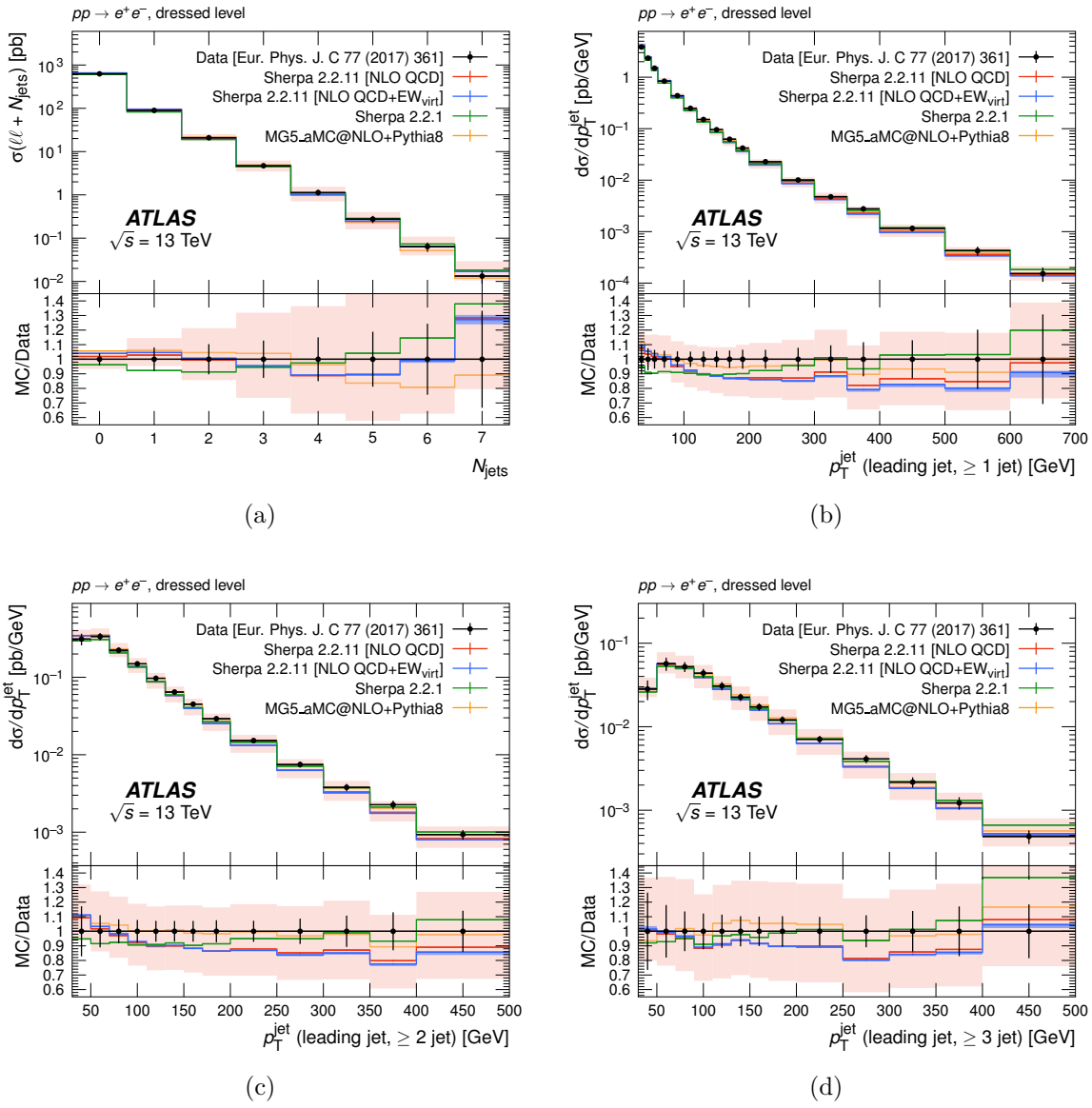

Figure 6. Comparisons between generator-level $Z \to ee$ predictions and measured data points. The red uncertainty band includes the envelope of the 7-point scale variations around the SHERPA 2.2.11 NLO QCD prediction. The blue uncertainty band is the envelope of multiplicative and exponentiated NLO $\mathrm{EW}_{\mathrm{virt}}$ schemes around the additive NLO $\mathrm{EW}_{\mathrm{virt}}$ prediction. Data points are taken from ATLAS measurements at $\sqrt{s} = 13\,\mathrm{TeV}$ [67].

4.1 Speed characterization

The time it takes to generate a single event, or the per-event CPU cost, is highly dependent on the configuration of the MC generator: for example, the perturbative accuracy of the cross-section in both the strong and electroweak couplings, the number of extra partons at matrix-element level, the matrix-element to parton-shower matching algorithm, and the scale-setting algorithm. Moreover, additional scale and PDF predictions used to evaluate sources of theoretical uncertainty are routinely stored in the nominal sample as alternative

JHEP08(2022)089

generator weights. Depending on the number of additional predictions and the methodology with which one evaluates the variation weight, significant CPU cost can be incurred. This section quantifies the per-event CPU cost of configurations with varying *perturbative accuracy* and Sherpa-specific scale-setting and clustering algorithms, collectively referred to as *additional features*. The $pp \to e^{\pm}e^{\mp}$ + jets process is used as a representative process, and events are generated using Sherpa 2.2.11. Additionally, a comparison between the MadGraph5_aMC@NLO+Pythia FxFx merged set-up and Sherpa is included, where a dedicated Sherpa configuration ensures that the same perturbative accuracy and a similar scale-setting algorithm is used in the two event generators.

Benchmarking of the MC configurations takes place on a dedicated machine that has no additional computing load. The machine utilizes an Intel(R) Xeon(R) E5-2667 v2 CPU with a base 3.30 GHz clock speed and a 4.0 GHz boost capability under single-core operation, which has 2 sockets with 8 cores each (16 physical CPU cores). A Western Digital Black 7200 rpm 2 TB hard-drive (HDD) is used as non-volatile memory, whilst 4× 8192 MB Samsung DDR3 with 1600 million transfers per second (MT/s) (Model: M393B1G70QH0) is used for dynamic volatile memory. The corresponding machine is benchmarked using the HEP-SPEC2006 (HS06) standard [68], a real application-level suite of seven C++ [69] benchmarks derived from the SPEC CPU2006 standard, that tests integer and floating-point operational performance of the host machine. The HS06 score is obtained with hyper-threading disabled, and all physical processor cores configured as independent single-core nodes with HEP-SPEC2006 compiled with gcc in 32-bit mode. The corresponding HS06 score for each CPU second was found to be 20.97 HS06 seconds. It should be noted that platform dependencies, single-core versus multi-core mode operation, and configuration variations of the CPU can yield a variance of the HS06 score of approximately 20%.

Event generation times in seconds are monitored event-by-event, where care is taken to exclude any initialization steps associated with the software application. Two key classes of metrics are obtained: the mean CPU time per event and associated standard deviation as extracted from the sampled events, and the median per-event time in addition to the ±25% quantiles. All CPU times are then converted to the HS06 standard using the score 1 second = 20.97 HS06 seconds.

4.1.1 Perturbative accuracy

The *perturbative accuracy* class of set-ups quantifies the effect of increasing perturbative accuracy in the strong coupling constant. Within this class of set-ups, three distinct classes exist: pure LO, pure NLO, and mixed NLO+LO. Set-ups with an increasing number of extra partons produced at matrix-element level, ranging from zero to five extra partons, are studied.

The event generation HS06 cost per event for the *perturbative accuracy* set-ups are shown in figure 7. The LO set-ups are considerably faster than the NLO set-ups, partly because of the smaller number of diagrams that need to be sampled, but also due to the higher complexity of the multi-jet merging algorithms when applied to NLO vs. LO events. In the class of NLO set-ups, the results are categorized as a function of the number of NLO emissions and compared between pure NLO set-ups and one with up to five additional jets

JHEP08(2022)089

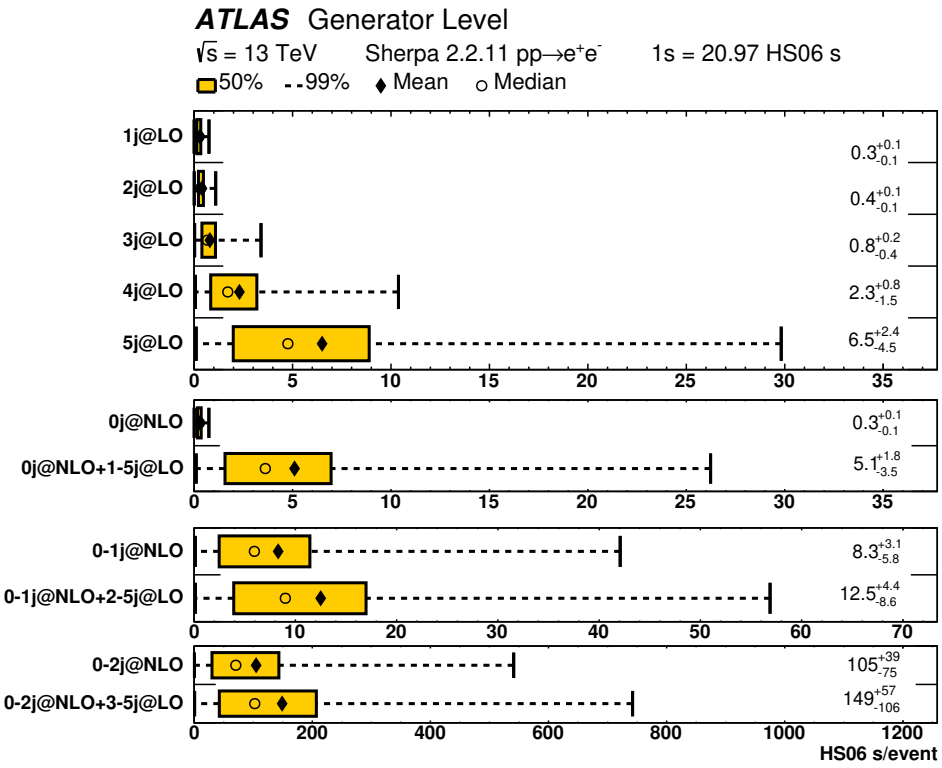

Figure 7. The time in HS06 seconds per event for various configurations that vary the QCD accuracy of the sample and number of extra partons. The markers show the mean and median values, and the box shows the ±25% quantiles. The whiskers show the 99% containment bounds, while the numbers on the right show the mean and standard deviation of the sample. Each canvas has a different x-axis range. One second equals 20.97 HS06 seconds on the specific machine used.

at LO accuracy. For the 0j@NLO set-up, the pure NLO set-up is extremely fast and on a similar scale to LO set-ups with a similar number of final-state partons. When adding in the 5j@LO legs to the 0j@NLO set-up, the execution time increases and is roughly of the same order of magnitude as the pure 5j@LO set-up. The fact that the 0j@NLO+1–5j@LO set-up is faster than the pure 5j@LO set-up is attributed to the ∼15% increase in the cross section for the $2 \to 2$ process when going from LO to NLO. As such, in the NLO set-up the $2 \to 2$ process is sampled more often and is faster than processes with more final-state partons, leading to an overall decrease in the average time per event. When adding more NLO diagrams to the calculation, there is approximately a tenfold increase in the event generation time for each additional NLO contribution. The difference with and without the LO legs is relatively small compared to the increase when moving from 1j@NLO to 2j@NLO.

While the configurations with up to one extra parton at LO or NLO in the strong coupling are shown to be much faster, the cross-sections for these configurations are known to miss important contributions and severely underestimate the total cross-section [70–72]. In order to meet the requirements of the ATLAS physics programme, which demands

JHEP08(2022)089

accurate predictions for phase spaces selecting multiple jets and is thus sensitive to these higher-order QCD contributions, it is mandatory for the matrix elements to include the highest perturbative accuracy that available theoretical tools and computational resources allow. Therefore, the QCD accuracy for the Sherpa 2.2.11 configuration is chosen to be 0–2@NLO+3,4,5j@LO. Most of the CPU cost originates from the 2j@NLO contribution, but can be reduced with various well-motivated approximations as described in the next section.

4.1.2 Additional features

The *features* class of set-ups quantifies the effect of various approximations or additional predictions included in the Sherpa 2.2.11 configuration relative to a reference configuration. The reference configuration uses a configuration similar to the Sherpa 2.2.11 configuration in table 1, but removes the H_{T}' scale for $\mathbb{H}$-events shown in eq. (2.1), the NLO $\mathrm{EW}_{\mathrm{virt}}$ corrections shown in section 3.1, the scale and PDF variations, and uses the $2 \to 4$ core process for the evaluation of the differential K-factor for LO matrix elements as done for the Sherpa 2.2.1 set-up. Each feature is evaluated independently by adding them one-by-one above the reference set-up, so that the CPU cost of each additional feature can be quantified.

In order to reduce the CPU budget of the costly 2j@NLO contribution, an H_{T}' scale choice is used for $\mathbb{H}$-events. The default merging scale requires independent calculations for the real-emission correction and all associated dipole subtraction terms in the $\mathbb{H}$-events. The number of dipole terms grows as n^3 with the number of external partons (n), and for each of those dipole terms the clustering algorithm requires a runtime proportional to $(n-1)^2$. Therefore, the expected speed-up when using the H_{T}' scale is particularly large for $\mathbb{H}$-events at large multiplicities. As shown in figure 8, a factor of three reduction in the per-event generation time is achieved when using an H_{T}' scale for $\mathbb{H}$-events. The clustering scheme that uses a simplified $2 \to 2$ core process to evaluate the differential K-factor was found to have consistent per-event CPU times compared to the setup using the $2 \to 4$ core process.

The additional predictions include NLO $\mathrm{EW}_{\mathrm{virt}}$ corrections in three schemes, as described in section 3.1, and over 300 additional predictions for scale and PDF uncertainties. As shown at the bottom of figure 8, the NLO $\mathrm{EW}_{\mathrm{virt}}$ corrections, and scale and PDF uncertainties, each independently increase the event generation time by up to 40%. Although the additional scale and PDF predictions increase the event generation time, they are produced at a significantly smaller CPU cost than generating over 300 different predictions individually, and improve the accuracy of the prediction.

The results in figure 8 clearly show it is possible to reduce the per-event CPU time by up to a factor of three, provided that the features do not negatively impact the physic modelling performance. In order to illustrate the effect on the modelling, the reference setup is first modified by switching to the H_{T}' scale for $\mathbb{H}$-events (blue), and again by using the inclusive + exclusive clustering scheme (green). Additionally, the Sherpa 2.2.11 set-up with all additional features added simultaneously is included for comparison. As can be seen in figure 9, the cross-sections are largely unchanged across a wide range of H_{T} and p_{T}^{V}

JHEP08(2022)089

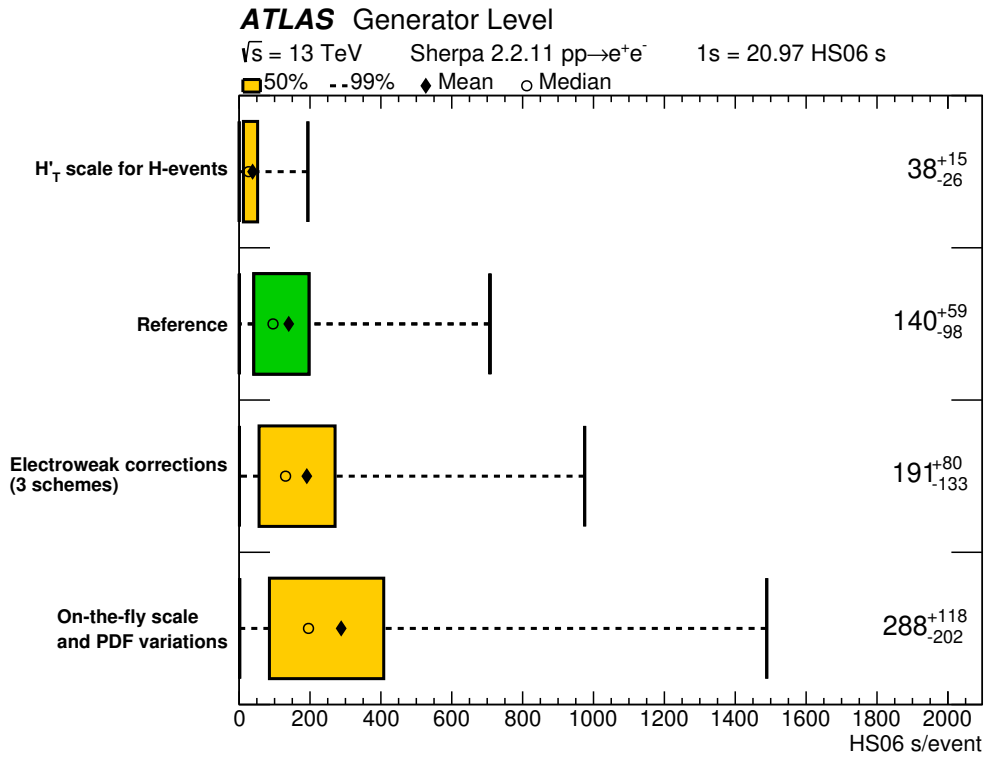

Figure 8. The time in HS06 seconds per event for various features that affect the event generation time. The markers show the mean and median values, and the box shows the ±25% quantiles. The whiskers show the 99% containment bounds, while the numbers on the right show the mean and standard deviation of the sample. All set-ups are accurate to 0–2j@NLO+3,4,5j@LO in the QCD coupling. One second equals 20.97 HS06 seconds on the specific machine used.

phase spaces. The largest differences observed are with the modified H_{T}' scale for $\mathbb{H}$-events for intermediate H_{T} and p_{T}^{V} values, but amount to less than 5% and are well within the uncertainty band formed from variations of the renormalization and factorization scales. Given these small differences and the significant reduction in the per-event CPU time, both the H_{T}' scale and the modified clustering scheme are adopted as the default in the 2.2.11 $V+$jets sample.

4.1.3 Generator comparisons

This section presents a comparison of the CPU time for the Sherpa and MadGraph5_aMC@NLO+Pythia configurations when the major differences between generator-specific approaches are factored out. In particular, the two generators have different approaches to setting the renormalization scale and in this paper it is set at different perturbative accuracies. The NLO multi-jet merging approach in Sherpa is constructed so as to account for the resummation of soft-collinear higher-order corrections originating in the phase space available to gluon decays. This is achieved by a suitable setting of the renormalization scale, which should correspond to the nodal transverse momentum in a

JHEP08(2022)089

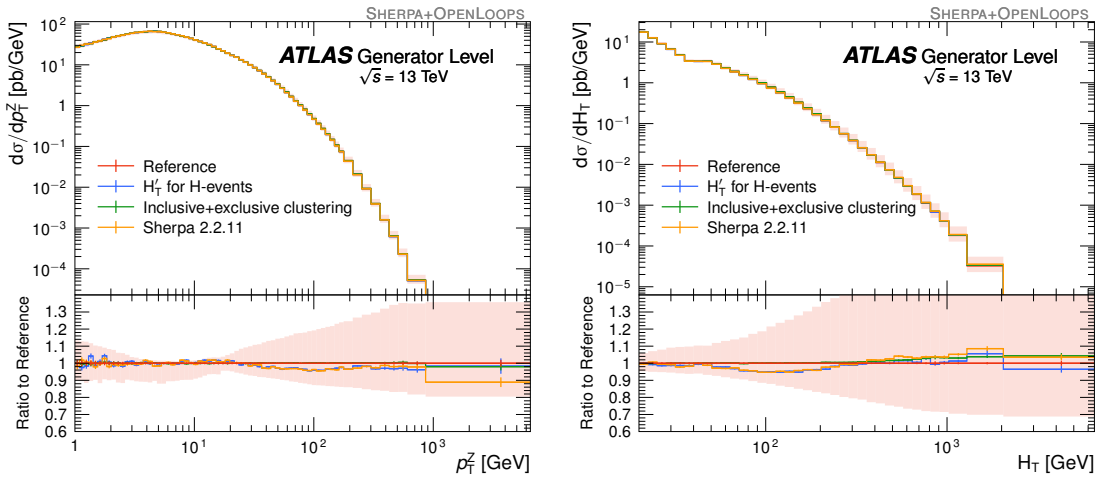

(a) (b)

Figure 9. Differential distributions of (a) the dilepton transverse momentum and (b) scalar sum of the jet momenta for $Z \to ee$ generator-level events. The H'_T scale and the inclusive + exclusive clustering scheme are added to the reference set-up. The SHERPA 2.2.11 configuration contains all changes simultaneously. The uncertainty band includes the envelope of the 7-point scale variations of the reference prediction.

parton-shower branching tree for each gluon emission [73, 74]. In order to identify this scale, the event needs to be clustered using a sequential recombination algorithm, whose computational complexity grows as n^2 as the number of external partons, n, increases. On the other hand, the MADGRAPH5_aMC@NLO+PYTHIA configuration discussed in the paper uses an event-level scale choice which requires significantly less CPU resources than the recombination algorithm used in SHERPA.

For a comparison of the CPU budget between the SHERPA and MADGRAPH5_aMC@NLO+PYTHIA event generators, the recombination algorithm of SHERPA was disabled and replaced with an event-level renormalization scale choice defined by the scalar sum of all out-going partons. This event-level scale choice is applied to all aspects of the calculation and not just the $\mathbb{H}$-events discussed in the previous section. In both the SHERPA and MADGRAPH5_aMC@NLO+PYTHIA set-ups, the perturbative accuracy of the matrix-element calculation is specified as 0–2j@NLO in QCD coupling.

An average time per event calculated from 1000 events is extracted for both the SHERPA and MADGRAPH5_aMC@NLO+PYTHIA set-ups. In this procedure, the matrix-element and parton-shower matching efficiency is taken into account in the MADGRAPH5_aMC@NLO+PYTHIA set-up and amounts to 38%. The average event times for the SHERPA and MADGRAPH5_aMC@NLO+PYTHIA configurations were 19.4 and 26.4 HS06 seconds, respectively. Therefore, the SHERPA configuration is approximately 30% faster than the MADGRAPH5_aMC@NLO+PYTHIA set-up. It is worth noting that the default scale-setting procedure used in SHERPA results in over a factor of five increase in the CPU cost when compared with the same 0–2j@NLO set-up shown in figure 7. While this implies that the scale-setting procedure is a significant component of the total CPU

JHEP08(2022)089

budget in the majority of the SHERPA configurations used by ATLAS, it is important to ensure an accurate description of vector bosons produced with many jets. In particular, when using an event-level H_{T}' scale the SHERPA prediction under-estimates the data by up to 30% for phase-spaces with multiple jet emissions in $W+$jets and $Z+$jets selections.

4.2 Statistical enhancement methods

The probability of sampling an event with a specific phase-space configuration is dictated by the differential partonic cross-section. This poses a problem from a sampling coverage perspective as regions of phase space with small production cross-sections, for example $V+$jets processes in which the transverse momentum of the vector boson is large, are rarely sampled. Therefore, although the speed with which events can be generated is a key ingredient in generating large MC samples quickly, it is not the whole picture.

The question of *phase-space sample coverage* is a problematic one from a logistical perspective, because regions of interest to BSM searches often have small production cross-sections, whilst regions studied by SM precision measurements often have high production cross-sections. In order to address the statistical needs for the broad ATLAS physics programme, smart phase-space sampling/biasing methods are required. Section 4.2.1 details the deployment of enhancement strategies that either divide up the integration problem into multiple regions or bias the integrand to artificially increase the sample rate of specific phase-space points.

The weighted mode of operation of event generators can introduce statistical features that alter the statistical power of each sampled event. The precision of the MC estimated integral is dependent on an array of factors ranging from the number of sampled points, to the variance of the event weights. Since biasing techniques alter the phase-space sample rate, additional sources of variance are introduced, which can degrade the statistical precision of a sample. The statistical features of the event weight distribution are studied in section 4.2.2 for an array of enhancement techniques.

4.2.1 Sample biasing and statistical precision

Monte Carlo integration numerically approximates a definite integral by randomly sampling a set of N_{gen} points within the integral domain according to a probability density function. For scattering experiments this integral represents the cross-section, whereby each sampled point represents an event with a generation probability defined by the differential partonic cross-section. MC event generators operating in a weighted mode therefore assign each event a weight (w) based on the generation probability, such that the cross section is approximated by the average of the weights $\langle w \rangle$,[1] [75]. With this in mind, the relative statistical uncertainty of a MC sample across the entire generated phase space[2] is given by:

$$\frac{\hat{\sigma}_{\hat{N}}}{\hat{N}} = \frac{\sqrt{\sum_i w_i^2}}{\sum_i w_i} = \frac{1}{\sqrt{N_{\mathrm{gen}}}} \sqrt{1 + \frac{s_w^2}{\langle w \rangle^2}}, \tag{4.1}$$

[1] The MC estimator of the cross-section integral is equivalent to the product of the event weight mean and integral volume.

[2] In order for this to be used for a subset of the phase space it should be corrected by the ratio of the event weight sum entering the sub-space over the total number of events.

JHEP08(2022)089

where $\hat{\sigma}_{\hat{N}}$ is the sample error, $\hat{N}$ is the expected event yield given N_{gen} sampled phase space points, and s_w^2 is the event weight variance. The last square-root factor of eq. (4.1) is referred to as the *statistical dilution factor*, which originates from the presence of non-unit event weights. Consequently, samples containing a large variance of event weights will have a significantly reduced statistical precision.

This statistical picture is complicated by the introduction of negative event weights, as a result of the MC@NLO method [76]. The presence of negative weights not only increases the event weight variance, but also introduces an additional source of statistical suppression, thereby further reducing the statistical precision of a generated MC sample. The above relative statistical uncertainty formalism of eq. (4.1) can be reparameterized in terms of the negative-weight fraction f_{nw} as given by:

$$\frac{\hat{\sigma}_{\hat{N}}}{\hat{N}} = \frac{1}{\sqrt{N_{\text{gen}}} \cdot (1 - 2f_{\text{nw}})},$$

where a constant non-zero event weight of $w = \pm c$ is assumed, and f_{nw} is the negative-weight fraction defined as $f_{\text{nw}} = \sum_i^{N_{\text{gen}}^-} |w_i| / \sum_i^{N_{\text{gen}}} |w_i|$, for N_{gen} total and N_{gen}^- negative-weight events. The asymptotic limit of $f_{\text{nw}} = 0.5$ can be seen to induce an infinitely large error. The statistical precision of the generated MC samples is studied below, using the four key parameters obtained above: $[N_{\text{gen}}, \langle w \rangle, s_w^2, f_{\text{nw}}]$. These are referred to as *numerical efficiency parameters*.

Given the strong reliance of the MC statistical precision on the number of sampled events, N_{gen}, the question of how to sufficiently populate remote phase-space regions for a precise prediction is crucial. For example, in the $V+$jets case study, high-H_{T} phase-space regions are mainly populated from topologies with high parton multiplicity. The resulting cross-section contribution to a more inclusive generator phase space is therefore small, due to the suppression caused by powers of α_{S}. Therefore, when generating a MC sample inclusive of H_{T}, the high H_{T} region will be sparsely populated. Establishing an enhancement strategy to address this must therefore meet two key criteria: it should exert control over the phase-space sampling in a versatile way, and induce minimal variance in the event weight.

To address this, three enhancement techniques are tested, which offer varying levels of control over how events are sampled from the generated phase space. These are divided into two categories, referred to as *discrete*, and *continuous* in the following. As per the name, all methods enhance the probability of sampling an event according to one or more kinematic observables, where the exact definition of each observable is limited to anything that can be constructed from the four-momenta of the matrix-element final-state particles.

In the discrete case, MC samples are *sliced* according to kinematic observables, $\mathcal{O}$, by constructing exclusive integration boundaries between which the MC generator would sample. This discrete technique is referred to as a *sliced enhancement* strategy. An illustration of the sliced enhancement strategy for $pp \to e^+e^- +$jets is given in figure 10, in which the distribution of unweighted events and the resulting differential cross-section is shown as a function of $\log_{10}(\max(H_{\text{T}}, p_{\text{T}}^V))$. Six phase-space slices are generated with internal

JHEP08(2022)089

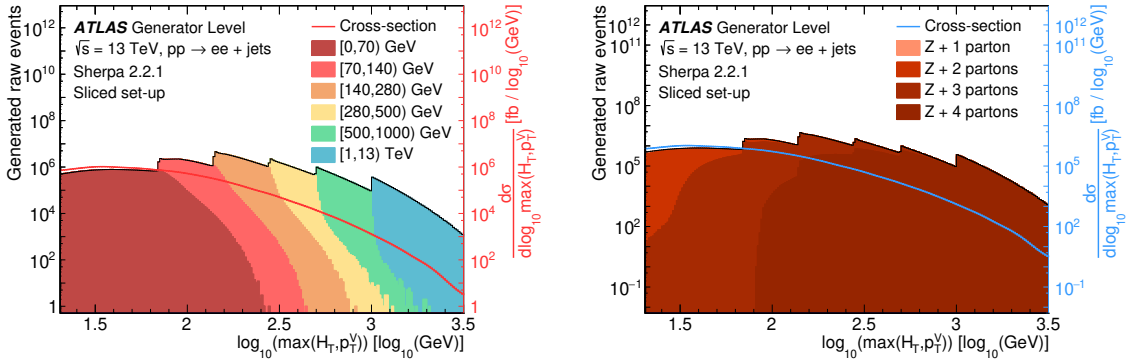

(a) Boundary Breakdown.

(b) Jet Multiplicity Breakdown.

Figure 10. Distribution of unweighted $pp \to e^+e^- +$jets MC sampled events and differential cross-section for the sliced enhancement as a function of the slicing observable, $\log_{10}(\max(H_{\mathrm{T}}, p_{\mathrm{T}}^V))$. Events are sliced according to the $\max(H_{\mathrm{T}}, p_{\mathrm{T}}^V)$ variable. The unweighted distribution is split either (a) according to the phase-space sampling slices, or (b) according to the final-state jet multiplicity. In (b) the Z+1 parton contribution is small and only visible in the top left of the distribution.

boundaries at $\max(H_{\mathrm{T}}, p_{\mathrm{T}}^V) = [70, 140, 280, 500, 1000]$ GeV, shown as coloured bands in figure 10(a), clearly illustrating the composite nature of the MC sample. The discontinuities in the unweighted event distribution at the integration boundaries are the result of generating each phase-space slice with a different effective luminosity. Figure 10(b) contains the same information, split according to the final-state parton multiplicity, demonstrating that events with high parton multiplicity mostly populate the large-$\max(H_{\mathrm{T}}, p_{\mathrm{T}}^V)$ phase-space region.

The phase-space slices shown in figure 10 are not perfectly aligned with the integration boundaries, due to a disparity in the p_{T}^V and H_{T} definitions used at the matrix-element integration stage versus those at the matrix-element final-state level (as shown in the figure). Specifically, for NLO processes the hard-scattering matrix element can contain an additional parton emission, which would be matched between the matrix element and parton shower via the colour-exact variant of the MC@NLO algorithm [33]. At the integration step this emission is not present, and so only the on-shell final-state partons are used to define H_{T} and p_{T}^V. This feature is unique to the slicing strategy, which, as shown in the following section, has significant consequences for the statistical precision of the sample at the internal boundaries.

In contrast, *continuous* enhancement techniques artificially scale the probability density function by a biasing function $e(\vec{\mathcal{O}})$, where $\vec{\mathcal{O}}$ is a set of observables. Following the transformation the resulting cross-section is non-physical, so each sampled event is corrected by the inverse of the biasing function, $w_{i,n}^{\mathrm{bias}} = e(\vec{\mathcal{O}})^{-1}$, as an event-weight multiplier after event generation.

Two instances of this type of technique are considered, referred to as the *differential enhancement* and *analytic enhancement* strategies:

- **Differential enhancement:** the biasing function is set to the inverse of the differential cross-section as a function of a single observable for each parton-multiplicity

JHEP08(2022)089

final state, $e_n(\mathcal{O}) = (\mathrm{d}\sigma_n/\mathrm{d}\mathcal{O})^{-1}$, where the subscript n denotes the number of final-state partons. This is applied within some kinematic bounds defined by the user, $\alpha < \mathcal{O} < \beta$.

- **Analytic enhancement:** the biasing function is an analytic formula parameterized according to a set of observables independent of the final-state multiplicity n, i.e. $e(\vec{\mathcal{O}})$.

Figure 11 illustrates the effect of the continuous enhancement techniques on the unweighted event sample rate versus that predicted by the differential cross-section, for both the differential (figure 11(a)), and analytic (figure 11(b)) strategies. The observable of choice is $\max(H_\mathrm{T}, p_\mathrm{T}^V)$ with the former using a log form, $\log_{10}(\max(H_\mathrm{T}, p_\mathrm{T}^V))$, and the latter using a squared form, $(\max(H_\mathrm{T}, p_\mathrm{T}^V)/20)^2$. The squared form was empirically selected to balance the production rate of the low and high $\max(H_\mathrm{T}, p_\mathrm{T}^V)$ regions.[3]

Unlike the discrete sliced enhancement strategy, the unweighted event sample rate varies smoothly as a function of the enhancement observable(s), which has profound consequences for the statistical precision of the sample (as explored in the following section). It should be noted that the differential enhancement scheme samples events more uniformly than the analytic scheme. This is most notable when comparing the individual parton-multiplicity subprocesses between the differential and analytic enhancement schemes. This feature is native to the differential enhancement scheme because the sampling probability density function is biased using the inverse of the differential cross-section. Therefore, the transformed probability density function from which events are sampled is approximately uniform as a function of the biasing observable. The sharp change in sample rate at $\log_{10}(\max(H_\mathrm{T}, p_\mathrm{T}^V)) \approx 3.3$ for the differential enhancement approach is a consequence of an upper bound on the differential enhancement strategy of $\max(H_\mathrm{T}, p_\mathrm{T}^V) \approx 2\,\mathrm{TeV}$, after which the sample rate is dictated by the cross section. Achieving this level of uniformity with the analytic scheme ultimately requires some fine tuning of the observables and analytic functional form, but with this comes versatility and flexibility in controlling the sample rate.

Each of the three techniques have their own set of strengths and weaknesses, in terms of phase-space sampling speed (generation time), phase-space sampling control, and statistical precision. Some of these features are already visible in figures 10 and 11, for example the smoother sampling coverage of the continuous enhancement strategies compared to the sliced enhancement strategies. The impact of these features on the performance of each sample is explored in the following subsection.

4.2.2 Quantitative assessment

Using the two Sherpa configurations outlined in section 2.1, an assessment of the statistical precision of the discrete and continuous enhancement strategies for $pp \to e^+e^- + \text{jets}$ and

[3] The available statistics from the 2.2.1 configuration, which were extended many times during the Run 2 period, serve as an indicator of the phase spaces probed by the ATLAS physics programme. Therefore, the functional form of the analytic enhancement was selected to mimic the phase-space coverage of the 2.2.1 sliced samples.

JHEP08(2022)089

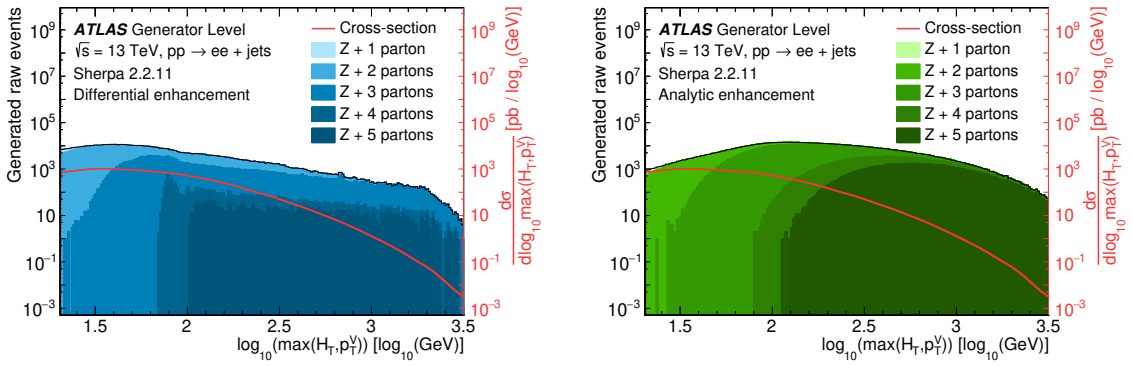

(a) (b)

Figure 11. Distribution of unweighted MC sampled events for the SHERPA configurations with (a) differential and (b) analytic enhancement as a function of $\log_{10}(\max(H_{\mathrm{T}}, p_{\mathrm{T}}^{V}))$. The differential enhancement is specified using $\log_{10}(\max(H_{\mathrm{T}}, p_{\mathrm{T}}^{V}))$ function, while the analytical enhancement uses the $(\max(H_{\mathrm{T}}, p_{\mathrm{T}}^{V})/20)^2$ function. In (b) the Z+1 parton contribution is small and only visible in the top left of the distribution.

$pp \to \mu^+\mu^- +$jets is performed. The $\max(H_{\mathrm{T}}, p_{\mathrm{T}}^{V})$ sliced 2.2.1 configuration serves as a reference sample, due to its status as the default configuration for modelling $V+$jets processes within the ATLAS physics programme, when evaluating the performance of the new continuous enhancement 2.2.11 configurations. The assessment frames the statistical precision of each sample within the context of the four MC numerical efficiency parameters previously defined, $[N_{\mathrm{gen}}, \langle w \rangle, s_w^2, f_{\mathrm{nw}}]$.

As demonstrated by figures 10 and 11, the differential distribution of sampled events is of key interest when assessing the statistical performance of the aforementioned enhancement strategies. With this in mind, and in order to provide a comparison that is sensitive to the distribution of events, not the absolute inclusive quantity, the inclusive phase space of each sample is limited to a total of 10 million unweighted events, $N_{\mathrm{gen}} = 10^7$.

Figure 12 shows the distribution of event weights as a function of $\max(H_{\mathrm{T}}, p_{\mathrm{T}}^{V})$, normalized to unit area, for the 2.2.1 (figure 12(a)), 2.2.11 differential enhancement (figure 12(b)), and 2.2.11 analytic enhancement (figure 12(c)) configurations. The mean weight and root-mean-square deviation as a function of $\max(H_{\mathrm{T}}, p_{\mathrm{T}}^{V})$ are given by the red markers.

As observed in figure 10, the discrete $\max(H_{\mathrm{T}}, p_{\mathrm{T}}^{V})$ slices of the 2.2.1 configuration are visible as differently coloured bands. Given that the assigned event weight is proportional to the amplitude of the matrix element and the infinitesimal phase-space element evaluated for the event kinematics, the mean weight and variance of each slice must differ. This is because each slice populates a unique and exclusive region of phase space. Therefore, when constructing the inclusive sample each phase-space slice contributes a single unique mode to the event weight distribution.

Similar observations can be made for the differential enhancement strategy, figure 12(b), where discrete bands that become increasingly distinguishable towards higher $\max(H_{\mathrm{T}}, p_{\mathrm{T}}^{V})$ values are observed. These bands arise as a result of the dependency of the

JHEP08(2022)089

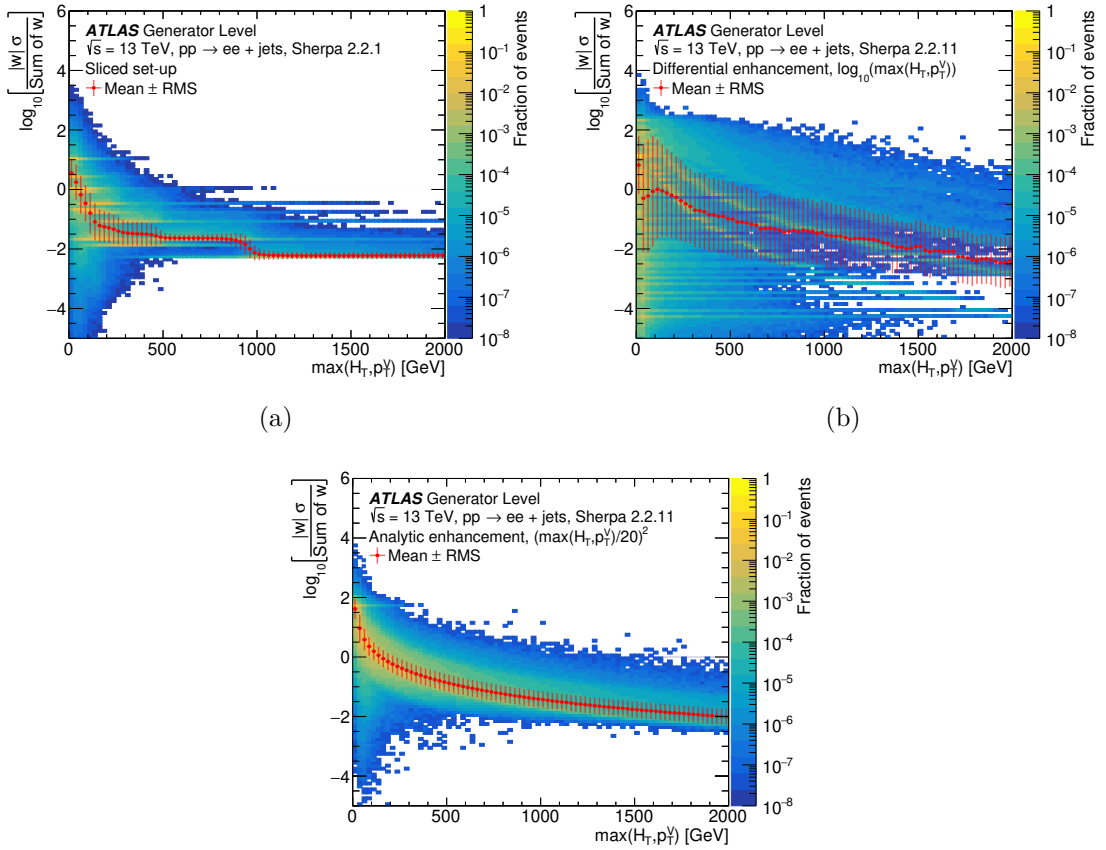

Figure 12. Distributions of the logarithm of the absolute value of the event weight (w) times cross section (σ) divided by the sum of event weights as a function of $\max(H_{\mathrm{T}}, p_{\mathrm{T}}^{V})$ for the (a) sliced, (b) differential enhancement and (c) analytic enhancement SHERPA configurations. The distributions are normalized to unity.

differential enhancement strategy on the final-state parton multiplicity; each $2 \to n$ process is enhanced by its own inverse differential cross-section as outlined in section 4.2.1. Given the correlation of H_{T} and p_{T}^{V} with the parton multiplicity of the hard-scatter process, for any given $\max(H_{\mathrm{T}}, p_{\mathrm{T}}^{V})$ value two different parton-multiplicity final states experience uniquely different biasing weights. The resulting event weight distribution is therefore multimodal in nature, which has negative consequences on the statistical precision of the sample as discussed below.

In contrast, the analytic enhancement strategy of the 2.2.11 configuration is independent of the hard-scatter final-state parton multiplicity, and with no discrete integration boundaries a smooth event weight distribution is obtained as a function of $\max(H_{\mathrm{T}}, p_{\mathrm{T}}^{V})$, as demonstrated by figure 12(c).

With this in mind, figure 13 summarizes the statistical precision of the three enhancement strategies as a function of $\max(H_{\mathrm{T}}, p_{\mathrm{T}}^{V})$ and p_{T}^{V}. The top panel shows the $pp \to e^{+}e^{-} + \text{jets}$ differential cross-section (black) generated at $\sqrt{s} = 13\,\text{TeV}$ with an effective integrated luminosity of $139\,\text{fb}^{-1}$ for p_{T}^{V} in figure 13(a) and $\max(H_{\mathrm{T}}, p_{\mathrm{T}}^{V})$ in fig-

JHEP08(2022)089

ure 13(b). The top panel in each case also superimposes the relative statistical uncertainty as a function of the kinematic observable. The middle panel shows the differential behaviour of the statistical dilution factor resulting from the event weight variance, as given by eq. (4.1), whilst the third panel shows the differential negative-weight fraction.

From figure 13 it can be seen that the differential enhancement strategy gives the least precise prediction. This is the direct result of the event weight variance induced by the parton-multiplicity-dependent biasing, which manifests in the form of a large statistical dilution factor. In the comparisons shown, this dilution factor exceeds that of both the 2.2.1 and 2.2.11 configurations for $p_{\mathrm{T}}^{V} > 100\,\mathrm{GeV}$ and $\max(H_{\mathrm{T}}, p_{\mathrm{T}}^{V}) > 150\,\mathrm{GeV}$, and does so by almost an order of magnitude in the high $\max(H_{\mathrm{T}}, p_{\mathrm{T}}^{V})$ and p_{T}^{V} regions.

In the comparison of the analytic and sliced enhancement strategies the conclusions are, however, slightly more nuanced. The statistical precision of the differential cross-section predicted by the 2.2.11 analytic enhancement strategy either matches or exceeds that of the 2.2.1 sliced enhancement strategy. Furthermore, the statistical dilution factor and negative-weight fraction of the analytic enhancement strategy is far less variable than that of the sliced enhancement strategy. The superior statistical precision and stability of the 2.2.11 configuration is attributed to two key factors.

The first is the removal of phase-space slicing during the MC integration step. Specifically, the 2.2.1 phase-space slices are only exclusive at the matrix-element level during integration, in which the on-shell final-state partons (void of NLO parton emission matching) and V boson decay products are used to construct p_{T}^{V} and H_{T}. After parton showering and hadronization, the observables are defined by hadron clustered jets, and electroweak showered leptons. Consequently, the disparity in the definition of the H_{T} and p_{T}^{V} observables means that the phase-space slices overlap at the internal integration boundaries when using the hadron-level definitions. Therefore, at the internal phase-space boundaries a small overlap results in a multimodal event weight distribution and so an increased event weight variance. Given the higher density of integration boundaries in the $\max(H_{\mathrm{T}}, p_{\mathrm{T}}^{V}) < 280\,\mathrm{GeV}$ region (see section 2.1), the size and variability of the dilution factor is larger.

This intrinsic feature ultimately limits the scalability of the sliced enhancement strategy, because should a sample with finer integration slices be required, the growing number of internal boundaries will induce an increased statistical dilution effect. Effectively, the scheme must sacrifice statistical precision in order to gain more control of the sample rate across the generated phase space.

The second key factor is a reduction of the negative-weight fraction in the 2.2.11 configuration. An overall inclusive reduction of the negative-weight fraction from ∼18% to ∼9% was achieved by neglecting sub-leading gluon spin and colour correlations in the MC@NLO matching. Furthermore, by using the $2 \to 2$ process to define the local NLO/LO reweighting K-factor for the 2.2.11 configuration, instead of the $2 \to 4$ process as done for the 2.2.1 configuration, the fraction of negative weights shifts from the high cross-section regions at low p_{T}^{V} and H_{T} into the low cross-section tails. As a result, the statistical dilution in the highest cross-section regions is reduced, thereby significantly increasing the overall statistical precision of the sample.

Despite the superior statistical precision of the analytic enhancement strategy, and the versatility of the analytic form (sample rate can be tuned to suit the physics use case), the

JHEP08(2022)089

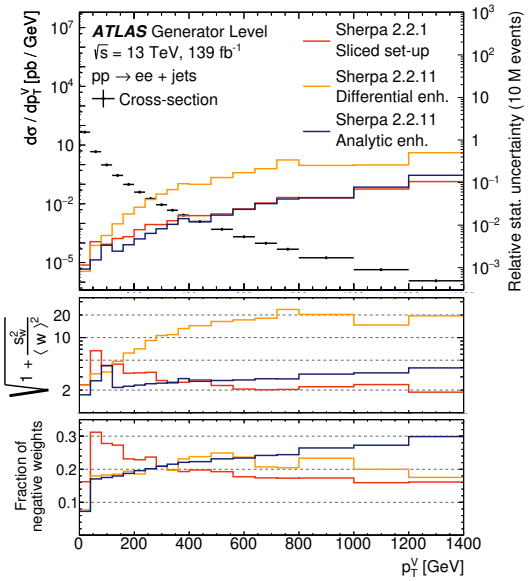

(a) $pp \to e^+e^- +$jets as function of p_{T}^V.

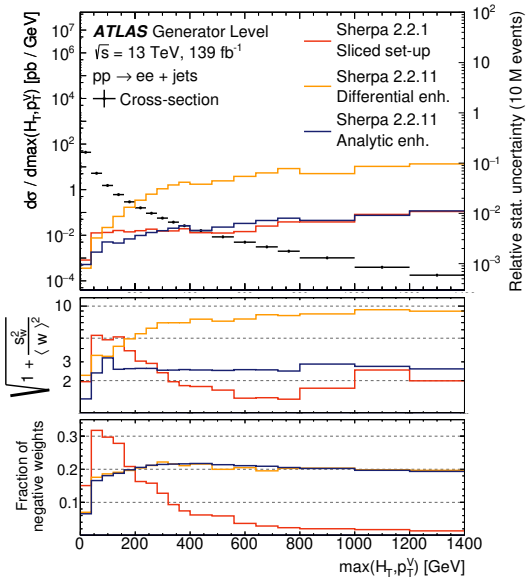

(b) $pp \to e^+e^- +$jets as function of $\max(H_{\mathrm{T}}, p_{\mathrm{T}}^V)$.

Figure 13. Differential cross-section of $pp \to e^+e^- +$jets as a function of (a) p_{T}^V and (b) $\max(H_{\mathrm{T}}, p_{\mathrm{T}}^V)$ in black, as read from the left axis. The relative differential uncertainty of said cross-section for the three enhancement schemes is shown superimposed and should be read from the right axis. The first panel shows the differential efficiency factor resulting from the weight spread, whilst the second panel shows the negative-weight fraction, as a function of p_{T}^V and $\max(H_{\mathrm{T}}, p_{\mathrm{T}}^V)$.

subdomain sampling capability of the sliced enhancement strategy is still invaluable. With this in mind, a hybrid scheme is possible in which multiple analytically enhanced samples exclusive in their phase-space slicing can be combined. This is demonstrated in figure 14 in which the aforementioned $\max(H_{\mathrm{T}}, p_{\mathrm{T}}^V)$ analytically enhanced 2.2.11 configuration sample (red) is shown as a function of the invariant mass of the dimuon system ($m_{\mu\mu}$) for $pp \to \mu^+\mu^- +$jets, along with the resulting differential cross-section (black). Due to the off-shell suppression, the ability of the $\max(H_{\mathrm{T}}, p_{\mathrm{T}}^V)$ enhanced sample to populate off-pole-mass regions is limited.

Consequently, a supplementary 2.2.11 configuration using an $(m_V/100)^2$ enhancement with a dimuon invariant mass requirement of $m_{\mu\mu} > 120\,\mathrm{GeV}$ is generated. This is combined with the 2.2.11 $\max(H_{\mathrm{T}}, p_{\mathrm{T}}^V)$ enhanced sample by vetoing events below $m_{\mu\mu} = 120\,\mathrm{GeV}$ in the $\max(H_{\mathrm{T}}, p_{\mathrm{T}}^V)$ sample. The resulting combined sample, as shown by the orange line in figure 14, has a smaller relative statistical uncertainty in the $m_{\mu\mu} > 120\,\mathrm{GeV}$ region due to the larger statistical population, and the reduced statistical dilution factor in the $m_{\mu\mu} > 120\,\mathrm{GeV}$ region. The negative-weight fraction is unaffected by the biasing and subsequent combination procedure, as demonstrated.

4.3 Impact on computing resources

The inclusive $V+$jets cross-section is sufficiently large that the computing resources required to match the dataset's integrated luminosity are significant and difficult to achieve

JHEP08(2022)089

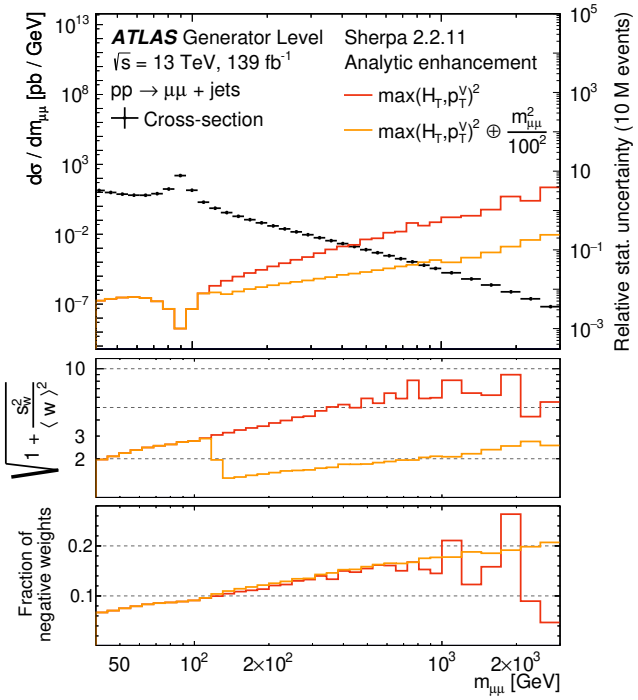

Figure 14. Differential cross-section of $pp \to \mu^+\mu^- +$jets as a function of $m_{\mu\mu}$ in black, as read from the left axis. The relative differential uncertainty for the $\max(H_{\mathrm{T}}, p_{\mathrm{T}}^V)$ analytic enhancement Sherpa 2.2.11 configuration and the $m_{\mu\mu} + \max(H_{\mathrm{T}}, p_{\mathrm{T}}^V)$ analytic enhancement Sherpa 2.2.11 configuration, is shown superimposed and should be read from the right axis. The first panel shows the differential efficiency factor resulting from the weight spread, whilst the second panel shows the negative-weight fraction, as a function of $m_{\mu\mu}$.

across the wide range of phase space required for physics analyses. Moreover, as the LHC physics programme advances it continues to explore extreme regions of phase space often requiring computationally expensive higher-order strong and electroweak corrections. As shown in the previous section, this higher accuracy requires additional resources but these can be reduced through well-motivated approximations with minimal impact on the physics modelling. In this section, the computing resources for the Sherpa 2.2.11 and 2.2.1 configurations are compared in order to quantify the combined effect of the various improvements described in this paper.

4.3.1 Per-event CPU cost for production configurations

The per-event CPU time of the final production versions of the Sherpa 2.2.1 and 2.2.11 configurations (see table 1) are characterized in the same way as in section 4.1. Sherpa 2.2.1 is considered a legacy configuration from which the latest Sherpa 2.2.11 setup can be measured against. The 2.2.11 configuration contains all the additional features described in section 4.1.2, where the virtual electroweak corrections and on-the-fly scale and PDF uncertainties lead to longer event generation times, while the H_{T}' scale definition for $\mathbb{H}$-

JHEP08(2022)089

Phase-space strategy	Mean [s/event]	Mean [HS06 s/event]	Fraction of events [%]
SHERPA 2.2.11 configuration			
$\left(\frac{\max(H_{\mathrm{T}},p_{\mathrm{T}}^{V})}{20}\right)^{2}$ analytic enhancement	17.9 ± 0.2	375 ± 4	100
SHERPA 2.2.1 configuration			
$0 < \max(H_{\mathrm{T}}, p_{\mathrm{T}}^{V}) < 70\,\mathrm{GeV}$	4.7 ± 0.5	99 ± 11	31
$70 < \max(H_{\mathrm{T}}, p_{\mathrm{T}}^{V}) < 140\,\mathrm{GeV}$	34.6 ± 2.3	725 ± 48	27
$140 < \max(H_{\mathrm{T}}, p_{\mathrm{T}}^{V}) < 280\,\mathrm{GeV}$	36.8 ± 1.2	772 ± 25	19
$280 < \max(H_{\mathrm{T}}, p_{\mathrm{T}}^{V}) < 500\,\mathrm{GeV}$	53.7 ± 2.2	1126 ± 46	11
$500 < \max(H_{\mathrm{T}}, p_{\mathrm{T}}^{V}) < 1000\,\mathrm{GeV}$	67.6 ± 3.0	1418 ± 63	9
$\max(H_{\mathrm{T}}, p_{\mathrm{T}}^{V}) > 1000\,\mathrm{GeV}$	108.4 ± 5.7	2273 ± 120	3

Table 3. Mean CPU cost for the SHERPA configurations in seconds and HS06 seconds. The HS06 conversion factor used was 1 second = 20.97 HS06 seconds. The uncertainty corresponds to the standard deviation of multiple trials. The fraction of events corresponds to the number of events in a given slice to the total number generated across all slices.

events and the alternative clustering scheme lead to shorter event generation times. In addition, the analytic enhancement described in section 4.2.1 is included and biases the sampled events. The 2.2.1 configuration contains on-the-fly scale and PDF variations, and was sliced into discrete samples in the $\max(H_{\mathrm{T}}, p_{\mathrm{T}}^{V})$ variable. The CPU time of each for the $\max(H_{\mathrm{T}}, p_{\mathrm{T}}^{V})$ slices was characterized independently. The mean values in seconds per event and HS06 seconds per event are shown in table 3. Each configuration was run five times and the standard deviation of the results is quoted as the *trial* error and amounts to less than 5% for all configurations.

As can be seen from the table, the event generation time for the high-$\max(H_{\mathrm{T}}, p_{\mathrm{T}}^{V})$ 2.2.1 slices is considerably longer than the slices at lower values, since $2 \to n$ processes with higher n dominate the higher-$\max(H_{\mathrm{T}}, p_{\mathrm{T}}^{V})$ slices and are more computationally challenging. Since these multi-jet merged setups are primarily used in phase-spaces with jet selections, the intermediate to higher-$\max(H_{\mathrm{T}}, p_{\mathrm{T}}^{V})$ slices are most relevant to analyses.

4.3.2 Generated effective luminosity

The effective luminosity of a generated MC dataset can be used as a metric to quantify the MC sample size and compare the performance of the different configurations. It is defined to be:

$$\mathcal{L}_{\mathrm{eff}}(x_b) = \frac{N(x_b)^{\mathrm{eff}}}{\sigma(x_b)},$$

where x_b is the center of bin b of a generic observable, $\sigma(x_b)$ is the total cross-section in bin b, and $N(x_b)^{\mathrm{eff}}$ is the effective number of events in bin b. The effective number of events is computed from weighted events and defined to be:

$$N(x_b)^{\mathrm{eff}} = \frac{\left(\sum_i w_i\right)^2}{\left(\sum_i w_i^2\right)},$$

JHEP08(2022)089

where w_i corresponds to the generator event weights in the sample, and the sum extends over events that are contained within bin b.

In order to facilitate the comparison of all the Sherpa configurations in table 1, the total number of events in each generated sample is normalized to a common benchmark of 200 M events. Since the 2.2.1 configuration is separated into discrete samples based on the $\max(H_{\mathrm{T}}, p_{\mathrm{T}}^{V})$ quantity, the number of events that populate each of the individual $\max(H_{\mathrm{T}}, p_{\mathrm{T}}^{V})$ slices needs to be specified. For the purposes of these comparisons, the actual number of events generated by the ATLAS collaboration in each of the discrete $\max(H_{\mathrm{T}}, p_{\mathrm{T}}^{V})$ slices is assumed, and interpreted as the overall demand from ATLAS. The fraction of events in each of the slices is shown in the last column of table 3. The sum of all the slices are then normalized to 200 M for comparison with the continuous enhancement samples.

The effective luminosity in each generated MC sample as a function of the boson transverse momentum and the total sum of jet transverse momenta (H_{T}) are shown in figure 15. The Sherpa 2.2.11 configuration provides an effective luminosity similar to that from the sliced Sherpa 2.2.1 set-up across a wide range of phase spaces, and exceeds the ATLAS Run 2 dataset's integrated luminosity for intermediate to high p_{T}^{V} and H_{T} selections. When comparing the effective luminosity of the 2.2.11 and 2.2.1 set-ups in the low p_{T}^{V} and H_{T} regions, the two configurations have comparable performance overall, with maximum differences of 30%. For high p_{T}^{V} and H_{T} selections, the spread of weights and the negative-weight fraction are slightly higher in the Sherpa 2.2.11 set-up than in 2.2.1, which is reflected by the reduced effective luminosity in the tails of the Sherpa 2.2.11 set-up. However, both set-ups already exceed the dataset's integrated luminosity by over an order of magnitude. On the other hand, the extremely large spread of weights present in the differential enhancement Sherpa 2.2.11 configuration has a detrimental effect on the effective luminosity, which can be over two orders of magnitude lower than that of the Sherpa 2.2.11 configuration when using the analytic enhancement scheme. The differential enhancement configuration fails to reach the Run 2 dataset's integrated luminosity across the most of the phase space.

Besides providing comparable performance to the 2.2.1 setup the effective luminosity of the 2.2.11 set-up is more uniform than in the 2.2.1 configuration. As discussed in section 4.2.2, discrete slicing causes a migration between slices, which produces an artificially large spread of weights. This effect is most pronounced near the slice boundaries and degrades the effective luminosity in those regions When using a continuous enhancement method as done in the Sherpa 2.2.11 configurations, such an effect is no longer present, improving the uniformity of the effective luminosity across values of key variables used in physics analyses. This is clearly observable in the H_{T} distribution in figure 15 around the slice boundaries 280 GeV and 1000 GeV.

Beyond the improvement in the generated effective luminosity, the Sherpa 2.2.11 configuration costs less than the 2.2.1 set-up from a CPU standpoint, despite the former containing additional LO QCD legs and virtual electroweak corrections. Using the mean values for the CPU cost and the relative number of events in each of the slices found in table 3, the total HS06 CPU cost to produce these 200 M events in the Sherpa 2.2.1 and 2.2.11

JHEP08(2022)089

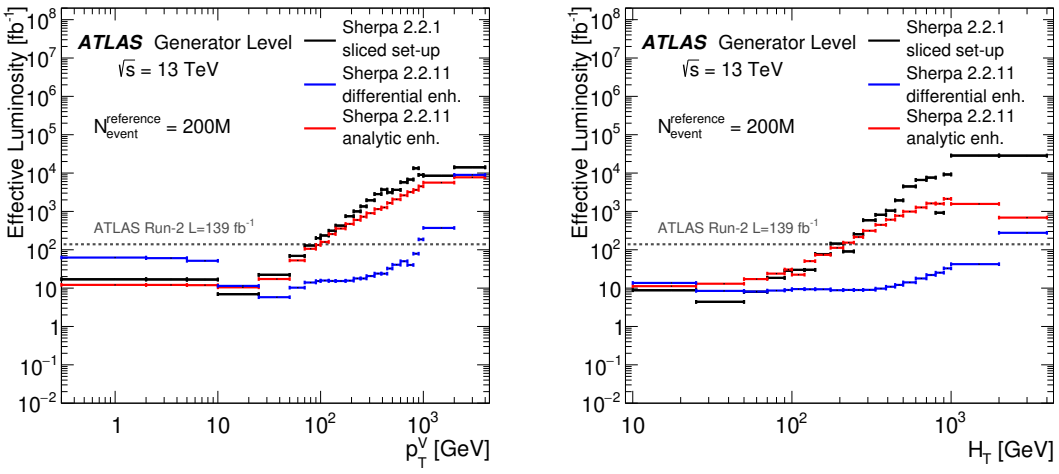

(a) (b)

Figure 15. Differential distributions of the effective luminosity of each of the SHERPA configurations as a function of (a) p_{T}^{V}, and (b) H_{T}. All samples have been scaled to a common reference value of 200 M events. The truncated lowest bin includes events with p_{T}^{V} or H_{T} down to zero in the calculation.

configurations is 140×10^3 MHS06 seconds and 75×10^3 MHS06 seconds, respectively. This represents nearly a factor of two reduction in the computing resources needed to obtain the results shown in figure 15. While the improvements in generated effective luminosity arise largely from the improved numerical efficiency parameters discussed in section 4.2.2, the overall decrease in CPU cost originates from the various approximations that were shown in section 4.1 to reduce the per-event generation time by over a factor of three.

Looking towards the HL-LHC, the integrated luminosity of the data set is expected to be at least $3000\,\mathrm{fb}^{-1}$. Assuming the same sampling pattern as given by figure 15, in which the MC effective luminosity matches or exceeds that of the data for p_{T}^{V} and H_{T} greater than approximately 100 GeV, roughly 10 billion events will be required for each of the leptonic decay modes of the Z boson. Accounting for the leptonic W boson decay modes as well, roughly 330 billion events will be needed to match the data set luminosity at the HL-LHC. With the developments in the latest SHERPA 2.2.11 setup presented in this paper, the CPU cost for this would be 3.8 MHS06 years. Assuming an aggressive research and development (R&D) programme over the following decade, the CPU budget allocated to event generation is 3.2 MHS06 for the year of 2031 [77]. Therefore the latest SHERPA 2.2.11 setup would exceed the yearly budget by 16% while the SHERPA 2.2.1 configuration would exceed the yearly resources by 132%. Despite exceeding the yearly budget, the reduction in the computing resources represents an important milestone towards meeting the computing budget for the HL-LHC. Further CPU reductions aimed at reducing the costly additional features shown in section 4.1.2 are expected to bring the latest SHERPA 2.2.11 setup below the allocated yearly resources and enable the usage of a second alternative multi-jet merged V+jets setup, such as the MADGRAPH5_aMC@NLO+PYTHIA described in this paper.

JHEP08(2022)089

5 Conclusions

The production of a single vector boson plus jets is an important process for study at the LHC and an integral part of the ATLAS physics programme. State-of-the-art predictions for single boson production are routinely used in comparisons with data measurements, and serve as an important ingredient for the modelling of backgrounds in measurements of other SM processes or searches for physics beyond the SM. As such, an accurate description of $V+$jets processes, along with good statistical coverage across a wide range of phase spaces, is crucial for the success of the ATLAS physics programme.

This paper highlights a series of recent modelling and computational improvements in the Sherpa event generator developed beyond the 2.2.1 set-up used by ATLAS for the last several years. The theoretical changes were shown to improve the description of data for a variety of measurements, and provide additional higher-order electroweak corrections for future measurements to probe. The major CPU bottlenecks in the event generation time were identified, and various approximations were implemented that reduce the per-event time by up to a factor of three. Together with a continuous statistical enhancement technique, the resources required to produce the Sherpa 2.2.11 configuration were reduced by up to a factor of two relative to the 2.2.1 configuration. In addition, the performance of the first alternative ATLAS multi-jet MadGraph5_aMC@NLO+Pythia configuration using FxFx merging with a similar perturbative accuracy to the Sherpa prediction was shown.

In summary, the MC configurations reported in this paper form the base standard of single vector boson plus jets simulation moving into the third run period (Run 3) of the LHC for ATLAS analyses. They also demonstrate that selective scale choices, appropriate phase space biasing algorithms, and negative weight treatments are appropriate techniques capable of reducing the CPU foot print of MC simulation moving into the HL-LHC era. However, although the changes made in the Sherpa 2.2.11 configuration will provide sufficient CPU savings such that a complementary higher order MC prediction (such as that presented by the MadGraph5_aMC@NLO+Pythia configuration) can be produced without increasing the total CPU foot print, the aforementioned improvements only represent the conservative R&D programme outlined in ref. [77]. Therefore, in order to reduce the total CPU usage of MC simulation to within the projected HL-LHC CPU budget, a more aggressive computational R&D programme in the field of MC simulation will be required moving into the future.

Acknowledgments

We thank CERN for the very successful operation of the LHC, as well as the support staff from our institutions without whom ATLAS could not be operated efficiently.

We acknowledge the support of ANPCyT, Argentina; YerPhI, Armenia; ARC, Australia; BMWFW and FWF, Austria; ANAS, Azerbaijan; SSTC, Belarus; CNPq and FAPESP, Brazil; NSERC, NRC and CFI, Canada; CERN; ANID, Chile; CAS, MOST and NSFC, China; Minciencias, Colombia; MSMT CR, MPO CR and VSC CR, Czech

JHEP08(2022)089

Republic; DNRF and DNSRC, Denmark; IN2P3-CNRS and CEA-DRF/IRFU, France; SRNSFG, Georgia; BMBF, HGF and MPG, Germany; GSRI, Greece; RGC and Hong Kong SAR, China; ISF and Benoziyo Center, Israel; INFN, Italy; MEXT and JSPS, Japan; CNRST, Morocco; NWO, The Netherlands; RCN, Norway; MEiN, Poland; FCT, Portugal; MNE/IFA, Romania; JINR; MES of Russia and NRC KI, Russian Federation; MESTD, Serbia; MSSR, Slovakia; ARRS and MIZŠ, Slovenia; DSI/NRF, South Africa; MICINN, Spain; SRC and Wallenberg Foundation, Sweden; SERI, SNSF and Cantons of Bern and Geneva, Switzerland; MOST, Taiwan; TAEK, Turkey; STFC, U.K.; DOE and NSF, U.S.A.. In addition, individual groups and members have received support from BCKDF, CANARIE, Compute Canada and CRC, Canada; COST, ERC, ERDF, Horizon 2020 and Marie Skłodowska-Curie Actions, European Union; Investissements d'Avenir Labex, Investissements d'Avenir Idex and ANR, France; DFG and AvH Foundation, Germany; Herakleitos, Thales and Aristeia programmes co-financed by EU-ESF and the Greek NSRF, Greece; BSF-NSF and GIF, Israel; Norwegian Financial Mechanism 2014–2021, Norway; NCN and NAWA, Poland; La Caixa Banking Foundation, CERCA Programme Generalitat de Catalunya and PROMETEO and GenT Programmes Generalitat Valenciana, Spain; Göran Gustafssons Stiftelse, Sweden; The Royal Society and Leverhulme Trust, U.K..

The crucial computing support from all WLCG partners is acknowledged gratefully, in particular from CERN, the ATLAS Tier-1 facilities at TRIUMF (Canada), NDGF (Denmark, Norway, Sweden), CC-IN2P3 (France), KIT/GridKA (Germany), INFN-CNAF (Italy), NL-T1 (The Netherlands), PIC (Spain), ASGC (Taiwan), RAL (U.K.) and BNL (U.S.A.), the Tier-2 facilities worldwide and large non-WLCG resource providers. Major contributors of computing resources are listed in ref. [78].

A Equations for modified Catani-Seymour splitting kernels

A.1 Final-initial dipoles

The eikonal factors appearing in the Catani-Seymour splitting functions [79] are changed as:

$$\frac{1}{1-\tilde{z}_i+(1-x_{a,ij})}-1 \;\to\; \frac{\tilde{z}_i}{1-\tilde{z}_i+(1-x_{a,ij})}.$$

This leads to an additional contribution to the $\bar{K}$ operators of the form

$$2\log\frac{2-x_{a,ij}}{1-x_{a,ij}}.$$

A.2 Initial-final dipoles

The eikonal factors appearing in the Catani-Seymour splitting functions [79] are changed as:

$$\frac{1}{1-x_{a,ik}+u_i}-1 \;\to\; \frac{x_{a,ik}}{1-x_{a,ik}+u_i}\,.$$

This leads to an additional contribution to the $\bar{K}$ terms of the form

$$2\log\frac{2-x_{a,ik}}{1-x_{a,ik}}\,.$$

JHEP08(2022)089

A.3 Initial-initial dipoles

The light-cone momentum fractions are modified as $x_{i,ab} \to x_{i,ab} + \tilde{v}_i$, and the eikonal factors appearing in the Catani-Seymour splitting functions [79] are redefined as follows:

$$\frac{1}{1-x_{i,ab}} - 1 \;\to\; \frac{x_{i,ab}+\tilde{v}_i}{1-x_{i,ab}}\,.$$

The collinear term for $q \to q$ is changed according to:

$$(1-\epsilon)(1-x_{i,ab}) \;\to\; (1-\epsilon)(1-x_{i,ab}-\tilde{v}_i)\,.$$

The collinear kernel for $q \to g$ is changed according to:

$$2\frac{1-x_{i,ab}}{x_{i,ab}} + (1-\epsilon)x_{i,ab} \;\to\; 2\frac{1-x_{i,ab}-\tilde{v}_i}{x_{i,ab}+\tilde{v}_i} + (1-\epsilon)(x_{i,ab}+\tilde{v}_i)\,.$$

The collinear terms for $g \to g$ are changed according to:

$$\frac{1-x_{i,ab}}{x_{i,ab}} + x_{i,ab}(1-x_{i,ab}) \;\to\; \frac{1-x_{i,ab}-\tilde{v}_i}{x_{i,ab}+\tilde{v}_i} + (x_{i,ab}+\tilde{v}_i)(1-x_{i,ab}-\tilde{v}_i)\,.$$

The collinear kernel for $g \to q$ is changed according to:

$$1 - \frac{2x_{i,ab}(1-x_{i,ab})}{1-\epsilon} \;\to\; 1 - \frac{2(x_{i,ab}+\tilde{v}_i)(1-x_{i,ab}-\tilde{v}_i)}{1-\epsilon}\,.$$

This leads to an additional contribution to the $\tilde{K}$ operators of the form:

$$\begin{aligned}
q \to q: &\quad 1 + x_{i,ab} \\
q \to g: &\quad 1 - x_{i,ab} + 2\,\frac{\log x}{x} \\
g \to g: &\quad 3 - x_{i,ab}(4 - 3x_{i,ab}) + 2\,\frac{\log x}{x} \\
g \to q: &\quad -(1-x_{i,ab})(1-3x_{i,ab})\,.
\end{aligned}$$

Open Access. This article is distributed under the terms of the Creative Commons Attribution License (CC-BY 4.0), which permits any use, distribution and reproduction in any medium, provided the original author(s) and source are credited. SCOAP^3 supports the goals of the International Year of Basic Sciences for Sustainable Development.

References

[1] L. Evans and P. Bryant eds., *LHC Machine*, 2008 *JINST* **3** S08001 [INSPIRE].

[2] ATLAS collaboration, *The ATLAS Experiment at the CERN Large Hadron Collider*, 2008 *JINST* **3** S08003 [INSPIRE].

[3] ATLAS collaboration, *Measurement of the associated production of a Higgs boson decaying into b-quarks with a vector boson at high transverse momentum in pp collisions at* $\sqrt{s} = 13$ *TeV with the ATLAS detector*, *Phys. Lett. B* **816** (2021) 136204 [arXiv:2008.02508] [INSPIRE].

JHEP08(2022)089

[4] ATLAS collaboration, *Measurement of the production cross section for a Higgs boson in association with a vector boson in the $H \to WW^* \to \ell\nu\ell\nu$ channel in pp collisions at $\sqrt{s} = 13$ TeV with the ATLAS detector*, *Phys. Lett. B* **798** (2019) 134949 [arXiv:1903.10052] [INSPIRE].

[5] ATLAS collaboration, *Measurement of the $t\bar{t}$ production cross-section in the lepton+jets channel at $\sqrt{s} = 13$ TeV with the ATLAS experiment*, *Phys. Lett. B* **810** (2020) 135797 [arXiv:2006.13076] [INSPIRE].

[6] ATLAS collaboration, *Measurements of top-quark pair spin correlations in the $e\mu$ channel at $\sqrt{s} = 13$ TeV using pp collisions in the ATLAS detector*, *Eur. Phys. J. C* **80** (2020) 754 [arXiv:1903.07570] [INSPIRE].

[7] ATLAS collaboration, *Search for squarks and gluinos in final states with one isolated lepton, jets, and missing transverse momentum at $\sqrt{s} = 13$ with the ATLAS detector*, *Eur. Phys. J. C* **81** (2021) 600 [*Erratum ibid.* **81** (2021) 956] [arXiv:2101.01629] [INSPIRE].

[8] ATLAS collaboration, *Searches for electroweak production of supersymmetric particles with compressed mass spectra in $\sqrt{s} = 13$ TeV pp collisions with the ATLAS detector*, *Phys. Rev. D* **101** (2020) 052005 [arXiv:1911.12606] [INSPIRE].

[9] ATLAS collaboration, *Search for new phenomena with top quark pairs in final states with one lepton, jets, and missing transverse momentum in pp collisions at $\sqrt{s} = 13$ TeV with the ATLAS detector*, *JHEP* **04** (2021) 174 [arXiv:2012.03799] [INSPIRE].

[10] P. Calafiura, J. Catmore, D. Costanzo and A. Di Girolamo, *ATLAS HL-LHC Computing Conceptual Design Report*, CERN-LHCC-2020-015 (2020) [LHCC-G-178] [https://doi.org/10.3204/PUBDB-2020-04972].

[11] HSF Physics Event Generator WG collaboration, *Challenges in Monte Carlo Event Generator Software for High-Luminosity LHC*, *Comput. Softw. Big Sci.* **5** (2021) 12 [arXiv:2004.13687] [INSPIRE].

[12] HEP Software Foundation collaboration, *A Roadmap for HEP Software and Computing R&D for the 2020s*, *Comput. Softw. Big Sci.* **3** (2019) 7 [arXiv:1712.06982] [INSPIRE].

[13] Sherpa collaboration, *Event Generation with Sherpa 2.2*, *SciPost Phys.* **7** (2019) 034 [arXiv:1905.09127] [INSPIRE].

[14] ATLAS collaboration, *ATLAS simulation of boson plus jets processes in Run 2*, ATL-PHYS-PUB-2017-006 (2017).

[15] J. Alwall et al., *The automated computation of tree-level and next-to-leading order differential cross sections, and their matching to parton shower simulations*, *JHEP* **07** (2014) 079 [arXiv:1405.0301] [INSPIRE].

[16] T. Sjöstrand, S. Mrenna and P.Z. Skands, *A Brief Introduction to PYTHIA 8.1*, *Comput. Phys. Commun.* **178** (2008) 852 [arXiv:0710.3820] [INSPIRE].

[17] ATLAS collaboration, *Differential cross-section measurements for the electroweak production of dijets in association with a Z boson in proton-proton collisions at ATLAS*, *Eur. Phys. J. C* **81** (2021) 163 [arXiv:2006.15458] [INSPIRE].

[18] ATLAS collaboration, *Search for squarks and gluinos in events with an isolated lepton, jets, and missing transverse momentum at $\sqrt{s} = 13$ TeV with the ATLAS detector*, *Phys. Rev. D* **96** (2017) 112010 [arXiv:1708.08232] [INSPIRE].

JHEP08(2022)089

[19] ATLAS collaboration, *Measurement of the transverse momentum distribution of Drell-Yan lepton pairs in proton-proton collisions at $\sqrt{s} = 13$ TeV with the ATLAS detector*, *Eur. Phys. J. C* **80** (2020) 616 [arXiv:1912.02844] [INSPIRE].

[20] ATLAS collaboration, *The ATLAS collaboration Software and Firmware*, ATL-SOFT-PUB-2021-001 (2021).

[21] T. Gleisberg and S. Höche, *Comix, a new matrix element generator*, *JHEP* **12** (2008) 039 [arXiv:0808.3674] [INSPIRE].

[22] F. Buccioni et al., *OpenLoops 2*, *Eur. Phys. J. C* **79** (2019) 866 [arXiv:1907.13071] [INSPIRE].

[23] F. Cascioli, P. Maierhöfer and S. Pozzorini, *Scattering Amplitudes with Open Loops*, *Phys. Rev. Lett.* **108** (2012) 111601 [arXiv:1111.5206] [INSPIRE].

[24] F. Buccioni, S. Pozzorini and M. Zoller, *On-the-fly reduction of open loops*, *Eur. Phys. J. C* **78** (2018) 70 [arXiv:1710.11452] [INSPIRE].

[25] A. Denner, S. Dittmaier and L. Hofer, *Collier: a fortran-based Complex One-Loop LIbrary in Extended Regularizations*, *Comput. Phys. Commun.* **212** (2017) 220 [arXiv:1604.06792] [INSPIRE].

[26] NNPDF collaboration, *Parton distributions for the LHC Run II*, *JHEP* **04** (2015) 040 [arXiv:1410.8849] [INSPIRE].

[27] S. Carrazza, S. Forte, Z. Kassabov, J.I. Latorre and J. Rojo, *An Unbiased Hessian Representation for Monte Carlo PDFs*, *Eur. Phys. J. C* **75** (2015) 369 [arXiv:1505.06736] [INSPIRE].

[28] M. Chiesa, F. Piccinini and A. Vicini, *Direct determination of $\sin^2\theta^{\ell}_{\rm eff}$ at hadron colliders*, *Phys. Rev. D* **100** (2019) 071302 [arXiv:1906.11569] [INSPIRE].

[29] S. Kallweit, J.M. Lindert, P. Maierhöfer, S. Pozzorini and M. Schönherr, *NLO electroweak automation and precise predictions for W+multijet production at the LHC*, *JHEP* **04** (2015) 012 [arXiv:1412.5157] [INSPIRE].

[30] S. Kallweit, J.M. Lindert, P. Maierhöfer, S. Pozzorini and M. Schönherr, *NLO QCD+EW predictions for V + jets including off-shell vector-boson decays and multijet merging*, *JHEP* **04** (2016) 021 [arXiv:1511.08692] [INSPIRE].

[31] D. Yennie, S. Frautschi and H. Suura, *The infrared divergence phenomena and high-energy processes*, *Ann. Phys.* **13** (1961) 379.

[32] M. Schönherr and F. Krauss, *Soft Photon Radiation in Particle Decays in SHERPA*, *JHEP* **12** (2008) 018 [arXiv:0810.5071] [INSPIRE].

[33] S. Höche, F. Krauss, M. Schönherr and F. Siegert, *A critical appraisal of NLO+PS matching methods*, *JHEP* **09** (2012) 049 [arXiv:1111.1220] [INSPIRE].

[34] S. Catani, F. Krauss, R. Kuhn and B.R. Webber, *QCD matrix elements + parton showers*, *JHEP* **11** (2001) 063 [hep-ph/0109231] [INSPIRE].

[35] S. Höche, F. Krauss, S. Schumann and F. Siegert, *QCD matrix elements and truncated showers*, *JHEP* **05** (2009) 053 [arXiv:0903.1219] [INSPIRE].

[36] S. Höche, F. Krauss, M. Schönherr and F. Siegert, *QCD matrix elements + parton showers: The NLO case*, *JHEP* **04** (2013) 027 [arXiv:1207.5030] [INSPIRE].

JHEP08(2022)089

[37] S. Schumann and F. Krauss, *A Parton shower algorithm based on Catani-Seymour dipole factorisation*, *JHEP* **03** (2008) 038 [arXiv:0709.1027] [INSPIRE].

[38] J.-C. Winter, F. Krauss and G. Soff, *A Modified cluster hadronization model*, *Eur. Phys. J. C* **36** (2004) 381 [hep-ph/0311085] [INSPIRE].

[39] ATLAS collaboration, *Studies on top-quark Monte Carlo modelling with Sherpa and MG5_aMC@NLO*, ATL-PHYS-PUB-2017-007 (2017).

[40] ALEPH, CDF, DELPHI, L3, OPAL and SLD collaborations, *Combined results on b-hadron production rates and decay properties*, hep-ex/0112028.

[41] Z. Bern et al., *Next-to-Leading Order $W + 5$-Jet Production at the LHC*, *Phys. Rev. D* **88** (2013) 014025 [arXiv:1304.1253] [INSPIRE].

[42] F. Dulat, S. Höche and S. Prestel, *Leading-Color Fully Differential Two-Loop Soft Corrections to QCD Dipole Showers*, *Phys. Rev. D* **98** (2018) 074013 [arXiv:1805.03757] [INSPIRE].

[43] K. Danziger, S. Höche and F. Siegert, *Reducing negative weights in Monte Carlo event generation with Sherpa*, arXiv:2110.15211 [INSPIRE].

[44] A. Schälicke and F. Krauss, *Implementing the ME+PS merging algorithm*, *JHEP* **07** (2005) 018 [hep-ph/0503281] [INSPIRE].

[45] E. Bothmann, M. Schönherr and S. Schumann, *Reweighting QCD matrix-element and parton-shower calculations*, *Eur. Phys. J. C* **76** (2016) 590 [arXiv:1606.08753] [INSPIRE].

[46] T.-J. Hou et al., *Progress in the CTEQ-TEA NNLO global QCD analysis*, arXiv:1908.11394 [INSPIRE].

[47] S. Bailey, T. Cridge, L.A. Harland-Lang, A.D. Martin and R.S. Thorne, *Parton distributions from LHC, HERA, Tevatron and fixed target data: MSHT20 PDFs*, *Eur. Phys. J. C* **81** (2021) 341 [arXiv:2012.04684] [INSPIRE].

[48] ATLAS collaboration, *ATLAS PYTHIA 8 tunes to 7 TeV data*, ATL-PHYS-PUB-2014-021 (2014).

[49] R.D. Ball et al., *Parton distributions with LHC data*, *Nucl. Phys. B* **867** (2013) 244 [arXiv:1207.1303] [INSPIRE].

[50] R. Frederix and S. Frixione, *Merging meets matching in MC@NLO*, *JHEP* **12** (2012) 061 [arXiv:1209.6215] [INSPIRE].

[51] NNPDF collaboration, *Illuminating the photon content of the proton within a global PDF analysis*, *SciPost Phys.* **5** (2018) 008 [arXiv:1712.07053] [INSPIRE].

[52] J.R. Andersen et al., *Les Houches 2013: Physics at TeV Colliders: Standard Model Working Group Report*, arXiv:1405.1067 [INSPIRE].

[53] C. Anastasiou, L.J. Dixon, K. Melnikov and F. Petriello, *High precision QCD at hadron colliders: Electroweak gauge boson rapidity distributions at NNLO*, *Phys. Rev. D* **69** (2004) 094008 [hep-ph/0312266] [INSPIRE].

[54] C. Bierlich et al., *Robust Independent Validation of Experiment and Theory: Rivet version 3*, *SciPost Phys.* **8** (2020) 026 [arXiv:1912.05451] [INSPIRE].

[55] J.-y. Chiu, F. Golf, R. Kelley and A.V. Manohar, *Electroweak Corrections in High Energy Processes using Effective Field Theory*, *Phys. Rev. D* **77** (2008) 053004 [arXiv:0712.0396] [INSPIRE].

JHEP08(2022)089

[56] Particle Data collaboration, *Review of Particle Physics*, *Phys. Rev. D* **98** (2018) 030001 [INSPIRE].

[57] ATLAS collaboration, *Measurement of the forward-backward asymmetry of electron and muon pair-production in pp collisions at $\sqrt{s} = 7$ TeV with the ATLAS detector*, *JHEP* **09** (2015) 049 [arXiv:1503.03709] [INSPIRE].

[58] ALEPH collaboration, *Measurement of the tau polarization at LEP*, *Eur. Phys. J. C* **20** (2001) 401 [hep-ex/0104038] [INSPIRE].

[59] ATLAS collaboration, *Measurement of τ polarisation in $Z/\gamma^* \to \tau\tau$ decays in proton-proton collisions at $\sqrt{s} = 8$ TeV with the ATLAS detector*, *Eur. Phys. J. C* **78** (2018) 163 [arXiv:1709.03490] [INSPIRE].

[60] S. Jadach and Z. Was, *QED $\mathcal{O}(\alpha^3)$ Radiative corrections to the reaction $e^+e^- \to \tau^+\tau^-$ including spin and mass effects*, *Acta Phys. Pol. B* **15** (1984) 1151 [*Erratum ibid.* **16** (1985) 483] [INSPIRE].

[61] S. Catani, S. Dittmaier, M.H. Seymour and Z. Trócsányi, *The Dipole formalism for next-to-leading order QCD calculations with massive partons*, *Nucl. Phys. B* **627** (2002) 189 [hep-ph/0201036] [INSPIRE].

[62] S. Frixione, Z. Kunszt and A. Signer, *Three jet cross-sections to next-to-leading order*, *Nucl. Phys. B* **467** (1996) 399 [hep-ph/9512328] [INSPIRE].

[63] S. Frixione, *A General approach to jet cross-sections in QCD*, *Nucl. Phys. B* **507** (1997) 295 [hep-ph/9706545] [INSPIRE].

[64] R. Frederix, S. Frixione, F. Maltoni and T. Stelzer, *Automation of next-to-leading order computations in QCD: The FKS subtraction*, *JHEP* **10** (2009) 003 [arXiv:0908.4272] [INSPIRE].

[65] ATLAS collaboration, *Measurement of the transverse momentum distribution of Drell-Yan lepton pairs in proton-proton collisions at $\sqrt{s} = 13$ TeV with the ATLAS detector*, *Eur. Phys. J. C* **80** (2020) 616 [arXiv:1912.02844] [INSPIRE].

[66] CMS collaboration, *Measurement of the differential cross sections for the associated production of a W boson and jets in proton-proton collisions at $\sqrt{s} = 13$ TeV*, *Phys. Rev. D* **96** (2017) 072005 [arXiv:1707.05979] [INSPIRE].

[67] ATLAS collaboration, *Measurements of the production cross section of a Z boson in association with jets in pp collisions at $\sqrt{s} = 13$ TeV with the ATLAS detector*, *Eur. Phys. J. C* **77** (2017) 361 [arXiv:1702.05725] [INSPIRE].

[68] M. Michelotto et al., *A comparison of HEP code with SPEC benchmarks on multi-core worker nodes*, *J. Phys. Conf. Ser.* **219** (2010) 052009 [INSPIRE].

[69] M. Wong, *C++ benchmarks in spec cpu2006*, *Comput. Archit. News* **35** (2007) 77.

[70] J.M. Campbell and R.K. Ellis, *Next-to-Leading Order Corrections to W^+ 2 jet and Z^+ 2 Jet Production at Hadron Colliders*, *Phys. Rev. D* **65** (2002) 113007 [hep-ph/0202176] [INSPIRE].

[71] A. Denner, S. Dittmaier, T. Kasprzik and A. Muck, *Electroweak corrections to W + jet hadroproduction including leptonic W-boson decays*, *JHEP* **08** (2009) 075 [arXiv:0906.1656] [INSPIRE].

[72] M. Rubin, G.P. Salam and S. Sapeta, *Giant QCD K-factors beyond NLO*, *JHEP* **09** (2010) 084 [arXiv:1006.2144] [INSPIRE].

JHEP08(2022)089

[73] D. Amati, A. Bassetto, M. Ciafaloni, G. Marchesini and G. Veneziano, *A Treatment of Hard Processes Sensitive to the Infrared Structure of QCD*, *Nucl. Phys. B* **173** (1980) 429 [INSPIRE].

[74] S. Catani, B.R. Webber and G. Marchesini, *QCD coherent branching and semiinclusive processes at large x*, *Nucl. Phys. B* **349** (1991) 635 [INSPIRE].

[75] K. Danziger, T. Janßen, S. Schumann and F. Siegert, *Accelerating Monte Carlo event generation — rejection sampling using neural network event-weight estimates*, *SciPost Phys.* **12** (2022) 164 [arXiv:2109.11964] [INSPIRE].

[76] S. Frixione and B.R. Webber, *Matching NLO QCD computations and parton shower simulations*, *JHEP* **06** (2002) 029 [hep-ph/0204244] [INSPIRE].

[77] ATLAS collaboration, *ATLAS Software and Computing HL-LHC Roadmap*, CERN-LHCC-2022-005 (2022).

[78] ATLAS collaboration, *ATLAS Computing Acknowledgements*, ATL-SOFT-PUB-2021-003 (2021).

[79] S. Catani and M.H. Seymour, *A General algorithm for calculating jet cross-sections in NLO QCD*, *Nucl. Phys. B* **485** (1997) 291 [*Erratum ibid.* **510** (1998) 503] [hep-ph/9605323] [INSPIRE].

JHEP08(2022)089

The ATLAS collaboration

G. Aad[99], B. Abbott[125], D.C. Abbott[100], A. Abed Abud[35], K. Abeling[52], D.K. Abhayasinghe[92], S.H. Abidi[28], A. Aboulhorma[34e], H. Abramowicz[158], H. Abreu[157], Y. Abulaiti[122], A.C. Abusleme Hoffman[143a], B.S. Acharya[65a,65b,n], B. Achkar[52], L. Adam[97], C. Adam Bourdarios[4], L. Adamczyk[82a], L. Adamek[163], S.V. Addepalli[25], J. Adelman[117], A. Adiguzel[11c,aa], S. Adorni[53], T. Adye[140], A.A. Affolder[142], Y. Afik[35], C. Agapopoulou[63], M.N. Agaras[13], J. Agarwala[69a,69b], A. Aggarwal[97], C. Agheorghiesei[26c], J.A. Aguilar-Saavedra[136f,136a,z], A. Ahmad[35], F. Ahmadov[78,x], W.S. Ahmed[101], X. Ai[45], G. Aielli[72a,72b], I. Aizenberg[176], M. Akbiyik[97], T.P.A. Åkesson[95], A.V. Akimov[108], K. Al Khoury[38], G.L. Alberghi[22b], J. Albert[172], P. Albicocco[50], M.J. Alconada Verzini[87], S. Alderweireldt[49], M. Aleksa[35], I.N. Aleksandrov[78], C. Alexa[26b], T. Alexopoulos[9], A. Alfonsi[116], F. Alfonsi[22b], M. Alhroob[125], B. Ali[138], S. Ali[155], M. Aliev[162], G. Alimonti[67a], C. Allaire[35], B.M.M. Allbrooke[153], P.P. Allport[20], A. Aloisio[68a,68b], F. Alonso[87], C. Alpigiani[145], E. Alunno Camelia[72a,72b], M. Alvarez Estevez[96], M.G. Alviggi[68a,68b], Y. Amaral Coutinho[79b], A. Ambler[101], L. Ambroz[131], C. Amelung[35], D. Amidei[103], S.P. Amor Dos Santos[136a], S. Amoroso[45], K.R. Amos[170], C.S. Amrouche[53], V. Ananiev[130], C. Anastopoulos[146], N. Andari[141], T. Andeen[10], J.K. Anders[19], S.Y. Andrean[44a,44b], A. Andreazza[67a,67b], S. Angelidakis[8], A. Angerami[38], A.V. Anisenkov[118b,118a], A. Annovi[70a], C. Antel[53], M.T. Anthony[146], E. Antipov[126], M. Antonelli[50], D.J.A. Antrim[17], F. Anulli[71a], M. Aoki[80], J.A. Aparisi Pozo[170], M.A. Aparo[153], L. Aperio Bella[45], N. Aranzabal[35], V. Araujo Ferraz[79a], C. Arcangeletti[50], A.T.H. Arce[48], E. Arena[89], J-F. Arguin[107], S. Argyropoulos[51], J.-H. Arling[45], A.J. Armbruster[35], A. Armstrong[167], O. Arnaez[163], H. Arnold[116], Z.P. Arrubarrena Tame[111], G. Artoni[71a,71b], H. Asada[113], K. Asai[123], S. Asai[160], N.A. Asbah[58], E.M. Asimakopoulou[168], L. Asquith[153], J. Assahsah[34d], K. Assamagan[28], R. Astalos[27a], R.J. Atkin[32a], M. Atkinson[169], N.B. Atlay[18], H. Atmani[59b], P.A. Atmasiddha[103], K. Augsten[138], S. Auricchio[68a,68b], V.A. Austrup[178], G. Avner[157], G. Avolio[35], M.K. Ayoub[14c], G. Azuelos[107,ai], D. Babal[27a], H. Bachacou[141], K. Bachas[159], A. Bachiu[33], F. Backman[44a,44b], A. Badea[58], P. Bagnaia[71a,71b], M. Bahmani[18], A.J. Bailey[170], V.R. Bailey[169], J.T. Baines[140], C. Bakalis[9], O.K. Baker[179], P.J. Bakker[116], E. Bakos[15], D. Bakshi Gupta[7], S. Balaji[154], R. Balasubramanian[116], E.M. Baldin[118b,118a], P. Balek[139], E. Ballabene[67a,67b], F. Balli[141], L.M. Baltes[60a], W.K. Balunas[31], J. Balz[97], E. Banas[83], M. Bandieramonte[135], A. Bandyopadhyay[23], S. Bansal[23], L. Barak[158], E.L. Barberio[102], D. Barberis[54b,54a], M. Barbero[99], G. Barbour[93], K.N. Barends[32a], T. Barillari[112], M-S. Barisits[35], J. Barkeloo[128], T. Barklow[150], R.M. Barnett[17], P. Baron[127], A. Baroncelli[59a], G. Barone[28], A.J. Barr[131], L. Barranco Navarro[44a,44b], F. Barreiro[96], J. Barreiro Guimarães da Costa[14a], U. Barron[158], S. Barsov[134], F. Bartels[60a], R. Bartoldus[150], G. Bartolini[99], A.E. Barton[88], P. Bartos[27a], A. Basalaev[45], A. Basan[97], M. Baselga[45], I. Bashta[73a,73b], A. Bassalat[63,af], M.J. Basso[163], C.R. Basson[98], R.L. Bates[56], S. Batlamous[34e], J.R. Batley[31], B. Batool[148], M. Battaglia[142], M. Bauce[71a,71b], F. Bauer[141,*], P. Bauer[23], A. Bayirli[11c], J.B. Beacham[48], T. Beau[132], P.H. Beauchemin[166], F. Becherer[51], P. Bechtle[23], H.P. Beck[19,p], K. Becker[174], C. Becot[45], A.J. Beddall[11c,ab], V.A. Bednyakov[78], C.P. Bee[152], T.A. Beermann[35], M. Begalli[79b], M. Begel[28], A. Behera[152], J.K. Behr[45], C. Beirao Da Cruz E Silva[35], J.F. Beirer[52,35], F. Beisiegel[23], M. Belfkir[121b], G. Bella[158], L. Bellagamba[22b], A. Bellerive[33], P. Bellos[20], K. Beloborodov[118b,118a], K. Belotskiy[109], N.L. Belyaev[109], D. Benchekroun[34a], Y. Benhammou[158], D.P. Benjamin[28], M. Benoit[28], J.R. Bensinger[25], S. Bentvelsen[116], L. Beresford[35], M. Beretta[50], D. Berge[18], E. Bergeaas Kuutmann[168], N. Berger[4], B. Bergmann[138], L.J. Bergsten[25], J. Beringer[17], S. Berlendis[6], G. Bernardi[132], C. Bernius[150], F.U. Bernlochner[23], T. Berry[92], P. Berta[139],

JHEP08(2022)089

I.A. Bertram[88], O. Bessidskaia Bylund[178], S. Bethke[112], A. Betti[41], A.J. Bevan[91], S. Bhatta[152], D.S. Bhattacharya[173], P. Bhattarai[25], V.S. Bhopatkar[5], R. Bi[135], R. Bi[28], R.M. Bianchi[135], O. Biebel[111], R. Bielski[128], N.V. Biesuz[70a,70b], M. Biglietti[73a], T.R.V. Billoud[138], M. Bindi[52], A. Bingul[11d], C. Bini[71a,71b], S. Biondi[22b,22a], A. Biondini[89], C.J. Birch-sykes[98], G.A. Bird[20,140], M. Birman[176], T. Bisanz[35], J.P. Biswal[2], D. Biswas[177,j], A. Bitadze[98], K. Bjørke[130], I. Bloch[45], C. Blocker[25], A. Blue[56], U. Blumenschein[91], J. Blumenthal[97], G.J. Bobbink[116], V.S. Bobrovnikov[118b,118a], M. Boehler[51], D. Bogavac[13], A.G. Bogdanchikov[118b,118a], C. Bohm[44a], V. Boisvert[92], P. Bokan[45], T. Bold[82a], M. Bomben[132], M. Bona[91], M. Boonekamp[141], C.D. Booth[92], A.G. Borbély[56], H.M. Borecka-Bielska[107], L.S. Borgna[93], G. Borissov[88], D. Bortoletto[131], D. Boscherini[22b], M. Bosman[13], J.D. Bossio Sola[35], K. Bouaouda[34a], J. Boudreau[135], E.V. Bouhova-Thacker[88], D. Boumediene[37], R. Bouquet[132], A. Boveia[124], J. Boyd[35], D. Boye[28], I.R. Boyko[78], J. Bracinik[20], N. Brahimi[59d,59c], G. Brandt[178], O. Brandt[31], F. Braren[45], B. Brau[100], J.E. Brau[128], W.D. Breaden Madden[56], K. Brendlinger[45], R. Brener[176], L. Brenner[35], R. Brenner[168], S. Bressler[176], B. Brickwedde[97], D. Britton[56], D. Britzger[112], I. Brock[23], G. Brooijmans[38], W.K. Brooks[143e], E. Brost[28], P.A. Bruckman de Renstrom[83], B. Brüers[45], D. Bruncko[27b], A. Bruni[22b], G. Bruni[22b], M. Bruschi[22b], N. Bruscino[71a,71b], L. Bryngemark[150], T. Buanes[16], Q. Buat[145], P. Buchholz[148], A.G. Buckley[56], I.A. Budagov[78], M.K. Bugge[130], O. Bulekov[109], B.A. Bullard[58], S. Burdin[89], C.D. Burgard[45], A.M. Burger[126], B. Burghgrave[7], J.T.P. Burr[31], C.D. Burton[10], J.C. Burzynski[149], E.L. Busch[38], V. Büscher[97], P.J. Bussey[56], J.M. Butler[24], C.M. Buttar[56], J.M. Butterworth[93], W. Buttinger[140], C.J. Buxo Vazquez[104], A.R. Buzykaev[118b,118a], G. Cabras[22b], S. Cabrera Urbán[170], D. Caforio[55], H. Cai[135], V.M.M. Cairo[150], O. Cakir[3a], N. Calace[35], P. Calafiura[17], G. Calderini[132], P. Calfayan[64], G. Callea[56], L.P. Caloba[79b], D. Calvet[37], S. Calvet[37], T.P. Calvet[99], M. Calvetti[70a,70b], R. Camacho Toro[132], S. Camarda[35], D. Camarero Munoz[96], P. Camarri[72a,72b], M.T. Camerlingo[73a,73b], D. Cameron[130], C. Camincher[172], M. Campanelli[93], A. Camplani[39], V. Canale[68a,68b], A. Canesse[101], M. Cano Bret[76], J. Cantero[96], Y. Cao[169], F. Capocasa[25], M. Capua[40b,40a], A. Carbone[67a,67b], R. Cardarelli[72a], J.C.J. Cardenas[7], F. Cardillo[170], G. Carducci[40b,40a], T. Carli[35], G. Carlino[68a], B.T. Carlson[135], E.M. Carlson[172,164a], L. Carminati[67a,67b], M. Carnesale[71a,71b], S. Caron[115], E. Carquin[143e], S. Carrá[45], G. Carratta[22b,22a], J.W.S. Carter[163], T.M. Carter[49], D. Casadei[32c], M.P. Casado[13,g], A.F. Casha[163], E.G. Castiglia[179], F.L. Castillo[60a], L. Castillo Garcia[13], V. Castillo Gimenez[170], N.F. Castro[136a,136e], A. Catinaccio[35], J.R. Catmore[130], V. Cavaliere[28], N. Cavalli[22b,22a], V. Cavasinni[70a,70b], E. Celebi[11c], F. Celli[131], M.S. Centonze[66a,66b], K. Cerny[127], A.S. Cerqueira[79a], A. Cerri[153], L. Cerrito[72a,72b], F. Cerutti[17], A. Cervelli[22b], S.A. Cetin[11c,ab], Z. Chadi[34a], D. Chakraborty[117], M. Chala[136f], J. Chan[177], W.S. Chan[116], W.Y. Chan[89], J.D. Chapman[31], B. Chargeishvili[156b], D.G. Charlton[20], T.P. Charman[91], M. Chatterjee[19], S. Chekanov[5], S.V. Chekulaev[164a], G.A. Chelkov[78,ad], A. Chen[103], B. Chen[158], B. Chen[172], C. Chen[59a], H. Chen[14c], H. Chen[28], J. Chen[59c], J. Chen[25], S. Chen[133], S.J. Chen[14c], X. Chen[59c], X. Chen[14b], Y. Chen[59a], C.L. Cheng[177], H.C. Cheng[61a], A. Cheplakov[78], E. Cheremushkina[45], E. Cherepanova[78], R. Cherkaoui El Moursli[34e], E. Cheu[6], K. Cheung[62], L. Chevalier[141], V. Chiarella[50], G. Chiarelli[70a], G. Chiodini[66a], A.S. Chisholm[20], A. Chitan[26b], Y.H. Chiu[172], M.V. Chizhov[78], K. Choi[10], A.R. Chomont[71a,71b], Y. Chou[100], E.Y.S. Chow[116], T. Chowdhury[32f], L.D. Christopher[32f], M.C. Chu[61a], X. Chu[14a,14d], J. Chudoba[137], J.J. Chwastowski[83], D. Cieri[112], K.M. Ciesla[83], V. Cindro[90], A. Ciocio[17], F. Cirotto[68a,68b], Z.H. Citron[176,k], M. Citterio[67a], D.A. Ciubotaru[26b], B.M. Ciungu[163], A. Clark[53], P.J. Clark[49], J.M. Clavijo Columbie[45], S.E. Clawson[98], C. Clement[44a,44b], L. Clissa[22b,22a], Y. Coadou[99], M. Cobal[65a,65c], A. Coccaro[54b], R.F. Coelho Barrue[136a], R. Coelho Lopes De Sa[100], S. Coelli[67a], H. Cohen[158], A.E.C. Coimbra[35], B. Cole[38], J. Collot[57], P. Conde Muiño[136a,136g],

JHEP08(2022)089

S.H. Connell[32c], I.A. Connelly[56], E.I. Conroy[131], F. Conventi[68a,aj], H.G. Cooke[20], A.M. Cooper-Sarkar[131], F. Cormier[171], L.D. Corpe[35], M. Corradi[71a,71b], E.E. Corrigan[95], F. Corriveau[101,w], M.J. Costa[170], F. Costanza[4], D. Costanzo[146], B.M. Cote[124], G. Cowan[92], J.W. Cowley[31], K. Cranmer[122], S. Crépé-Renaudin[57], F. Crescioli[132], M. Cristinziani[148], M. Cristoforetti[74a,74b,b], V. Croft[166], G. Crosetti[40b,40a], A. Cueto[35], T. Cuhadar Donszelmann[167], H. Cui[14a,14d], Z. Cui[6], A.R. Cukierman[150], W.R. Cunningham[56], F. Curcio[40b,40a], P. Czodrowski[35], M.M. Czurylo[60b], M.J. Da Cunha Sargedas De Sousa[59a], J.V. Da Fonseca Pinto[79b], C. Da Via[98], W. Dabrowski[82a], T. Dado[46], S. Dahbi[32f], T. Dai[103], C. Dallapiccola[100], M. Dam[39], G. D'amen[28], V. D'Amico[73a,73b], J. Damp[97], J.R. Dandoy[133], M.F. Daneri[29], M. Danninger[149], V. Dao[35], G. Darbo[54b], S. Darmora[5], A. Dattagupta[128], S. D'Auria[67a,67b], C. David[164b], T. Davidek[139], D.R. Davis[48], B. Davis-Purcell[33], I. Dawson[91], K. De[7], R. De Asmundis[68a], M. De Beurs[116], S. De Castro[22b,22a], N. De Groot[115], P. de Jong[116], H. De la Torre[104], A. De Maria[14c], A. De Salvo[71a], U. De Sanctis[72a,72b], M. De Santis[72a,72b], A. De Santo[153], J.B. De Vivie De Regie[57], D.V. Dedovich[78], J. Degens[116], A.M. Deiana[41], J. Del Peso[96], F. Del Rio[60a], F. Deliot[141], C.M. Delitzsch[46], M. Della Pietra[68a,68b], D. Della Volpe[53], A. Dell'Acqua[35], L. Dell'Asta[67a,67b], M. Delmastro[4], P.A. Delsart[57], S. Demers[179], M. Demichev[78], S.P. Denisov[119], L. D'Eramo[117], D. Derendarz[83], F. Derue[132], P. Dervan[89], K. Desch[23], K. Dette[163], C. Deutsch[23], P.O. Deviveiros[35], F.A. Di Bello[71a,71b], A. Di Ciaccio[72a,72b], L. Di Ciaccio[4], A. Di Domenico[71a,71b], C. Di Donato[68a,68b], A. Di Girolamo[35], G. Di Gregorio[70a,70b], A. Di Luca[74a,74b,b], B. Di Micco[73a,73b], R. Di Nardo[73a,73b], C. Diaconu[99], F.A. Dias[116], T. Dias Do Vale[149], M.A. Diaz[143a], F.G. Diaz Capriles[23], M. Didenko[170], E.B. Diehl[103], S. Díez Cornell[45], C. Diez Pardos[148], C. Dimitriadi[23,168], A. Dimitrievska[17], W. Ding[14b], J. Dingfelder[23], I-M. Dinu[26b], S.J. Dittmeier[60b], F. Dittus[35], F. Djama[99], T. Djobava[156b], J.I. Djuvsland[16], M.A.B. Do Vale[144], D. Dodsworth[25], C. Doglioni[98,95], J. Dolejsi[139], Z. Dolezal[139], M. Donadelli[79c], B. Dong[59c], J. Donini[37], A. D'onofrio[14c], M. D'Onofrio[89], J. Dopke[140], A. Doria[68a], M.T. Dova[87], A.T. Doyle[56], E. Drechsler[149], E. Dreyer[176], A.S. Drobac[166], D. Du[59a], T.A. du Pree[116], F. Dubinin[108], M. Dubovsky[27a], E. Duchovni[176], G. Duckeck[111], O.A. Ducu[35,26b], D. Duda[112], A. Dudarev[35], M. D'uffizi[98], L. Duflot[63], M. Dührssen[35], C. Dülsen[178], A.E. Dumitriu[26b], M. Dunford[60a], S. Dungs[46], K. Dunne[44a,44b], A. Duperrin[99], H. Duran Yildiz[3a], M. Düren[55], A. Durglishvili[156b], B. Dutta[45], B.L. Dwyer[117], G.I. Dyckes[17], M. Dyndal[82a], S. Dysch[98], B.S. Dziedzic[83], B. Eckerova[27a], M.G. Eggleston[48], E. Egidio Purcino De Souza[79b], L.F. Ehrke[53], G. Eigen[16], K. Einsweiler[17], T. Ekelof[168], Y. El Ghazali[34b], H. El Jarrari[34e], A. El Moussaouy[34a], V. Ellajosyula[168], M. Ellert[168], F. Ellinghaus[178], A.A. Elliot[91], N. Ellis[35], J. Elmsheuser[28], M. Elsing[35], D. Emeliyanov[140], A. Emerman[38], Y. Enari[160], I. Ene[17], J. Erdmann[46], A. Ereditato[19], P.A. Erland[83], M. Errenst[178], M. Escalier[63], C. Escobar[170], E. Etzion[158], G. Evans[136a], H. Evans[64], M.O. Evans[153], A. Ezhilov[134], S. Ezzarqtouni[34a], F. Fabbri[56], L. Fabbri[22b,22a], G. Facini[174], V. Fadeyev[142], R.M. Fakhrutdinov[119], S. Falciano[71a], P.J. Falke[23], S. Falke[35], J. Faltova[139], Y. Fan[14a], Y. Fang[14a], G. Fanourakis[43], M. Fanti[67a,67b], M. Faraj[59c], A. Farbin[7], A. Farilla[73a], E.M. Farina[69a,69b], T. Farooque[104], S.M. Farrington[49], F. Fassi[34e], D. Fassouliotis[8], M. Faucci Giannelli[72a,72b], W.J. Fawcett[31], L. Fayard[63], O.L. Fedin[134,o], G. Fedotov[134], M. Feickert[169], L. Feligioni[99], A. Fell[146], D.E. Fellers[128], C. Feng[59b], M. Feng[14b], M.J. Fenton[167], A.B. Fenyuk[119], S.W. Ferguson[42], J.A. Fernandez Pretel[51], J. Ferrando[45], A. Ferrari[168], P. Ferrari[116], R. Ferrari[69a], D. Ferrere[53], C. Ferretti[103], F. Fiedler[97], A. Filipčič[90], F. Filthaut[115], M.C.N. Fiolhais[136a,136c,a], L. Fiorini[170], F. Fischer[148], W.C. Fisher[104], T. Fitschen[20,63], I. Fleck[148], P. Fleischmann[103], T. Flick[178], L. Flores[133], M. Flores[32d], L.R. Flores Castillo[61a], F.M. Follega[74a,74b], N. Fomin[16], J.H. Foo[163], B.C. Forland[64], A. Formica[141], A.C. Forti[98], E. Fortin[99], A.W. Fortman[58], M.G. Foti[17], L. Fountas[8],

JHEP08(2022)089

D. Fournier[63], H. Fox[88], P. Francavilla[70a,70b], S. Francescato[58], M. Franchini[22b,22a], S. Franchino[60a], D. Francis[35], L. Franco[4], L. Franconi[19], M. Franklin[58], G. Frattari[71a,71b], A.C. Freegard[91], P.M. Freeman[20], W.S. Freund[79b], E.M. Freundlich[46], D. Froidevaux[35], J.A. Frost[131], Y. Fu[59a], M. Fujimoto[123], E. Fullana Torregrosa[170], J. Fuster[170], A. Gabrielli[22b,22a], A. Gabrielli[35], P. Gadow[45], G. Gagliardi[54b,54a], L.G. Gagnon[17], G.E. Gallardo[131], E.J. Gallas[131], B.J. Gallop[140], R. Gamboa Goni[91], K.K. Gan[124], S. Ganguly[160], J. Gao[59a], Y. Gao[49], F.M. Garay Walls[143a], B. Garcia[28], C. García[170], J.E. García Navarro[170], J.A. García Pascual[14a], M. Garcia-Sciveres[17], R.W. Gardner[36], D. Garg[76], R.B. Garg[150], S. Gargiulo[51], C.A. Garner[163], V. Garonne[28], S.J. Gasiorowski[145], P. Gaspar[79b], G. Gaudio[69a], P. Gauzzi[71a,71b], I.L. Gavrilenko[108], A. Gavrilyuk[120], C. Gay[171], G. Gaycken[45], E.N. Gazis[9], A.A. Geanta[26b], C.M. Gee[142], J. Geisen[95], M. Geisen[97], C. Gemme[54b], M.H. Genest[57], S. Gentile[71a,71b], S. George[92], W.F. George[20], T. Geralis[43], L.O. Gerlach[52], P. Gessinger-Befurt[35], M. Ghasemi Bostanabad[172], A. Ghosh[167], A. Ghosh[6], B. Giacobbe[22b], S. Giagu[71a,71b], N. Giangiacomi[163], P. Giannetti[70a], A. Giannini[59a], S.M. Gibson[92], M. Gignac[142], D.T. Gil[82b], B.J. Gilbert[38], D. Gillberg[33], G. Gilles[116], N.E.K. Gillwald[45], L. Ginabat[132], D.M. Gingrich[2,ai], M.P. Giordani[65a,65c], P.F. Giraud[141], G. Giugliarelli[65a,65c], D. Giugni[67a], F. Giuli[72a,72b], I. Gkialas[8,h], P. Gkountoumis[9], L.K. Gladilin[110], C. Glasman[96], G.R. Gledhill[128], M. Glisic[128], I. Gnesi[40b,d], Y. Go[28], M. Goblirsch-Kolb[25], D. Godin[107], S. Goldfarb[102], T. Golling[53], D. Golubkov[119], J.P. Gombas[104], A. Gomes[136a,136b], R. Goncalves Gama[52], R. Gonçalo[136a,136c], G. Gonella[128], L. Gonella[20], A. Gongadze[78], F. Gonnella[20], J.L. Gonski[38], S. González de la Hoz[170], S. Gonzalez Fernandez[13], R. Gonzalez Lopez[89], C. Gonzalez Renteria[17], R. Gonzalez Suarez[168], S. Gonzalez-Sevilla[53], G.R. Gonzalvo Rodriguez[170], R.Y. González Andana[49], L. Goossens[35], N.A. Gorasia[20], P.A. Gorbounov[120], H.A. Gordon[28], B. Gorini[35], E. Gorini[66a,66b], A. Gorišek[90], A.T. Goshaw[48], M.I. Gostkin[78], C.A. Gottardo[115], M. Gouighri[34b], V. Goumarre[45], A.G. Goussiou[145], N. Govender[32c], C. Goy[4], I. Grabowska-Bold[82a], K. Graham[33], E. Gramstad[130], S. Grancagnolo[18], M. Grandi[153], V. Gratchev[134], P.M. Gravila[26f], F.G. Gravili[66a,66b], H.M. Gray[17], C. Grefe[23], I.M. Gregor[45], P. Grenier[150], K. Grevtsov[45], C. Grieco[13], A.A. Grillo[142], K. Grimm[30,l], S. Grinstein[13,u], J.-F. Grivaz[63], S. Groh[97], E. Gross[176], J. Grosse-Knetter[52], C. Grud[103], A. Grummer[114], J.C. Grundy[131], L. Guan[103], W. Guan[177], C. Gubbels[171], J.G.R. Guerrero Rojas[170], F. Guescini[112], D. Guest[18], R. Gugel[97], A. Guida[45], T. Guillemin[4], S. Guindon[35], F. Guo[14a], J. Guo[59c], L. Guo[63], Y. Guo[103], R. Gupta[45], S. Gurbuz[23], G. Gustavino[35], M. Guth[53], P. Gutierrez[125], L.F. Gutierrez Zagazeta[133], C. Gutschow[93], C. Guyot[141], C. Gwenlan[131], C.B. Gwilliam[89], E.S. Haaland[130], A. Haas[122], M. Habedank[45], C. Haber[17], H.K. Hadavand[7], A. Hadef[97], S. Hadzic[112], M. Haleem[173], J. Haley[126], J.J. Hall[146], G.D. Hallewell[99], L. Halser[19], K. Hamano[172], H. Hamdaoui[34e], M. Hamer[23], G.N. Hamity[49], J. Han[59b], K. Han[59a], L. Han[14c], L. Han[59a], S. Han[17], Y.F. Han[163], K. Hanagaki[80,s], M. Hance[142], D.A. Hangal[38], M.D. Hank[36], R. Hankache[98], E. Hansen[95], J.B. Hansen[39], J.D. Hansen[39], P.H. Hansen[39], K. Hara[165], D. Harada[53], T. Harenberg[178], S. Harkusha[105], Y.T. Harris[131], P.F. Harrison[174], N.M. Hartman[150], N.M. Hartmann[111], Y. Hasegawa[147], A. Hasib[49], S. Haug[19], R. Hauser[104], M. Havranek[138], C.M. Hawkes[20], R.J. Hawkings[35], S. Hayashida[113], D. Hayden[104], C. Hayes[103], R.L. Hayes[171], C.P. Hays[131], J.M. Hays[91], H.S. Hayward[89], F. He[59a], Y. He[161], Y. He[132], M.P. Heath[49], V. Hedberg[95], A.L. Heggelund[130], N.D. Hehir[91], C. Heidegger[51], K.K. Heidegger[51], W.D. Heidorn[77], J. Heilman[33], S. Heim[45], T. Heim[17], B. Heinemann[45,ag], J.G. Heinlein[133], J.J. Heinrich[128], L. Heinrich[35], J. Hejbal[137], L. Helary[45], A. Held[122], C.M. Helling[171], S. Hellman[44a,44b], C. Helsens[35], R.C.W. Henderson[88], L. Henkelmann[31], A.M. Henriques Correia[35], H. Herde[150], Y. Hernández Jiménez[152], H. Herr[97], M.G. Herrmann[111],

JHEP08(2022)089

T. Herrmann[47], G. Herten[51], R. Hertenberger[111], L. Hervas[35], N.P. Hessey[164a], H. Hibi[81], E. Higón-Rodriguez[170], S.J. Hillier[20], I. Hinchliffe[17], F. Hinterkeuser[23], M. Hirose[129], S. Hirose[165], D. Hirschbuehl[178], B. Hiti[90], O. Hladik[137], J. Hobbs[152], R. Hobincu[26e], S. Höche[r], N. Hod[176], M.C. Hodgkinson[146], B.H. Hodkinson[31], A. Hoecker[35], J. Hofer[45], D. Hohn[51], T. Holm[23], M. Holzbock[112], L.B.A.H. Hommels[31], B.P. Honan[98], J. Hong[59c], T.M. Hong[135], Y. Hong[52], J.C. Honig[51], A. Hönle[112], B.H. Hooberman[169], W.H. Hopkins[5], Y. Horii[113], L.A. Horyn[36], S. Hou[155], J. Howarth[56], J. Hoya[87], M. Hrabovsky[127], A. Hrynevich[106], T. Hryn'ova[4], P.J. Hsu[62], S.-C. Hsu[145], Q. Hu[38], S. Hu[59c], Y.F. Hu[14a,14d,ak], D.P. Huang[93], X. Huang[14c], Y. Huang[59a], Y. Huang[14a], Z. Hubacek[138], M. Huebner[23], F. Huegging[23], T.B. Huffman[131], M. Huhtinen[35], S.K. Huiberts[16], R. Hulsken[57], N. Huseynov[12,ac], J. Huston[104], J. Huth[58], R. Hyneman[150], S. Hyrych[27a], G. Iacobucci[53], G. Iakovidis[28], I. Ibragimov[148], L. Iconomidou-Fayard[63], P. Iengo[35], R. Iguchi[160], T. Iizawa[53], Y. Ikegami[80], A. Ilg[19], N. Ilic[163], H. Imam[34a], T. Ingebretsen Carlson[44a,44b], G. Introzzi[69a,69b], M. Iodice[73a], V. Ippolito[71a,71b], M. Ishino[160], W. Islam[177], C. Issever[18,45], S. Istin[11c,al], H. Ito[175], J.M. Iturbe Ponce[61a], R. Iuppa[74a,74b], A. Ivina[176], J.M. Izen[42], V. Izzo[68a], P. Jacka[137], P. Jackson[1], R.M. Jacobs[45], B.P. Jaeger[149], C.S. Jagfeld[111], G. Jäkel[178], K. Jakobs[51], T. Jakoubek[176], J. Jamieson[56], K.W. Janas[82a], G. Jarlskog[95], A.E. Jaspan[89], T. Javůrek[35], M. Javurkova[100], F. Jeanneau[141], L. Jeanty[128], J. Jejelava[156a,y], P. Jenni[51,e], S. Jézéquel[4], J. Jia[152], Z. Jia[14c], Y. Jiang[59a], S. Jiggins[49], J. Jimenez Pena[112], S. Jin[14c], A. Jinaru[26b], O. Jinnouchi[161], H. Jivan[32f], P. Johansson[146], K.A. Johns[6], C.A. Johnson[64], D.M. Jones[31], E. Jones[174], R.W.L. Jones[88], T.J. Jones[89], J. Jovicevic[15], X. Ju[17], J.J. Junggeburth[35], A. Juste Rozas[13,u], S. Kabana[143d], A. Kaczmarska[83], M. Kado[71a,71b], H. Kagan[124], M. Kagan[150], A. Kahn[38], A. Kahn[133], C. Kahra[97], T. Kaji[175], E. Kajomovitz[157], N. Kakati[176], C.W. Kalderon[28], A. Kamenshchikov[163], N.J. Kang[142], Y. Kano[113], D. Kar[32f], K. Karava[131], M.J. Kareem[164b], E. Karentzos[51], I. Karkanias[159], S.N. Karpov[78], Z.M. Karpova[78], V. Kartvelishvili[88], A.N. Karyukhin[119], E. Kasimi[159], C. Kato[59d], J. Katzy[45], S. Kaur[33], K. Kawade[147], K. Kawagoe[86], T. Kawaguchi[113], T. Kawamoto[141], G. Kawamura[52], E.F. Kay[172], F.I. Kaya[166], S. Kazakos[13], V.F. Kazanin[118b,118a], Y. Ke[152], J.M. Keaveney[32a], R. Keeler[172], J.S. Keller[33], A.S. Kelly[93], D. Kelsey[153], J.J. Kempster[20], J. Kendrick[20], K.E. Kennedy[38], O. Kepka[137], S. Kersten[178], B.P. Kerševan[90], S. Ketabchi Haghighat[163], M. Khandoga[132], A. Khanov[126], A.G. Kharlamov[118b,118a], T. Kharlamova[118b,118a], E.E. Khoda[145], T.J. Khoo[18], G. Khoriauli[173], E. Khramov[78], J. Khubua[156b], M. Kiehn[35], A. Kilgallon[128], E. Kim[161], Y.K. Kim[36], N. Kimura[93], A. Kirchhoff[52], D. Kirchmeier[47], C. Kirfel[23], J. Kirk[140], A.E. Kiryunin[112], T. Kishimoto[160], D.P. Kisliuk[163], C. Kitsaki[9], O. Kivernyk[23], M. Klassen[60a], C. Klein[33], L. Klein[173], M.H. Klein[103], M. Klein[89], U. Klein[89], P. Klimek[35], A. Klimentov[28], F. Klimpel[112], T. Klingl[23], T. Klioutchnikova[35], F.F. Klitzner[111], P. Kluit[116], S. Kluth[112], E. Kneringer[75], T.M. Knight[163], A. Knue[51], D. Kobayashi[86], R. Kobayashi[84], M. Kocian[150], T. Kodama[160], P. Kodys[139], D.M. Koeck[153], P.T. Koenig[23], T. Koffas[33], N.M. Köhler[35], M. Kolb[141], I. Koletsou[4], T. Komarek[127], K. Köneke[51], A.X.Y. Kong[1], T. Kono[123], V. Konstantinides[93], N. Konstantinidis[93], B. Konya[95], R. Kopeliansky[64], S. Koperny[82a], K. Korcyl[83], K. Kordas[159], G. Koren[158], A. Korn[93], S. Korn[52], I. Korolkov[13], N. Korotkova[110], B. Kortman[116], O. Kortner[112], S. Kortner[112], W.H. Kostecka[117], V.V. Kostyukhin[148,162], A. Kotsokechagia[63], A. Kotwal[48], A. Koulouris[35], A. Kourkoumeli-Charalampidi[69a,69b], C. Kourkoumelis[8], E. Kourlitis[5], O. Kovanda[153], R. Kowalewski[172], W. Kozanecki[141], A.S. Kozhin[119], V.A. Kramarenko[110], G. Kramberger[90], P. Kramer[97], M.W. Krasny[132], A. Krasznahorkay[35], J.A. Kremer[97], J. Kretzschmar[89], K. Kreul[18], P. Krieger[163], F. Krieter[111], S. Krishnamurthy[100], A. Krishnan[60b], M. Krivos[139], K. Krizka[17], K. Kroeninger[46], H. Kroha[112], J. Kroll[137], J. Kroll[133], K.S. Krowpman[104], U. Kruchonak[78], H. Krüger[23], N. Krumnack[77], M.C. Kruse[48],

JHEP08(2022)089

J.A. Krzysiak[83], A. Kubota[161], O. Kuchinskaia[162], S. Kuday[3a], D. Kuechler[45], J.T. Kuechler[45], S. Kuehn[35], T. Kuhl[45], V. Kukhtin[78], Y. Kulchitsky[105,ac], S. Kuleshov[143c], M. Kumar[32f], N. Kumari[99], M. Kuna[57], A. Kupco[137], T. Kupfer[46], O. Kuprash[51], H. Kurashige[81], L.L. Kurchaninov[164a], Y.A. Kurochkin[105], A. Kurova[109], E.S. Kuwertz[35], M. Kuze[161], A.K. Kvam[145], J. Kvita[127], T. Kwan[101], K.W. Kwok[61a], C. Lacasta[170], F. Lacava[71a,71b], H. Lacker[18], D. Lacour[132], N.N. Lad[93], E. Ladygin[78], B. Laforge[132], T. Lagouri[143d], S. Lai[52], I.K. Lakomiec[82a], N. Lalloue[57], J.E. Lambert[125], S. Lammers[64], W. Lampl[6], C. Lampoudis[159], E. Lançon[28], U. Landgraf[51], M.P.J. Landon[91], V.S. Lang[51], J.C. Lange[52], R.J. Langenberg[100], A.J. Lankford[167], F. Lanni[28], K. Lantzsch[23], A. Lanza[69a], A. Lapertosa[54b,54a], J.F. Laporte[141], T. Lari[67a], F. Lasagni Manghi[22b], M. Lassnig[35], V. Latonova[137], T.S. Lau[61a], A. Laudrain[97], A. Laurier[33], M. Lavorgna[68a,68b], S.D. Lawlor[92], Z. Lawrence[98], M. Lazzaroni[67a,67b], B. Le[98], B. Leban[90], A. Lebedev[77], M. LeBlanc[35], T. LeCompte[5], F. Ledroit-Guillon[57], A.C.A. Lee[93], G.R. Lee[16], L. Lee[58], S.C. Lee[155], L.L. Leeuw[32c], B. Lefebvre[164a], H.P. Lefebvre[92], M. Lefebvre[172], C. Leggett[17], K. Lehmann[149], G. Lehmann Miotto[35], W.A. Leight[100], A. Leisos[159,t], M.A.L. Leite[79c], C.E. Leitgeb[45], R. Leitner[139], K.J.C. Leney[41], T. Lenz[23], S. Leone[70a], C. Leonidopoulos[49], A. Leopold[151], C. Leroy[107], R. Les[104], C.G. Lester[31], M. Levchenko[134], J. Levêque[4], D. Levin[103], L.J. Levinson[176], D.J. Lewis[20], B. Li[14b], B. Li[59b], C. Li[59a], C-Q. Li[59c,59d], H. Li[59a], H. Li[59b], H. Li[59b], J. Li[59c], K. Li[145], L. Li[59c], M. Li[14a,14d], Q.Y. Li[59a], S. Li[59d,59c,c], T. Li[59b], X. Li[45], Z. Li[59b], Z. Li[131], Z. Li[101], Z. Li[89], Z. Liang[14a], M. Liberatore[45], B. Liberti[72a], K. Lie[61c], J. Lieber Marin[79b], K. Lin[104], R.A. Linck[64], R.E. Lindley[6], J.H. Lindon[2], A. Linss[45], E. Lipeles[133], A. Lipniacka[16], T.M. Liss[169,ah], A. Lister[171], J.D. Little[4], B. Liu[14a], B.X. Liu[149], D. Liu[59d,59c], J.B. Liu[59a], J.K.K. Liu[31], K. Liu[59d,59c], M. Liu[59a], M.Y. Liu[59a], P. Liu[14a], Q. Liu[59d,145,59c], X. Liu[59a], Y. Liu[45], Y. Liu[14c,14d], Y.L. Liu[103], Y.W. Liu[59a], M. Livan[69a,69b], J. Llorente Merino[149], S.L. Lloyd[91], E.M. Lobodzinska[45], P. Loch[6], S. Loffredo[72a,72b], T. Lohse[18], K. Lohwasser[146], M. Lokajicek[137], J.D. Long[169], I. Longarini[71a,71b], L. Longo[66a,66b], R. Longo[169], I. Lopez Paz[35], A. Lopez Solis[45], J. Lorenz[111], N. Lorenzo Martinez[4], A.M. Lory[111], A. Lösle[51], X. Lou[44a,44b], X. Lou[14a], A. Lounis[63], J. Love[5], P.A. Love[88], J.J. Lozano Bahilo[170], G. Lu[14a,14d], M. Lu[76], S. Lu[133], Y.J. Lu[62], H.J. Lubatti[145], C. Luci[71a,71b], F.L. Lucio Alves[14c], A. Lucotte[57], F. Luehring[64], I. Luise[152], O. Lundberg[151], B. Lund-Jensen[151], N.A. Luongo[128], M.S. Lutz[158], D. Lynn[28], H. Lyons[89], R. Lysak[137], E. Lytken[95], F. Lyu[14a], V. Lyubushkin[78], T. Lyubushkina[78], H. Ma[28], L.L. Ma[59b], Y. Ma[93], D.M. Mac Donell[172], G. Maccarrone[50], J.C. MacDonald[146], R. Madar[37], W.F. Mader[47], J. Maeda[81], T. Maeno[28], M. Maerker[47], V. Magerl[51], J. Magro[65a,65c], D.J. Mahon[38], C. Maidantchik[79b], A. Maio[136a,136b,136d], K. Maj[82a], O. Majersky[27a], S. Majewski[128], N. Makovec[63], V. Maksimovic[15], B. Malaescu[132], Pa. Malecki[83], V.P. Maleev[134], F. Malek[57], D. Malito[40b,40a], U. Mallik[76], C. Malone[31], S. Maltezos[9], S. Malyukov[78], J. Mamuzic[170], G. Mancini[50], J.P. Mandalia[91], I. Mandić[90], L. Manhaes de Andrade Filho[79a], I.M. Maniatis[159], M. Manisha[141], J. Manjarres Ramos[47], D.C. Mankad[176], K.H. Mankinen[95], A. Mann[111], A. Manousos[75], B. Mansoulie[141], S. Manzoni[35], A. Marantis[159,t], G. Marchiori[132], M. Marcisovsky[137], L. Marcoccia[72a,72b], C. Marcon[95], M. Marinescu[20], M. Marjanovic[125], Z. Marshall[17], S. Marti-Garcia[170], T.A. Martin[174], V.J. Martin[49], B. Martin dit Latour[16], L. Martinelli[71a,71b], M. Martinez[13,u], P. Martinez Agullo[170], V.I. Martinez Outschoorn[100], P. Martinez Suarez[13], S. Martin-Haugh[140], V.S. Martoiu[26b], A.C. Martyniuk[93], A. Marzin[35], S.R. Maschek[112], L. Masetti[97], T. Mashimo[160], J. Masik[98], A.L. Maslennikov[118b,118a], L. Massa[22b], P. Massarotti[68a,68b], P. Mastrandrea[70a,70b], A. Mastroberardino[40b,40a], T. Masubuchi[160], T. Mathisen[168], A. Matic[111], N. Matsuzawa[160], J. Maurer[26b], B. Maček[90], D.A. Maximov[118b,118a], R. Mazini[155], I. Maznas[159], S.M. Mazza[142], C. Mc Ginn[28], J.P. Mc Gowan[101], S.P. Mc Kee[103], T.G. McCarthy[112], W.P. McCormack[17], E.F. McDonald[102],

JHEP08(2022)089

A.E. McDougall[116], J.A. Mcfayden[153], G. Mchedlidze[156b], M.A. McKay[41], R.P. Mckenzie[32f], D.J. Mclaughlin[93], K.D. McLean[172], S.J. McMahon[140], P.C. McNamara[102], R.A. McPherson[172,w], J.E. Mdhluli[32f], S. Meehan[35], T. Megy[37], S. Mehlhase[111], A. Mehta[89], B. Meirose[42], D. Melini[157], B.R. Mellado Garcia[32f], A.H. Melo[52], F. Meloni[45], A. Melzer[23], E.D. Mendes Gouveia[136a], A.M. Mendes Jacques Da Costa[20], H.Y. Meng[163], L. Meng[88], S. Menke[112], M. Mentink[35], E. Meoni[40b,40a], C. Merlassino[131], L. Merola[68a,68b], C. Meroni[67a], G. Merz[103], O. Meshkov[108,110], J.K.R. Meshreki[148], J. Metcalfe[5], A.S. Mete[5], C. Meyer[64], J-P. Meyer[141], M. Michetti[18], R.P. Middleton[140], L. Mijović[49], G. Mikenberg[176], M. Mikestikova[137], M. Mikuž[90], H. Mildner[146], A. Milic[163], C.D. Milke[41], D.W. Miller[36], L.S. Miller[33], A. Milov[176], D.A. Milstead[44a,44b], T. Min[14c], A.A. Minaenko[119], I.A. Minashvili[156b], L. Mince[56], A.I. Mincer[122], B. Mindur[82a], M. Mineev[78], Y. Minegishi[160], Y. Mino[84], L.M. Mir[13], M. Miralles Lopez[170], M. Mironova[131], T. Mitani[175], A. Mitra[174], V.A. Mitsou[170], O. Miu[163], P.S. Miyagawa[91], Y. Miyazaki[86], A. Mizukami[80], J.U. Mjörnmark[95], T. Mkrtchyan[60a], M. Mlynarikova[117], T. Moa[44a,44b], S. Mobius[52], K. Mochizuki[107], P. Moder[45], P. Mogg[111], A.F. Mohammed[14a], S. Mohapatra[38], G. Mokgatitswane[32f], B. Mondal[148], S. Mondal[138], K. Mönig[45], E. Monnier[99], L. Monsonis Romero[170], J. Montejo Berlingen[35], M. Montella[124], F. Monticelli[87], N. Morange[63], A.L. Moreira De Carvalho[136a], M. Moreno Llácer[170], C. Moreno Martinez[13], P. Morettini[54b], S. Morgenstern[174], D. Mori[149], M. Morii[58], M. Morinaga[160], V. Morisbak[130], A.K. Morley[35], A.P. Morris[93], L. Morvaj[35], P. Moschovakos[35], B. Moser[116], M. Mosidze[156b], T. Moskalets[51], P. Moskvitina[115], J. Moss[30,m], E.J.W. Moyse[100], S. Muanza[99], J. Mueller[135], R. Mueller[19], D. Muenstermann[88], G.A. Mullier[95], J.J. Mullin[133], D.P. Mungo[67a,67b], J.L. Munoz Martinez[13], F.J. Munoz Sanchez[98], M. Murin[98], W.J. Murray[174,140], A. Murrone[67a,67b], J.M. Muse[125], M. Muškinja[17], C. Mwewa[28], A.G. Myagkov[119,ad], A.J. Myers[7], A.A. Myers[135], G. Myers[64], M. Myska[138], B.P. Nachman[17], O. Nackenhorst[46], A.Nag Nag[47], K. Nagai[131], K. Nagano[80], J.L. Nagle[28], E. Nagy[99], A.M. Nairz[35], Y. Nakahama[80], K. Nakamura[80], H. Nanjo[129], F. Napolitano[60a], R. Narayan[41], E.A. Narayanan[114], I. Naryshkin[134], M. Naseri[33], C. Nass[23], G. Navarro[21a], J. Navarro-Gonzalez[170], R. Nayak[158], P.Y. Nechaeva[108], F. Nechansky[45], T.J. Neep[20], A. Negri[69a,69b], M. Negrini[22b], C. Nellist[115], C. Nelson[101], K. Nelson[103], S. Nemecek[137], M. Nessi[35,f], M.S. Neubauer[169], F. Neuhaus[97], J. Neundorf[45], R. Newhouse[171], P.R. Newman[20], C.W. Ng[135], Y.S. Ng[18], Y.W.Y. Ng[167], B. Ngair[34e], H.D.N. Nguyen[107], R.B. Nickerson[131], R. Nicolaidou[141], D.S. Nielsen[39], J. Nielsen[142], M. Niemeyer[52], N. Nikiforou[10], V. Nikolaenko[119,ad], I. Nikolic-Audit[132], K. Nikolopoulos[20], P. Nilsson[28], H.R. Nindhito[53], A. Nisati[71a], N. Nishu[2], R. Nisius[112], S.J. Noacco Rosende[87], T. Nobe[160], D.L. Noel[31], Y. Noguchi[84], I. Nomidis[132], M.A. Nomura[28], M.B. Norfolk[146], R.R.B. Norisam[93], J. Novak[90], T. Novak[45], O. Novgorodova[47], L. Novotny[138], R. Novotny[114], L. Nozka[127], K. Ntekas[167], E. Nurse[93], F.G. Oakham[33,ai], J. Ocariz[132], A. Ochi[81], I. Ochoa[136a], J.P. Ochoa-Ricoux[143a], S. Oda[86], S. Odaka[80], S. Oerdek[168], A. Ogrodnik[82a], A. Oh[98], C.C. Ohm[151], H. Oide[161], R. Oishi[160], M.L. Ojeda[45], Y. Okazaki[84], M.W. O'Keefe[89], Y. Okumura[160], A. Olariu[26b], L.F. Oleiro Seabra[136a], S.A. Olivares Pino[143d], D. Oliveira Damazio[28], D. Oliveira Goncalves[79a], J.L. Oliver[167], M.J.R. Olsson[167], A. Olszewski[83], J. Olszowska[83], Ö.O. Öncel[23], D.C. O'Neil[149], A.P. O'neill[19], A. Onofre[136a,136e], P.U.E. Onyisi[10], R.G. Oreamuno Madriz[117], M.J. Oreglia[36], G.E. Orellana[87], D. Orestano[73a,73b], N. Orlando[13], R.S. Orr[163], V. O'Shea[56], R. Ospanov[59a], G. Otero y Garzon[29], H. Otono[86], P.S. Ott[60a], G.J. Ottino[17], M. Ouchrif[34d], J. Ouellette[28], F. Ould-Saada[130], A. Ouraou[141,*], M. Owen[56], R.E. Owen[140], K.Y. Oyulmaz[11c], V.E. Ozcan[11c], N. Ozturk[7], S. Ozturk[11c,ab], J. Pacalt[127], H.A. Pacey[31], K. Pachal[48], A. Pacheco Pages[13], C. Padilla Aranda[13], S. Pagan Griso[17], G. Palacino[64], S. Palazzo[49], S. Palestini[35], M. Palka[82b], J. Pan[179], D.K. Panchal[10], C.E. Pandini[53], J.G. Panduro Vazquez[92], P. Pani[45], G. Panizzo[65a,65c],

JHEP08(2022)089

L. Paolozzi[53], C. Papadatos[107], S. Parajuli[41], A. Paramonov[5], C. Paraskevopoulos[9], D. Paredes Hernandez[61b], B. Parida[176], T.H. Park[163], A.J. Parker[30], M.A. Parker[31], F. Parodi[54b,54a], E.W. Parrish[117], V.A. Parrish[49], J.A. Parsons[38], U. Parzefall[51], B. Pascual Dias[107], L. Pascual Dominguez[158], V.R. Pascuzzi[17], F. Pasquali[116], E. Pasqualucci[71a], S. Passaggio[54b], F. Pastore[92], P. Pasuwan[44a,44b], J.R. Pater[98], A. Pathak[177], J. Patton[89], T. Pauly[35], J. Pearkes[150], M. Pedersen[130], R. Pedro[136a], S.V. Peleganchuk[118b,118a], O. Penc[137], C. Peng[61b], H. Peng[59a], M. Penzin[162], B.S. Peralva[79a], A.P. Pereira Peixoto[57], L. Pereira Sanchez[44a,44b], D.V. Perepelitsa[28], E. Perez Codina[164a], M. Perganti[9], L. Perini[67a,67b], H. Pernegger[35], S. Perrella[35], A. Perrevoort[115], K. Peters[45], R.F.Y. Peters[98], B.A. Petersen[35], T.C. Petersen[39], E. Petit[99], V. Petousis[138], C. Petridou[159], A. Petrukhin[148], M. Pettee[17], N.E. Pettersson[35], K. Petukhova[139], A. Peyaud[141], R. Pezoa[143e], L. Pezzotti[35], G. Pezzullo[179], T. Pham[102], P.W. Phillips[140], M.W. Phipps[169], G. Piacquadio[152], E. Pianori[17], F. Piazza[67a,67b], R. Piegaia[29], D. Pietreanu[26b], A.D. Pilkington[98], M. Pinamonti[65a,65c], J.L. Pinfold[2], C. Pitman Donaldson[93], D.A. Pizzi[33], L. Pizzimento[72a,72b], A. Pizzini[116], M.-A. Pleier[28], V. Plesanovs[51], V. Pleskot[139], E. Plotnikova[78], R. Poettgen[95], R. Poggi[53], L. Poggioli[132], I. Pogrebnyak[104], D. Pohl[23], I. Pokharel[52], S. Polacek[139], G. Polesello[69a], A. Poley[149,164a], R. Polifka[138], A. Polini[22b], C.S. Pollard[131], Z.B. Pollock[124], V. Polychronakos[28], D. Ponomarenko[109], L. Pontecorvo[35], S. Popa[26a], G.A. Popeneciu[26d], L. Portales[4], D.M. Portillo Quintero[164a], S. Pospisil[138], P. Postolache[26c], K. Potamianos[131], I.N. Potrap[78], C.J. Potter[31], H. Potti[1], T. Poulsen[45], J. Poveda[170], G. Pownall[45], M.E. Pozo Astigarraga[35], A. Prades Ibanez[170], P. Pralavorio[99], M.M. Prapa[43], D. Price[98], M. Primavera[66a], M.A. Principe Martin[96], M.L. Proffitt[145], N. Proklova[109], K. Prokofiev[61c], F. Prokoshin[78], G. Proto[72a,72b], S. Protopopescu[28], J. Proudfoot[5], M. Przybycien[82a], D. Pudzha[134], P. Puzo[63], D. Pyatiizbyantseva[109], J. Qian[103], Y. Qin[98], T. Qiu[91], A. Quadt[52], M. Queitsch-Maitland[23], G. Rabanal Bolanos[58], D. Rafanoharana[51], F. Ragusa[67a,67b], J.A. Raine[53], S. Rajagopalan[28], K. Ran[14a,14d], V. Raskina[132], D.F. Rassloff[60a], S. Rave[97], B. Ravina[56], I. Ravinovich[176], M. Raymond[35], A.L. Read[130], N.P. Readioff[146], D.M. Rebuzzi[69a,69b], G. Redlinger[28], K. Reeves[42], D. Reikher[158], A. Reiss[97], A. Rej[148], C. Rembser[35], A. Renardi[45], M. Renda[26b], M.B. Rendel[112], A.G. Rennie[56], S. Resconi[67a], M. Ressegotti[54b,54a], E.D. Resseguie[17], S. Rettie[93], B. Reynolds[124], E. Reynolds[17], M. Rezaei Estabragh[178], O.L. Rezanova[118b,118a], P. Reznicek[139], E. Ricci[74a,74b], R. Richter[112], S. Richter[44a,44b], E. Richter-Was[82b], M. Ridel[132], P. Rieck[122], P. Riedler[35], M. Rijssenbeek[152], A. Rimoldi[69a,69b], M. Rimoldi[45], L. Rinaldi[22b,22a], T.T. Rinn[169], M.P. Rinnagel[111], G. Ripellino[151], I. Riu[13], P. Rivadeneira[45], J.C. Rivera Vergara[172], F. Rizatdinova[126], E. Rizvi[91], C. Rizzi[53], B.A. Roberts[174], B.R. Roberts[17], S.H. Robertson[101,w], M. Robin[45], D. Robinson[31], C.M. Robles Gajardo[143e], M. Robles Manzano[97], A. Robson[56], A. Rocchi[72a,72b], C. Roda[70a,70b], S. Rodriguez Bosca[60a], Y. Rodriguez Garcia[21a], A. Rodriguez Rodriguez[51], A.M. Rodríguez Vera[164b], S. Roe[35], J.T. Roemer[167], A.R. Roepe[125], J. Roggel[178], O. Røhne[130], R.A. Rojas[172], B. Roland[51], C.P.A. Roland[64], J. Roloff[28], A. Romaniouk[109], M. Romano[22b], A.C. Romero Hernandez[169], N. Rompotis[89], M. Ronzani[122], L. Roos[132], S. Rosati[71a], B.J. Rosser[133], E. Rossi[163], E. Rossi[4], E. Rossi[68a,68b], L.P. Rossi[54b], L. Rossini[45], R. Rosten[124], M. Rotaru[26b], B. Rottler[51], D. Rousseau[63], D. Rousso[31], G. Rovelli[69a,69b], A. Roy[169], A. Rozanov[99], Y. Rozen[157], X. Ruan[32f], A.J. Ruby[89], T.A. Ruggeri[1], F. Rühr[51], A. Ruiz-Martinez[170], A. Rummler[35], Z. Rurikova[51], N.A. Rusakovich[78], H.L. Russell[172], L. Rustige[37], J.P. Rutherfoord[6], E.M. Rüttinger[146], K. Rybacki[88], M. Rybar[139], E.B. Rye[130], A. Ryzhov[119], J.A. Sabater Iglesias[53], P. Sabatini[170], L. Sabetta[71a,71b], H.F-W. Sadrozinski[142], R. Sadykov[78], F. Safai Tehrani[71a], B. Safarzadeh Samani[153], M. Safdari[150], S. Saha[101], M. Sahinsoy[112], A. Sahu[178], M. Saimpert[141], M. Saito[160], T. Saito[160], D. Salamani[35], G. Salamanna[73a,73b],

JHEP08(2022)089

A. Salnikov[150], J. Salt[170], A. Salvador Salas[13], D. Salvatore[40b,40a], F. Salvatore[153], A. Salzburger[35], D. Sammel[51], D. Sampsonidis[159], D. Sampsonidou[59d,59c], J. Sánchez[170], A. Sanchez Pineda[4], V. Sanchez Sebastian[170], H. Sandaker[130], C.O. Sander[45], I.G. Sanderswood[88], J.A. Sandesara[100], M. Sandhoff[178], C. Sandoval[21b], D.P.C. Sankey[140], A. Sansoni[50], C. Santoni[37], H. Santos[136a,136b], S.N. Santpur[17], A. Santra[176], K.A. Saoucha[146], A. Sapronov[78], J.G. Saraiva[136a,136d], J. Sardain[99], O. Sasaki[80], K. Sato[165], C. Sauer[60b], F. Sauerburger[51], E. Sauvan[4], P. Savard[163,ai], R. Sawada[160], C. Sawyer[140], L. Sawyer[94], I. Sayago Galvan[170], C. Sbarra[22b], A. Sbrizzi[22b,22a], T. Scanlon[93], J. Schaarschmidt[145], P. Schacht[112], D. Schaefer[36], U. Schäfer[97], A.C. Schaffer[63], D. Schaile[111], R.D. Schamberger[152], E. Schanet[111], C. Scharf[18], N. Scharmberg[98], V.A. Schegelsky[134], D. Scheirich[139], F. Schenck[18], M. Schernau[167], C. Schiavi[54b,54a], Z.M. Schillaci[25], E.J. Schioppa[66a,66b], M. Schioppa[40b,40a], B. Schlag[97], K.E. Schleicher[51], S. Schlenker[35], K. Schmieden[97], C. Schmitt[97], S. Schmitt[45], L. Schoeffel[141], A. Schoening[60b], P.G. Scholer[51], E. Schopf[131], M. Schott[97], J. Schovancova[35], S. Schramm[53], F. Schroeder[178], H-C. Schultz-Coulon[60a], M. Schumacher[51], B.A. Schumm[142], Ph. Schune[141], A. Schwartzman[150], T.A. Schwarz[103], Ph. Schwemling[141], R. Schwienhorst[104], A. Sciandra[142], G. Sciolla[25], F. Scuri[70a], F. Scutti[102], C.D. Sebastiani[89], K. Sedlaczek[46], P. Seema[18], S.C. Seidel[114], A. Seiden[142], B.D. Seidlitz[28], T. Seiss[36], C. Seitz[45], J.M. Seixas[79b], G. Sekhniaidze[68a], S.J. Sekula[41], L. Selem[4], N. Semprini-Cesari[22b,22a], S. Sen[48], L. Serin[63], L. Serkin[65a,65b], M. Sessa[73a,73b], H. Severini[125], S. Sevova[150], F. Sforza[54b,54a], A. Sfyrla[53], E. Shabalina[52], R. Shaheen[151], J.D. Shahinian[133], N.W. Shaikh[44a,44b], D. Shaked Renous[176], L.Y. Shan[14a], M. Shapiro[17], A. Sharma[35], A.S. Sharma[1], S. Sharma[45], P.B. Shatalov[120], K. Shaw[153], S.M. Shaw[98], P. Sherwood[93], L. Shi[93], C.O. Shimmin[179], Y. Shimogama[175], J.D. Shinner[92], I.P.J. Shipsey[131], S. Shirabe[53], M. Shiyakova[78], J. Shlomi[176], M.J. Shochet[36], J. Shojaii[102], D.R. Shope[151], S. Shrestha[124], E.M. Shrif[32f], M.J. Shroff[172], P. Sicho[137], A.M. Sickles[169], E. Sideras Haddad[32f], O. Sidiropoulou[35], A. Sidoti[22b], F. Siegert[47], Dj. Sijacki[15], F. Sili[87], J.M. Silva[20], M.V. Silva Oliveira[35], S.B. Silverstein[44a], S. Simion[63], R. Simoniello[35], N.D. Simpson[95], S. Simsek[11c], S. Sindhu[52], P. Sinervo[163], V. Sinetckii[110], S. Singh[149], S. Singh[163], S. Sinha[45], S. Sinha[32f], M. Sioli[22b,22a], I. Siral[128], S.Yu. Sivoklokov[110], J. Sjölin[44a,44b], A. Skaf[52], E. Skorda[95], P. Skubic[125], M. Slawinska[83], V. Smakhtin[176], B.H. Smart[140], J. Smiesko[139], S.Yu. Smirnov[109], Y. Smirnov[109], L.N. Smirnova[110,q], O. Smirnova[95], E.A. Smith[36], H.A. Smith[131], R. Smith[150], M. Smizanska[88], K. Smolek[138], A. Smykiewicz[83], A.A. Snesarev[108], H.L. Snoek[116], S. Snyder[28], R. Sobie[172,w], A. Soffer[158], C.A. Solans Sanchez[35], E.Yu. Soldatov[109], U. Soldevila[170], A.A. Solodkov[119], S. Solomon[51], A. Soloshenko[78], K. Solovieva[51], O.V. Solovyanov[119], V. Solovyev[134], P. Sommer[146], H. Son[166], A. Sonay[13], W.Y. Song[164b], A. Sopczak[138], A.L. Sopio[93], F. Sopkova[27b], V. Sothilingam[60a], S. Sottocornola[69a,69b], R. Soualah[121c], A.M. Soukharev[118b,118a], Z. Soumaimi[34e], D. South[45], S. Spagnolo[66a,66b], M. Spalla[112], M. Spangenberg[174], F. Spanò[92], D. Sperlich[51], G. Spigo[35], M. Spina[153], S. Spinali[88], D.P. Spiteri[56], M. Spousta[139], E.J. Staats[33], A. Stabile[67a,67b], R. Stamen[60a], M. Stamenkovic[116], A. Stampekis[20], M. Standke[23], E. Stanecka[83], B. Stanislaus[17], M.M. Stanitzki[45], M. Stankaityte[131], B. Stapf[45], E.A. Starchenko[119], G.H. Stark[142], J. Stark[99], D.M. Starko[164b], P. Staroba[137], P. Starovoitov[60a], S. Stärz[101], R. Staszewski[83], G. Stavropoulos[43], J. Steentoft[168], P. Steinberg[28], A.L. Steinhebel[128], B. Stelzer[149,164a], H.J. Stelzer[135], O. Stelzer-Chilton[164a], H. Stenzel[55], T.J. Stevenson[153], G.A. Stewart[35], M.C. Stockton[35], G. Stoicea[26b], M. Stolarski[136a], S. Stonjek[112], A. Straessner[47], J. Strandberg[151], S. Strandberg[44a,44b], M. Strauss[125], T. Strebler[99], P. Strizenec[27b], R. Ströhmer[173], D.M. Strom[128], L.R. Strom[45], R. Stroynowski[41], A. Strubig[44a,44b], S.A. Stucci[28], B. Stugu[16], J. Stupak[125], N.A. Styles[45], D. Su[150], S. Su[59a], W. Su[59d,145,59c], X. Su[59a,63], K. Sugizaki[160], V.V. Sulin[108], M.J. Sullivan[89], D.M.S. Sultan[74a,74b],

JHEP08(2022)089

L. Sultanaliyeva[108], S. Sultansoy[3c], T. Sumida[84], S. Sun[103], S. Sun[177], O. Sunneborn Gudnadottir[168], M.R. Sutton[153], M. Svatos[137], M. Swiatlowski[164a], T. Swirski[173], I. Sykora[27a], M. Sykora[139], T. Sykora[139], D. Ta[97], K. Tackmann[45,v], A. Taffard[167], R. Tafirout[164a], R.H.M. Taibah[132], R. Takashima[85], K. Takeda[81], E.P. Takeva[49], Y. Takubo[80], M. Talby[99], A.A. Talyshev[118b,118a], K.C. Tam[61b], N.M. Tamir[158], A. Tanaka[160], J. Tanaka[160], R. Tanaka[63], J. Tang[59c], Z. Tao[171], S. Tapia Araya[77], S. Tapprogge[97], A. Tarek Abouelfadl Mohamed[104], S. Tarem[157], K. Tariq[59b], G. Tarna[26b], G.F. Tartarelli[67a], P. Tas[139], M. Tasevsky[137], E. Tassi[40b,40a], G. Tateno[160], Y. Tayalati[34e], G.N. Taylor[102], W. Taylor[164b], H. Teagle[89], A.S. Tee[177], R. Teixeira De Lima[150], P. Teixeira-Dias[92], J.J. Teoh[116], K. Terashi[160], J. Terron[96], S. Terzo[13], M. Testa[50], R.J. Teuscher[163,w], N. Themistokleous[49], T. Theveneaux-Pelzer[18], O. Thielmann[178], D.W. Thomas[92], J.P. Thomas[20], E.A. Thompson[45], P.D. Thompson[20], E. Thomson[133], E.J. Thorpe[91], Y. Tian[52], V. Tikhomirov[108,ae], Yu.A. Tikhonov[118b,118a], S. Timoshenko[109], E.X.L. Ting[1], P. Tipton[179], S. Tisserant[99], S.H. Tlou[32f], A. Tnourji[37], K. Todome[22b,22a], S. Todorova-Nova[139], S. Todt[47], M. Togawa[80], J. Tojo[86], S. Tokár[27a], K. Tokushuku[80], R. Tombs[31], M. Tomoto[80,113], L. Tompkins[150], P. Tornambe[100], E. Torrence[128], H. Torres[47], E. Torró Pastor[170], M. Toscani[29], C. Tosciri[36], D.R. Tovey[146], A. Traeet[16], I.S. Trandafir[26b], C.J. Treado[122], T. Trefzger[173], A. Tricoli[28], I.M. Trigger[164a], S. Trincaz-Duvoid[132], D.A. Trischuk[171], W. Trischuk[163], B. Trocmé[57], A. Trofymov[63], C. Troncon[67a], F. Trovato[153], L. Truong[32c], M. Trzebinski[83], A. Trzupek[83], F. Tsai[152], M. Tsai[103], A. Tsiamis[159], P.V. Tsiareshka[105], A. Tsirigotis[159,t], V. Tsiskaridze[152], E.G. Tskhadadze[156a], M. Tsopoulou[159], Y. Tsujikawa[84], I.I. Tsukerman[120], V. Tsulaia[17], S. Tsuno[80], O. Tsur[157], D. Tsybychev[152], Y. Tu[61b], A. Tudorache[26b], V. Tudorache[26b], A.N. Tuna[35], S. Turchikhin[78], I. Turk Cakir[3a], R. Turra[67a], P.M. Tuts[38], S. Tzamarias[159], P. Tzanis[9], E. Tzovara[97], K. Uchida[160], F. Ukegawa[165], P.A. Ulloa Poblete[143b], G. Unal[35], M. Unal[10], A. Undrus[28], G. Unel[167], K. Uno[160], J. Urban[27b], P. Urquijo[102], G. Usai[7], R. Ushioda[161], M. Usman[107], Z. Uysal[11d], V. Vacek[138], B. Vachon[101], K.O.H. Vadla[130], T. Vafeiadis[35], C. Valderanis[111], E. Valdes Santurio[44a,44b], M. Valente[164a], S. Valentinetti[22b,22a], A. Valero[170], A. Vallier[99], J.A. Valls Ferrer[170], T.R. Van Daalen[145], P. Van Gemmeren[5], S. Van Stroud[93], I. Van Vulpen[116], M. Vanadia[72a,72b], W. Vandelli[35], M. Vandenbroucke[141], E.R. Vandewall[126], D. Vannicola[158], L. Vannoli[54b,54a], R. Vari[71a], E.W. Varnes[6], C. Varni[17], T. Varol[155], D. Varouchas[63], K.E. Varvell[154], M.E. Vasile[26b], L. Vaslin[37], G.A. Vasquez[172], F. Vazeille[37], D. Vazquez Furelos[13], T. Vazquez Schroeder[35], J. Veatch[52], V. Vecchio[98], M.J. Veen[116], I. Veliscek[131], L.M. Veloce[163], F. Veloso[136a,136c], S. Veneziano[71a], A. Ventura[66a,66b], A. Verbytskyi[112], M. Verducci[70a,70b], C. Vergis[23], M. Verissimo De Araujo[79b], W. Verkerke[116], J.C. Vermeulen[116], C. Vernieri[150], P.J. Verschuuren[92], M. Vessella[100], M.L. Vesterbacka[122], M.C. Vetterli[149,ai], A. Vgenopoulos[159], N. Viaux Maira[143e], T. Vickey[146], O.E. Vickey Boeriu[146], G.H.A. Viehhauser[131], L. Vigani[60b], M. Villa[22b,22a], M. Villaplana Perez[170], E.M. Villhauer[49], E. Vilucchi[50], M.G. Vincter[33], G.S. Virdee[20], A. Vishwakarma[49], C. Vittori[22b,22a], I. Vivarelli[153], V. Vladimirov[174], E. Voevodina[112], M. Vogel[178], P. Vokac[138], J. Von Ahnen[45], E. Von Toerne[23], B. Vormwald[35], V. Vorobel[139], K. Vorobev[109], M. Vos[170], J.H. Vossebeld[89], M. Vozak[116], L. Vozdecky[91], N. Vranjes[15], M. Vranjes Milosavljevic[15], V. Vrba[138,*], M. Vreeswijk[116], N.K. Vu[99], R. Vuillermet[35], O.V. Vujinovic[97], I. Vukotic[36], S. Wada[165], C. Wagner[100], W. Wagner[178], S. Wahdan[178], H. Wahlberg[87], R. Wakasa[165], M. Wakida[113], V.M. Walbrecht[112], J. Walder[140], R. Walker[111], W. Walkowiak[148], A.M. Wang[58], A.Z. Wang[177], C. Wang[59a], C. Wang[59c], H. Wang[17], J. Wang[61a], P. Wang[41], R.-J. Wang[97], R. Wang[58], R. Wang[5], S.M. Wang[155], S. Wang[59b], T. Wang[59a], W.T. Wang[76], W.X. Wang[59a], X. Wang[14c], X. Wang[169], X. Wang[59c], Y. Wang[59d], Z. Wang[103], Z. Wang[59d,48,59c], Z. Wang[103], A. Warburton[101], R.J. Ward[20], N. Warrack[56],

JHEP08(2022)089

A.T. Watson[20], M.F. Watson[20], G. Watts[145], B.M. Waugh[93], A.F. Webb[10], C. Weber[28], M.S. Weber[19], S.A. Weber[33], S.M. Weber[60a], C. Wei[59a], Y. Wei[131], A.R. Weidberg[131], J. Weingarten[46], M. Weirich[97], C. Weiser[51], T. Wenaus[28], B. Wendland[46], T. Wengler[35], N.S. Wenke[112], N. Wermes[23], M. Wessels[60a], K. Whalen[128], A.M. Wharton[88], A.S. White[58], A. White[7], M.J. White[1], D. Whiteson[167], L. Wickremasinghe[129], W. Wiedenmann[177], C. Wiel[47], M. Wielers[140], N. Wieseotte[97], C. Wiglesworth[39], L.A.M. Wiik-Fuchs[51], D.J. Wilbern[125], H.G. Wilkens[35], D.M. Williams[38], H.H. Williams[133], S. Williams[31], S. Willocq[100], P.J. Windischhofer[131], F. Winklmeier[128], B.T. Winter[51], M. Wittgen[150], M. Wobisch[94], A. Wolf[97], R. Wölker[131], J. Wollrath[167], M.W. Wolter[83], H. Wolters[136a,136c], V.W.S. Wong[171], A.F. Wongel[45], S.D. Worm[45], B.K. Wosiek[83], K.W. Woźniak[83], K. Wraight[56], J. Wu[14a,14d], S.L. Wu[177], X. Wu[53], Y. Wu[59a], Z. Wu[141,59a], J. Wuerzinger[131], T.R. Wyatt[98], B.M. Wynne[49], S. Xella[39], L. Xia[14c], M. Xia[14b], J. Xiang[61c], X. Xiao[103], M. Xie[59a], X. Xie[59a], I. Xiotidis[153], D. Xu[14a], H. Xu[59a], H. Xu[59a], L. Xu[59a], R. Xu[133], T. Xu[59a], W. Xu[103], Y. Xu[14b], Z. Xu[59b], Z. Xu[150], B. Yabsley[154], S. Yacoob[32a], N. Yamaguchi[86], Y. Yamaguchi[161], H. Yamauchi[165], T. Yamazaki[17], Y. Yamazaki[81], J. Yan[59c], S. Yan[131], Z. Yan[24], H.J. Yang[59c,59d], H.T. Yang[17], S. Yang[59a], T. Yang[61c], X. Yang[59a], X. Yang[14a], Y. Yang[41], Z. Yang[103,59a], W-M. Yao[17], Y.C. Yap[45], H. Ye[14c], J. Ye[41], S. Ye[28], I. Yeletskikh[78], M.R. Yexley[88], P. Yin[38], K. Yorita[175], C.J.S. Young[51], C. Young[150], M. Yuan[103], R. Yuan[59b,i], X. Yue[60a], M. Zaazoua[34e], B. Zabinski[83], G. Zacharis[9], E. Zaid[49], A.M. Zaitsev[119,ad], T. Zakareishvili[156b], N. Zakharchuk[33], S. Zambito[35], D. Zanzi[51], O. Zaplatilek[138], S.V. Zeißner[46], C. Zeitnitz[178], J.C. Zeng[169], D.T. Zenger Jr[25], O. Zenin[119], T. Ženiš[27a], S. Zenz[91], S. Zerradi[34a], D. Zerwas[63], B. Zhang[14c], D.F. Zhang[146], G. Zhang[14b], J. Zhang[5], K. Zhang[14a], L. Zhang[14c], M. Zhang[169], R. Zhang[177], S. Zhang[103], X. Zhang[59c], X. Zhang[59b], Z. Zhang[63], H. Zhao[145], P. Zhao[48], T. Zhao[59b], Y. Zhao[142], Z. Zhao[59a], A. Zhemchugov[78], Z. Zheng[150], D. Zhong[169], B. Zhou[103], C. Zhou[177], H. Zhou[6], N. Zhou[59c], Y. Zhou[6], C.G. Zhu[59b], C. Zhu[14a,14d], H.L. Zhu[59a], H. Zhu[14a], J. Zhu[103], Y. Zhu[59a], X. Zhuang[14a], K. Zhukov[108], V. Zhulanov[118b,118a], D. Zieminska[64], N.I. Zimine[78], S. Zimmermann[51,*], J. Zinsser[60b], M. Ziolkowski[148], L. Živković[15], A. Zoccoli[22b,22a], K. Zoch[53], T.G. Zorbas[146], O. Zormpa[43], W. Zou[38], L. Zwalinski[35].

[1] *Department of Physics, University of Adelaide, Adelaide, Australia*
[2] *Department of Physics, University of Alberta, Edmonton AB, Canada*
[3] [(a)] *Department of Physics, Ankara University, Ankara;* [(b)] *Istanbul Aydin University, Application and Research Center for Advanced Studies, Istanbul;* [(c)] *Division of Physics, TOBB University of Economics and Technology, Ankara, Turkey*
[4] *LAPP, Univ. Savoie Mont Blanc, CNRS/IN2P3, Annecy, France*
[5] *High Energy Physics Division, Argonne National Laboratory, Argonne IL, United States of America*
[6] *Department of Physics, University of Arizona, Tucson AZ, United States of America*
[7] *Department of Physics, University of Texas at Arlington, Arlington TX, United States of America*
[8] *Physics Department, National and Kapodistrian University of Athens, Athens, Greece*
[9] *Physics Department, National Technical University of Athens, Zografou, Greece*
[10] *Department of Physics, University of Texas at Austin, Austin TX, United States of America*
[11] [(a)] *Bahcesehir University, Faculty of Engineering and Natural Sciences, Istanbul;* [(b)] *Istanbul Bilgi University, Faculty of Engineering and Natural Sciences, Istanbul;* [(c)] *Department of Physics, Bogazici University, Istanbul;* [(d)] *Department of Physics Engineering, Gaziantep University, Gaziantep, Turkey*
[12] *Institute of Physics, Azerbaijan Academy of Sciences, Baku, Azerbaijan*
[13] *Institut de Física d'Altes Energies (IFAE), Barcelona Institute of Science and Technology, Barcelona, Spain*
[14] [(a)] *Institute of High Energy Physics, Chinese Academy of Sciences, Beijing;* [(b)] *Physics Department, Tsinghua University, Beijing;* [(c)] *Department of Physics, Nanjing University, Nanjing;* [(d)] *University of Chinese Academy of Science (UCAS), Beijing, China*

JHEP08(2022)089

[15] Institute of Physics, University of Belgrade, Belgrade, Serbia
[16] Department for Physics and Technology, University of Bergen, Bergen, Norway
[17] Physics Division, Lawrence Berkeley National Laboratory and University of California, Berkeley CA, United States of America
[18] Institut für Physik, Humboldt Universität zu Berlin, Berlin, Germany
[19] Albert Einstein Center for Fundamental Physics and Laboratory for High Energy Physics, University of Bern, Bern, Switzerland
[20] School of Physics and Astronomy, University of Birmingham, Birmingham, United Kingdom
[21] [(a)] Facultad de Ciencias y Centro de Investigaciónes, Universidad Antonio Nariño, Bogotá; [(b)] Departamento de Física, Universidad Nacional de Colombia, Bogotá, Colombia
[22] [(a)] Dipartimento di Fisica e Astronomia A. Righi, Università di Bologna, Bologna; [(b)] INFN Sezione di Bologna, Italy
[23] Physikalisches Institut, Universität Bonn, Bonn, Germany
[24] Department of Physics, Boston University, Boston MA, United States of America
[25] Department of Physics, Brandeis University, Waltham MA, United States of America
[26] [(a)] Transilvania University of Brasov, Brasov; [(b)] Horia Hulubei National Institute of Physics and Nuclear Engineering, Bucharest; [(c)] Department of Physics, Alexandru Ioan Cuza University of Iasi, Iasi; [(d)] National Institute for Research and Development of Isotopic and Molecular Technologies, Physics Department, Cluj-Napoca; [(e)] University Politehnica Bucharest, Bucharest; [(f)] West University in Timisoara, Timisoara, Romania
[27] [(a)] Faculty of Mathematics, Physics and Informatics, Comenius University, Bratislava; [(b)] Department of Subnuclear Physics, Institute of Experimental Physics of the Slovak Academy of Sciences, Kosice, Slovak Republic
[28] Physics Department, Brookhaven National Laboratory, Upton NY, United States of America
[29] Universidad de Buenos Aires, Facultad de Ciencias Exactas y Naturales, Departamento de Física, y CONICET, Instituto de Física de Buenos Aires (IFIBA), Buenos Aires, Argentina
[30] California State University, CA, United States of America
[31] Cavendish Laboratory, University of Cambridge, Cambridge, United Kingdom
[32] [(a)] Department of Physics, University of Cape Town, Cape Town; [(b)] iThemba Labs, Western Cape; [(c)] Department of Mechanical Engineering Science, University of Johannesburg, Johannesburg; [(d)] National Institute of Physics, University of the Philippines Diliman (Philippines); [(e)] University of South Africa, Department of Physics, Pretoria; [(f)] School of Physics, University of the Witwatersrand, Johannesburg, South Africa
[33] Department of Physics, Carleton University, Ottawa ON, Canada
[34] [(a)] Faculté des Sciences Ain Chock, Réseau Universitaire de Physique des Hautes Energies - Université Hassan II, Casablanca; [(b)] Faculté des Sciences, Université Ibn-Tofail, Kénitra; [(c)] Faculté des Sciences Semlalia, Université Cadi Ayyad, LPHEA-Marrakech; [(d)] LPMR, Faculté des Sciences, Université Mohamed Premier, Oujda; [(e)] Faculté des sciences, Université Mohammed V, Rabat; [(f)] Mohammed VI Polytechnic University, Ben Guerir, Morocco
[35] CERN, Geneva, Switzerland
[36] Enrico Fermi Institute, University of Chicago, Chicago IL, United States of America
[37] LPC, Université Clermont Auvergne, CNRS/IN2P3, Clermont-Ferrand, France
[38] Nevis Laboratory, Columbia University, Irvington NY, United States of America
[39] Niels Bohr Institute, University of Copenhagen, Copenhagen, Denmark
[40] [(a)] Dipartimento di Fisica, Università della Calabria, Rende; [(b)] INFN Gruppo Collegato di Cosenza, Laboratori Nazionali di Frascati, Italy
[41] Physics Department, Southern Methodist University, Dallas TX, United States of America
[42] Physics Department, University of Texas at Dallas, Richardson TX, United States of America
[43] National Centre for Scientific Research "Demokritos", Agia Paraskevi, Greece
[44] [(a)] Department of Physics, Stockholm University; [(b)] Oskar Klein Centre, Stockholm, Sweden
[45] Deutsches Elektronen-Synchrotron DESY, Hamburg and Zeuthen, Germany
[46] Fakultät Physik, Technische Universität Dortmund, Dortmund, Germany

JHEP08(2022)089

[47] Institut für Kern- und Teilchenphysik, Technische Universität Dresden, Dresden, Germany
[48] Department of Physics, Duke University, Durham NC, United States of America
[49] SUPA - School of Physics and Astronomy, University of Edinburgh, Edinburgh, United Kingdom
[50] INFN e Laboratori Nazionali di Frascati, Frascati, Italy
[51] Physikalisches Institut, Albert-Ludwigs-Universität Freiburg, Freiburg, Germany
[52] II. Physikalisches Institut, Georg-August-Universität Göttingen, Göttingen, Germany
[53] Département de Physique Nucléaire et Corpusculaire, Université de Genève, Genève, Switzerland
[54] [(a)] Dipartimento di Fisica, Università di Genova, Genova; [(b)] INFN Sezione di Genova, Italy
[55] II. Physikalisches Institut, Justus-Liebig-Universität Giessen, Giessen, Germany
[56] SUPA - School of Physics and Astronomy, University of Glasgow, Glasgow, United Kingdom
[57] LPSC, Université Grenoble Alpes, CNRS/IN2P3, Grenoble INP, Grenoble, France
[58] Laboratory for Particle Physics and Cosmology, Harvard University, Cambridge MA, United States of America
[59] [(a)] Department of Modern Physics and State Key Laboratory of Particle Detection and Electronics, University of Science and Technology of China, Hefei; [(b)] Institute of Frontier and Interdisciplinary Science and Key Laboratory of Particle Physics and Particle Irradiation (MOE), Shandong University, Qingdao; [(c)] School of Physics and Astronomy, Shanghai Jiao Tong University, Key Laboratory for Particle Astrophysics and Cosmology (MOE), SKLPPC, Shanghai; [(d)] Tsung-Dao Lee Institute, Shanghai, China
[60] [(a)] Kirchhoff-Institut für Physik, Ruprecht-Karls-Universität Heidelberg, Heidelberg; [(b)] Physikalisches Institut, Ruprecht-Karls-Universität Heidelberg, Heidelberg, Germany
[61] [(a)] Department of Physics, Chinese University of Hong Kong, Shatin, N.T., Hong Kong; [(b)] Department of Physics, University of Hong Kong, Hong Kong; [(c)] Department of Physics and Institute for Advanced Study, Hong Kong University of Science and Technology, Clear Water Bay, Kowloon, Hong Kong, China
[62] Department of Physics, National Tsing Hua University, Hsinchu, Taiwan
[63] IJCLab, Université Paris-Saclay, CNRS/IN2P3, 91405, Orsay, France
[64] Department of Physics, Indiana University, Bloomington IN, United States of America
[65] [(a)] INFN Gruppo Collegato di Udine, Sezione di Trieste, Udine; [(b)] ICTP, Trieste; [(c)] Dipartimento Politecnico di Ingegneria e Architettura, Università di Udine, Udine, Italy
[66] [(a)] INFN Sezione di Lecce; [(b)] Dipartimento di Matematica e Fisica, Università del Salento, Lecce, Italy
[67] [(a)] INFN Sezione di Milano; [(b)] Dipartimento di Fisica, Università di Milano, Milano, Italy
[68] [(a)] INFN Sezione di Napoli; [(b)] Dipartimento di Fisica, Università di Napoli, Napoli, Italy
[69] [(a)] INFN Sezione di Pavia; [(b)] Dipartimento di Fisica, Università di Pavia, Pavia, Italy
[70] [(a)] INFN Sezione di Pisa; [(b)] Dipartimento di Fisica E. Fermi, Università di Pisa, Pisa, Italy
[71] [(a)] INFN Sezione di Roma; [(b)] Dipartimento di Fisica, Sapienza Università di Roma, Roma, Italy
[72] [(a)] INFN Sezione di Roma Tor Vergata; [(b)] Dipartimento di Fisica, Università di Roma Tor Vergata, Roma, Italy
[73] [(a)] INFN Sezione di Roma Tre; [(b)] Dipartimento di Matematica e Fisica, Università Roma Tre, Roma, Italy
[74] [(a)] INFN-TIFPA; [(b)] Università degli Studi di Trento, Trento, Italy
[75] Institut für Astro- und Teilchenphysik, Leopold-Franzens-Universität, Innsbruck, Austria
[76] University of Iowa, Iowa City IA, United States of America
[77] Department of Physics and Astronomy, Iowa State University, Ames IA, United States of America
[78] Joint Institute for Nuclear Research, Dubna, Russia
[79] [(a)] Departamento de Engenharia Elétrica, Universidade Federal de Juiz de Fora (UFJF), Juiz de Fora; [(b)] Universidade Federal do Rio De Janeiro COPPE/EE/IF, Rio de Janeiro; [(c)] Instituto de Física, Universidade de São Paulo, São Paulo, Brazil
[80] KEK, High Energy Accelerator Research Organization, Tsukuba, Japan
[81] Graduate School of Science, Kobe University, Kobe, Japan
[82] [(a)] AGH University of Science and Technology, Faculty of Physics and Applied Computer Science, Krakow; [(b)] Marian Smoluchowski Institute of Physics, Jagiellonian University, Krakow, Poland

JHEP08(2022)089

[83] Institute of Nuclear Physics Polish Academy of Sciences, Krakow, Poland
[84] Faculty of Science, Kyoto University, Kyoto, Japan
[85] Kyoto University of Education, Kyoto, Japan
[86] Research Center for Advanced Particle Physics and Department of Physics, Kyushu University, Fukuoka, Japan
[87] Instituto de Física La Plata, Universidad Nacional de La Plata and CONICET, La Plata, Argentina
[88] Physics Department, Lancaster University, Lancaster, United Kingdom
[89] Oliver Lodge Laboratory, University of Liverpool, Liverpool, United Kingdom
[90] Department of Experimental Particle Physics, Jožef Stefan Institute and Department of Physics, University of Ljubljana, Ljubljana, Slovenia
[91] School of Physics and Astronomy, Queen Mary University of London, London, United Kingdom
[92] Department of Physics, Royal Holloway University of London, Egham, United Kingdom
[93] Department of Physics and Astronomy, University College London, London, United Kingdom
[94] Louisiana Tech University, Ruston LA, United States of America
[95] Fysiska institutionen, Lunds universitet, Lund, Sweden
[96] Departamento de Física Teorica C-15 and CIAFF, Universidad Autónoma de Madrid, Madrid, Spain
[97] Institut für Physik, Universität Mainz, Mainz, Germany
[98] School of Physics and Astronomy, University of Manchester, Manchester, United Kingdom
[99] CPPM, Aix-Marseille Université, CNRS/IN2P3, Marseille, France
[100] Department of Physics, University of Massachusetts, Amherst MA, United States of America
[101] Department of Physics, McGill University, Montreal QC, Canada
[102] School of Physics, University of Melbourne, Victoria, Australia
[103] Department of Physics, University of Michigan, Ann Arbor MI, United States of America
[104] Department of Physics and Astronomy, Michigan State University, East Lansing MI, United States of America
[105] B.I. Stepanov Institute of Physics, National Academy of Sciences of Belarus, Minsk, Belarus
[106] Research Institute for Nuclear Problems of Byelorussian State University, Minsk, Belarus
[107] Group of Particle Physics, University of Montreal, Montreal QC, Canada
[108] P.N. Lebedev Physical Institute of the Russian Academy of Sciences, Moscow, Russia
[109] National Research Nuclear University MEPhI, Moscow, Russia
[110] D.V. Skobeltsyn Institute of Nuclear Physics, M.V. Lomonosov Moscow State University, Moscow, Russia
[111] Fakultät für Physik, Ludwig-Maximilians-Universität München, München, Germany
[112] Max-Planck-Institut für Physik (Werner-Heisenberg-Institut), München, Germany
[113] Graduate School of Science and Kobayashi-Maskawa Institute, Nagoya University, Nagoya, Japan
[114] Department of Physics and Astronomy, University of New Mexico, Albuquerque NM, United States of America
[115] Institute for Mathematics, Astrophysics and Particle Physics, Radboud University/Nikhef, Nijmegen, The Netherlands
[116] Nikhef National Institute for Subatomic Physics and University of Amsterdam, Amsterdam, The Netherlands
[117] Department of Physics, Northern Illinois University, DeKalb IL, United States of America
[118] [(a)] Budker Institute of Nuclear Physics and NSU, SB RAS, Novosibirsk; [(b)] Novosibirsk State University Novosibirsk, Russia
[119] Institute for High Energy Physics of the National Research Centre Kurchatov Institute, Protvino, Russia
[120] Institute for Theoretical and Experimental Physics named by A.I. Alikhanov of National Research Centre "Kurchatov Institute", Moscow, Russia
[121] [(a)] New York University Abu Dhabi, Abu Dhabi; [(b)] United Arab Emirates University, Al Ain; [(c)] University of Sharjah, Sharjah, United Arab Emirates
[122] Department of Physics, New York University, New York NY, United States of America

JHEP08(2022)089

[123] Ochanomizu University, Otsuka, Bunkyo-ku, Tokyo, Japan
[124] Ohio State University, Columbus OH, United States of America
[125] Homer L. Dodge Department of Physics and Astronomy, University of Oklahoma, Norman OK, United States of America
[126] Department of Physics, Oklahoma State University, Stillwater OK, United States of America
[127] Palacký University, Joint Laboratory of Optics, Olomouc, Czech Republic
[128] Institute for Fundamental Science, University of Oregon, Eugene, OR, United States of America
[129] Graduate School of Science, Osaka University, Osaka, Japan
[130] Department of Physics, University of Oslo, Oslo, Norway
[131] Department of Physics, Oxford University, Oxford, United Kingdom
[132] LPNHE, Sorbonne Université, Université Paris Cité, CNRS/IN2P3, Paris, France
[133] Department of Physics, University of Pennsylvania, Philadelphia PA, United States of America
[134] Konstantinov Nuclear Physics Institute of National Research Centre "Kurchatov Institute", PNPI, St. Petersburg, Russia
[135] Department of Physics and Astronomy, University of Pittsburgh, Pittsburgh PA, United States of America
[136] [(a)] Laboratório de Instrumentação e Física Experimental de Partículas - LIP, Lisboa; [(b)] Departamento de Física, Faculdade de Ciências, Universidade de Lisboa, Lisboa; [(c)] Departamento de Física, Universidade de Coimbra, Coimbra; [(d)] Centro de Física Nuclear da Universidade de Lisboa, Lisboa; [(e)] Departamento de Física, Universidade do Minho, Braga; [(f)] Departamento de Física Teórica y del Cosmos, Universidad de Granada, Granada (Spain); [(g)] Instituto Superior Técnico, Universidade de Lisboa, Lisboa, Portugal
[137] Institute of Physics of the Czech Academy of Sciences, Prague, Czech Republic
[138] Czech Technical University in Prague, Prague, Czech Republic
[139] Charles University, Faculty of Mathematics and Physics, Prague, Czech Republic
[140] Particle Physics Department, Rutherford Appleton Laboratory, Didcot, United Kingdom
[141] IRFU, CEA, Université Paris-Saclay, Gif-sur-Yvette, France
[142] Santa Cruz Institute for Particle Physics, University of California Santa Cruz, Santa Cruz CA, United States of America
[143] [(a)] Departamento de Física, Pontificia Universidad Católica de Chile, Santiago; [(b)] Instituto de Investigación Multidisciplinario en Ciencia y Tecnología, y Departamento de Física, Universidad de La Serena; [(c)] Universidad Andres Bello, Department of Physics, Santiago; [(d)] Instituto de Alta Investigación, Universidad de Tarapacá, Arica; [(e)] Departamento de Física, Universidad Técnica Federico Santa María, Valparaíso, Chile
[144] Universidade Federal de São João del Rei (UFSJ), São João del Rei, Brazil
[145] Department of Physics, University of Washington, Seattle WA, United States of America
[146] Department of Physics and Astronomy, University of Sheffield, Sheffield, United Kingdom
[147] Department of Physics, Shinshu University, Nagano, Japan
[148] Department Physik, Universität Siegen, Siegen, Germany
[149] Department of Physics, Simon Fraser University, Burnaby BC, Canada
[150] SLAC National Accelerator Laboratory, Stanford CA, United States of America
[151] Department of Physics, Royal Institute of Technology, Stockholm, Sweden
[152] Departments of Physics and Astronomy, Stony Brook University, Stony Brook NY, United States of America
[153] Department of Physics and Astronomy, University of Sussex, Brighton, United Kingdom
[154] School of Physics, University of Sydney, Sydney, Australia
[155] Institute of Physics, Academia Sinica, Taipei, Taiwan
[156] [(a)] E. Andronikashvili Institute of Physics, Iv. Javakhishvili Tbilisi State University, Tbilisi; [(b)] High Energy Physics Institute, Tbilisi State University, Tbilisi, Georgia
[157] Department of Physics, Technion, Israel Institute of Technology, Haifa, Israel
[158] Raymond and Beverly Sackler School of Physics and Astronomy, Tel Aviv University, Tel Aviv, Israel

JHEP08(2022)089

[159] Department of Physics, Aristotle University of Thessaloniki, Thessaloniki, Greece
[160] International Center for Elementary Particle Physics and Department of Physics, University of Tokyo, Tokyo, Japan
[161] Department of Physics, Tokyo Institute of Technology, Tokyo, Japan
[162] Tomsk State University, Tomsk, Russia
[163] Department of Physics, University of Toronto, Toronto ON, Canada
[164] [(a)] TRIUMF, Vancouver BC; [(b)] Department of Physics and Astronomy, York University, Toronto ON, Canada
[165] Division of Physics and Tomonaga Center for the History of the Universe, Faculty of Pure and Applied Sciences, University of Tsukuba, Tsukuba, Japan
[166] Department of Physics and Astronomy, Tufts University, Medford MA, United States of America
[167] Department of Physics and Astronomy, University of California Irvine, Irvine CA, United States of America
[168] Department of Physics and Astronomy, University of Uppsala, Uppsala, Sweden
[169] Department of Physics, University of Illinois, Urbana IL, United States of America
[170] Instituto de Física Corpuscular (IFIC), Centro Mixto Universidad de Valencia - CSIC, Valencia, Spain
[171] Department of Physics, University of British Columbia, Vancouver BC, Canada
[172] Department of Physics and Astronomy, University of Victoria, Victoria BC, Canada
[173] Fakultät für Physik und Astronomie, Julius-Maximilians-Universität Würzburg, Würzburg, Germany
[174] Department of Physics, University of Warwick, Coventry, United Kingdom
[175] Waseda University, Tokyo, Japan
[176] Department of Particle Physics and Astrophysics, Weizmann Institute of Science, Rehovot, Israel
[177] Department of Physics, University of Wisconsin, Madison WI, United States of America
[178] Fakultät für Mathematik und Naturwissenschaften, Fachgruppe Physik, Bergische Universität Wuppertal, Wuppertal, Germany
[179] Department of Physics, Yale University, New Haven CT, United States of America

[a] Also at Borough of Manhattan Community College, City University of New York, New York NY, United States of America
[b] Also at Bruno Kessler Foundation, Trento, Italy
[c] Also at Center for High Energy Physics, Peking University, China
[d] Also at Centro Studi e Ricerche Enrico Fermi, Italy
[e] Also at CERN, Geneva, Switzerland
[f] Also at Département de Physique Nucléaire et Corpusculaire, Université de Genève, Genève, Switzerland
[g] Also at Departament de Fisica de la Universitat Autonoma de Barcelona, Barcelona, Spain
[h] Also at Department of Financial and Management Engineering, University of the Aegean, Chios, Greece
[i] Also at Department of Physics and Astronomy, Michigan State University, East Lansing MI, United States of America
[j] Also at Department of Physics and Astronomy, University of Louisville, Louisville, KY, United States of America
[k] Also at Department of Physics, Ben Gurion University of the Negev, Beer Sheva, Israel
[l] Also at Department of Physics, California State University, East Bay, United States of America
[m] Also at Department of Physics, California State University, Sacramento, United States of America
[n] Also at Department of Physics, King's College London, London, United Kingdom
[o] Also at Department of Physics, St. Petersburg State Polytechnical University, St. Petersburg, Russia
[p] Also at Department of Physics, University of Fribourg, Fribourg, Switzerland
[q] Also at Faculty of Physics, M.V. Lomonosov Moscow State University, Moscow, Russia
[r] Associated at Fermi National Accelerator Laboratory, Batavia IL, United States of America
[s] Also at Graduate School of Science, Osaka University, Osaka, Japan
[t] Also at Hellenic Open University, Patras, Greece

JHEP08(2022)089

[u] Also at Institucio Catalana de Recerca i Estudis Avancats, ICREA, Barcelona, Spain
[v] Also at Institut für Experimentalphysik, Universität Hamburg, Hamburg, Germany
[w] Also at Institute of Particle Physics (IPP), Canada
[x] Also at Institute of Physics, Azerbaijan Academy of Sciences, Baku, Azerbaijan
[y] Also at Institute of Theoretical Physics, Ilia State University, Tbilisi, Georgia
[z] Also at Instituto de Fisica Teorica, IFT-UAM/CSIC, Madrid, Spain
[aa] Also at Istanbul University, Dept. of Physics, Istanbul, Turkey
[ab] Also at Istinye University, Istanbul, Turkey
[ac] Also at Joint Institute for Nuclear Research, Dubna, Russia
[ad] Also at Moscow Institute of Physics and Technology State University, Dolgoprudny, Russia
[ae] Also at National Research Nuclear University MEPhI, Moscow, Russia
[af] Also at Physics Department, An-Najah National University, Nablus, Palestine
[ag] Also at Physikalisches Institut, Albert-Ludwigs-Universität Freiburg, Freiburg, Germany
[ah] Also at The City College of New York, New York NY, United States of America
[ai] Also at TRIUMF, Vancouver BC, Canada
[aj] Also at Università di Napoli Parthenope, Napoli, Italy
[ak] Also at University of Chinese Academy of Sciences (UCAS), Beijing, China
[al] Also at Yeditepe University, Physics Department, Istanbul, Turkey
[*] Deceased

JHEP08(2022)089